MULTIVARIABLE CONTROL SYSTEM DESIGN FOR A SUBMARINE

by

Kenneth A. Lively

B.S., M.S., University of Colorado (1976)

SUBMITTED IN PARTIAL FULFILLMENT OF THE
REQUIREMENTS FOR THE
DEGREES OF

MASTER OF SCIENCE

and

OCEAN ENGINEER

at the

MASSACHUSETTS INSTITUTE OF TECHNOLOGY

Signature of the Author Kenneth A Lively
Department of Ocean Engineering
Department of Electrical Engineering and Computer Science
May 11, 1984

Certified by Michael Athans
Professor Michael Athans,
Thesis Supervisor

Certified by Lena Valavani
Dr. Lena Valavani
Thesis Co-Supervisor

Certified by M J Triantafyllou
Professor Michael Triantafyllou
Thesis Reader

Accepted by _____
Professor Arthur Smith
Chairman, Electrical Engineering and Computer Science
Department Committee

Accepted by A. Douglas Carmichael
Professor A. D. Carmichael
Chairman, Ocean Engineering Department Committee

The author hereby grants to the U.S. Government permission to reproduce and to distribute copies of this thesis document in whole or in part.

Kenneth A Lively

Kenneth A. Lively

MULTIVARIABLE CONTROL SYSTEM DESIGN FOR A SUBMARINE

by

Kenneth A. Lively

Submitted to the Department of Electrical Engineering and Computer Science and to the Department of Ocean Engineering on May 11, 1983 in partial fulfillment of the requirements for the Degrees of Master of Science in Electrical Engineering and Computer Science and Ocean Engineer.

ABSTRACT

A nonlinear controller is designed for a full size submarine using the LQG/LTR procedure. Linear models of the submarine are developed at four different speeds and then analyzed using the method of modal analysis. The linear models are then augmented with integral control and a Kalman Filter transfer function is designed using some tools for loop shaping. The Loop Transfer Recovery technique is then applied to recover the Kalman Filter loop shapes. A polynomial data fit is performed on the resulting compensators to produce a nonlinear controller. Both the linear and the nonlinear controllers are extensively tested using a full nonlinear model of the submarine.

THESIS SUPERVISORS: Dr. Michael Athans, Professor of Systems Science and Engineering
Dr. Lena Valavani, Research Scientist, MIT Laboratory for Information and Decision Systems

ACKNOWLEDGEMENTS

I would like to thank my supervisors, Prof. Michael Athans and Dr. Lena Valavani for their help in shaping the ideas of this thesis and for their patience in seeing it through.

This thesis benefitted considerably from discussions with my fellow students Larry Dreher, George Goodman, and Logan Milliken.

I would also like to thank the Charles Stark Draper Laboratory for the computer support provided for this research and especially William Bonnice, who provided continual technical and programming support for the submarine model.

I am also indebted to CSDL for their loan of modem which permitted me to link the computer model of the submarine on the CSDL computer to the Honeyx control system software on the Multics computer at MIT.

This research was carried out at the MIT Laboratory for Information and Decision Systems with partial support provided by the Office of Naval Research under contract ONR/N00014-82-K-0582(NR 606-003).

Table of Contents

LIST OF FIGURES

LIST OF TABLES

Chapter 1

INTRODUCTION AND SUMMARY

1.1 Background

The technology for building multivariable control systems has advanced in the last several years and there is a very definite need for complex design examples to help engineers understand and further develop this powerful design methodology.

Multi-input, multi-output (MIMO) control system design is much more complex than either classical control system design or single-input, single-output (SISO) control system design. The engineer must use and manipulate the singular values of the loop transfer function matrix of the plant to determine the performance of the controller and this concept of singular values as a measure is at present relatively unknown to most control engineers. Therefore, it is necessary to apply the MIMO methodology to practical examples in order to display the power of this technique and

also to point out any shortcomings.

To date, non-trivial examples of MIMO design using the Linear Quadratic Gaussian procedure with Loop Transfer Recovery (LQG/LTR) are few in number (see [1] [2] for recent examples). This is in part due to the LQG/LTR technique having been only recently developed [3] [4] [5], and partly due to the significant effort required to develop and linearize a MIMO model, design the controller, and test the resulting design.

Previous controller designs for submarines have used the SISO design technique or classical design techniques [6] [7]. This thesis is believed to be the first (unclassified) example of a MIMO design on a full-size submarine. The LQG/LTR design methodology is used because it incorporates the dynamics of the plant (the submarine) into the compensator and thereby provides a vehicle for capturing the dynamics of the submarine at various speeds. This information can then be utilized to produce a nonlinear dynamic compensator that varies as some sensed parameter changes (gain scheduling), providing adaptive-like nonlinear control of the submarine over a variety of speed conditions and simultaneous maneuvers. In fact, the linearized models of the submarine were selected so as to <u>emphasize</u> the cross-coupling of the longitudinal and lateral dynamics.

1.2 Contributions of the Thesis

The main contribution of this thesis is to illustrate the multivariable LQG/LTR feedback control system design methodology for a maneuvering submarine, and, further, to demonstrate the utilization of gain scheduling to construct a nonlinear controller. The reader should not interpret the resulting controller design to be a final product, and further research is needed to use such controllers for all diverse submarine maneuvers.

The first stage of the design process is to achieve as complete an understanding of the submarine model as is possible. To accomplish this, the submarine model is linearized about an unconventional operating trajectory so as to capture longitudinal/lateral interactions. The resulting linear representation is decomposed into its modal representation. The modal matrices are then graphically displayed to visualize the dynamic behavior of the submarine and further manipulated to determine whether or not the required observability/controllability requirements of the LQG/LTR design process are met under various choices of control and output variables.

The controller design is based on the LQG/LTR methodology formulated by Doyle and Stein [3] [4], and refined by Athans [8].

The design effort concentrates on the frequency domain properties of the state space representations of the submarine model. Methods of shaping the singular values of the open loop plant transfer matrix are developed that guarantee the identical behavior of the singular values at both the high and low ends of the frequency spectrum. Scaling of the output variables is utilized to produce the desired loop shapes at frequencies near crossover.

The state variable used for gain scheduling was taken to be forward velocity in the body reference coordinate system. Although gain scheduling may also be desired based on roll angle (again in the body reference coordinate system), this would necessarily be in addition to the gain scheduling employed using forward velocity. Time domain plots of nonlinear simulations of the compensated system designed at a particular speed are presented to show the validity of that choice.

Gain scheduling of the compensator designs is accomplished by performing a least squares fit on the individual compensator parameters. An algorithm for producing the coefficients resulting from a quadratic polynomial least

squares fit to matrices is presented.

Finally, time domain plots of the gain scheduled LQG/LTR compensator being applied to the nonlinear submarine model are presented as a means of illustrating the resulting nonlinear design.

1.3 Outline of the Thesis

Chapter 2 describes the process used to model the submarine and the methods used to produce a linear state space representation. The computer implementation of the submarine nonlinear and linear models is briefly described. The chapter ends with a discussion of the reasoning used to select the output variables and presents the performance requirements imposed on the controller designs.

In Chapter 3, the eigenstructure of the linear model is studied using modal decomposition. Pole-zero information and singular value plots are also utilized to further display the structure of the open loop dynamics.

Chapter 4 contains the linear portion of the design, following the LQG/LTR methodology. Although the reader is assumed to be familiar with the work of Doyle and Stein [3], the notation being used is briefly summarized. Singular

value plots of the open loop submarine model plus compensator are presented for each design.

The gain scheduling method for the compensator parameters is presented in Chapter 5. Results of various nonlinear simulations are included to display the performance, focusing upon simultaneous evasive maneuvers.

Chapter 6 contains a summary, conclusions, and some proposed directions for further research.

Chapter 2

MATHEMATICAL MODEL OF THE SUBMARINE

2.1 Introduction

The submarine model used in this thesis is that implemented at the Charles Stark Draper Laboratory (CSDL) both as a real-time simulation facility and an analytical model generating facility. Details of the latter are given in [9].

This chapter discusses the equations used to model a submarine and presents a brief history of the implementation of the submarine model at the CSDL.

The software in its present form [10] provides the control system designer with several useful tools. The manner in which these tools are used to produce and validate the required linear models for a gain scheduling LQG/LTR controller is detailed, as well as the reasoning used to select the output variables.

The chapter ends with a section on performance requirements to be imposed on the controller design, thus setting the stage for analysis of the model in chapter 3 and finally the actual design of the controller in chapter 4.

2.2 Modeling of the Submarine

The generic model from which most submarine models are derived is that given in the original Naval Ship Research and Development Center (NSRDC) Report 2510 [11] entitled "Standard Equations of Motion for Submarine Simulation." The model used in this thesis is believed to be an improvement of the 'standard model' in that it includes the crossflow drag and vortex contribution terms for the five degrees of freedom (the straight ahead x-axis force is not included).

To establish the notation for describing the submarine motion, a brief description of the nonlinear equations of motion is presented.

Two reference frames are used in deriving the equations of motion for a submarine - the body reference frame and the earth reference frame. The former is used because hydrodynamic forces and inertias are more readily computed

in the submarine reference frame. For purposes of control and stability determination, we are also concerned with the motion of the submarine in the earth reference frame. The relationship of the motion of the submarine between these two reference frames is described by Euler's angles [12] Ψ, θ, and ϕ:

Ψ (Yaw) - rotation about the z axis

θ (Pitch) - rotation about the y axis

ϕ (Roll) - rotation about the x axis

where x, y, and z represent the body reference frame as it changes according to the indicated rotations and in the order given. The orientation of the submarine in its own reference frame is depicted in figure 2.1.

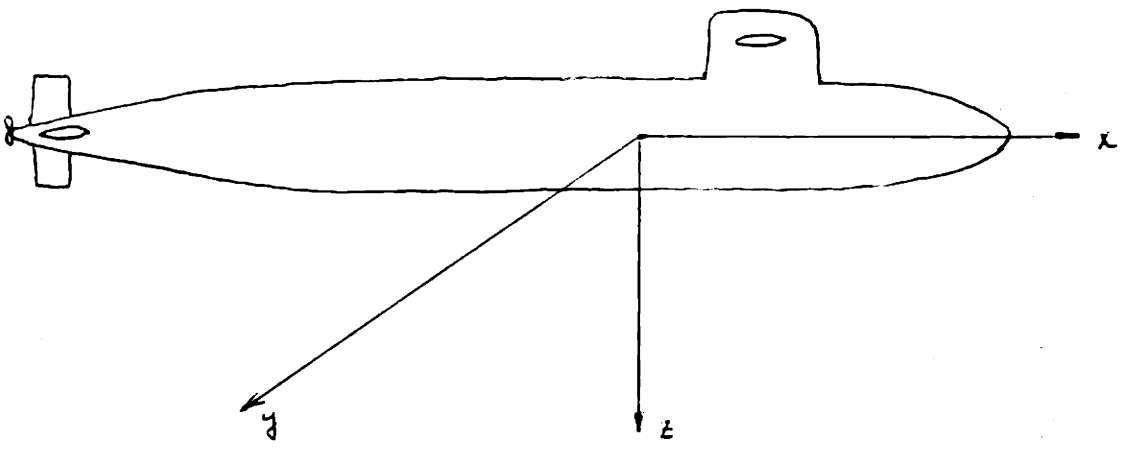

Figure 2.1 - Submarine Body Reference Frame Axes

The state vector for the submarine must therefore include the six degrees of freedom in its own reference frame, the three Euler angles, and any desired position variables to locate the submarine with respect to some earth frame reference point. For the purposes of this thesis, only the depth position variable is used and the state vector for the submarine model contains the states summarized in table 2.1.

Table 2.1. Submarine State Variables

$u = x_1(t)$ - forward velocity in feet/sec

$v = x_2(t)$ - lateral velocity in feet/sec

$w = x_3(t)$ - vertical velocity in feet/sec

$p = x_4(t)$ - roll rate in radians/sec

$q = x_5(t)$ - pitch rate in radians/sec

$r = x_6(t)$ - yaw rate in radians/sec

$\phi = x_7(t)$ - roll angle in radians

$\theta = x_8(t)$ - pitch angle in radians

$\Psi = x_9(t)$ - yaw angle in radians

$z = x_{10}(t)$ - depth in feet (positive downward)

Note: u, v, w, ϕ, and θ are in the body reference frame. All others are in the inertial reference frame.

It should be noted that the Euler angles only approximately describe the submarine roll, pitch, and yaw angles in the earth reference frame, with the approximation becoming more accurate as the magnitude of the Euler angles

approaches zero. This is due to the fact that, in transforming the coordinates from earth reference to body reference, the Euler angle rotations are applied sequentially, in the specific order Ψ, θ, and finally ϕ.

Using the state variables of table 2.1, the nonlinear equations of motion are derived using force and moment balances in the submarine rotating coordinate system. The forces and moments due to the submarine motion must be equal to the total forces and moments exerted by:

1. Hydrodynamic pressures
2. Control forces and moments
3. Propulsion or tow forces
4. Any other forces and moments

The reader is referred to the NSRDC Report 2510 [12] for details of the derivation of the nonlinear equations of motion and a description of the hydrodynamic coefficients describing the submarine geometry and control surfaces.

The submarine model used in this thesis has three control variables - rudders, stern planes, and fairwater planes (see figure 2.2). The propeller is constrained to turn at a constant rpm to reflect current operating procedures. The control surfaces on the submarine are locked together in the

sense that the port stern plane deflects the same as the starboard stern plane and similarly for the rudders and fairwater planes. Table 2.2 summarizes the nomenclature for the control surfaces.

Table 2.2. Submarine Control Surfaces

ds = $u_1(t)$ - stern planes deflection in radians

db = $u_2(t)$ - fairwater planes deflection in radians

dr = $u_3(t)$ - rudder deflection in radians

2.3 Implementation of the Model

Initially, the CSDL adapted model was implemented in the simulation lab at CSDL, resulting in a real time simulation. A Digital Equipment Corporation VAX 11-780 computer and a Computervision graphics display workstation are used to provide both computer print-out and visual display of submarine motion during various maneuvers. Joystick control is used to input commands to the control surfaces, with the state of the submarine being depicted in real time against an x-y grid on the graphics display. The display also includes simulated instrumentation to indicate the current status of the control surfaces and other selected parameters.

For the purposes of analytical studies geared to

controller design, the same set of nonlinear equations was later implemented on the IBM time sharing computer at CSDL. Considerable enhancement was added to the program during the transfer to aid the control system designer in his task. At present, capabilities of the software include:

1. Addition of a user-friendly executive routine to allow modification of parameters and selection of options for a particular simulation run. This routine then submits the tailored program for background execution.

2. The option of calculating $\underline{A}$ and $\underline{B}$ matrices that describe the linearization of the submarine about a particular nominal point, in the form

$$\dot{\underline{x}}(t) = \underline{A}\,\underline{x}(t) + \underline{B}\,\underline{u}(t).$$

3. The options of setting control surfaces to fixed values, varying the control surfaces over time according to values in a data file, calculation of the controls using full state feedback, or calculation of the controls using a LQG/LTR derived compensation.

4. Selection of computer print-out or plots (or both) of the state variables over time of either the nonlinear model or the linearized model.

5. The capability of searching for a local equilibrium

point for the nonlinear model that is close to a desired nominal point.

To closely simulate typical operating profiles of an actual submarine, the propeller rpm is kept constant during a particular run.

2.4 Generation of the Linear Models

To perform gain scheduling of compensator designs over a large speed range requires that several linear models of the submarine be developed. Extensive analysis of the submarine open loop dynamics, however, requires only a single model that captures most of the dynamic modes present in the submarine. As we remarked before, this linearized model was obtained to capture significant longitudinal-lateral interactions in simultaneous maneuvers.

The submarine modeled in this thesis (figure 2.2) is approximately 400 feet long, has the conventional stern configuration (stern control surfaces are in the shape of a cross), and planes mounted on the sail (fairwater planes). The lack of differential control for the control surfaces and the conventional stern configuration prevent any direct control over roll or roll rate of the submarine. For this

reason, the initial linear model should be such that roll does not dominate the submarine behavior nor is it absent either. The nominal point used for analysis uses a forward velocity of 20 knots, 5 degrees of rudder, and one degree on each of the planes. This places the submarine in a diving turn with the trajectory that of a helix. Other state variables are as determined by an equilibrium point search with these initial conditions. Analysis of this model is presented in the next chapter.

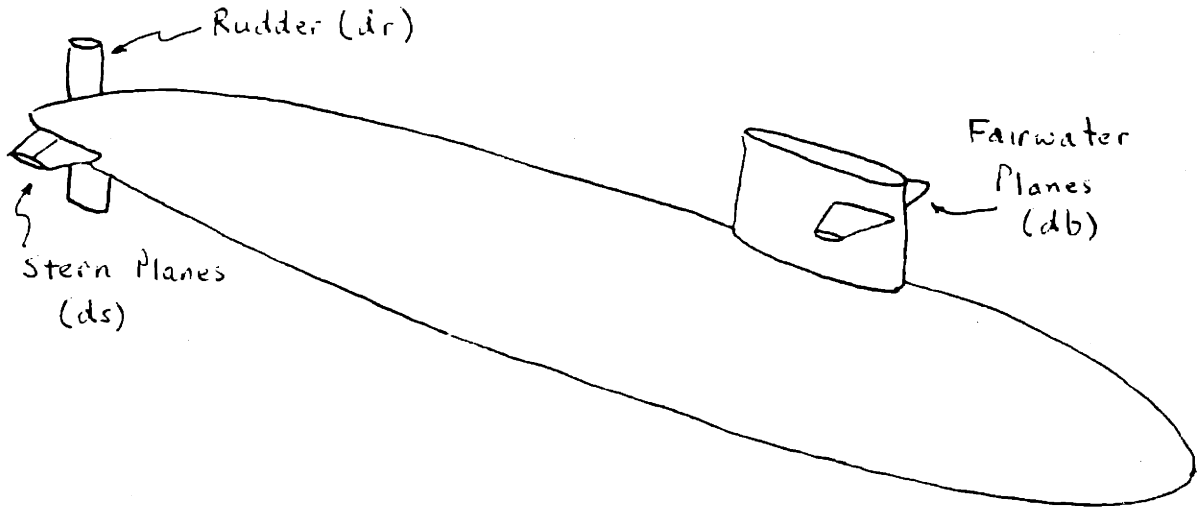

Figure 2.2. Submarine Control Surfaces

The control variables used in the controller designs are ds, db, and dr (refer to table 2.2), the angular deflections of the three control surfaces. Deflection limits, as imposed by the software, are 40 degrees for the stern planes and rudder, and 20 degrees for the sail planes.

Linearization of the nonlinear equations of motion is performed in a straightforward manner. A nominal point is determined by integrating the nonlinear equations of motion using a selected set of initial conditions, and an equilibrium point is found that corresponds to minimum accelerations for all state variables very near the steady state values determined from the integration of the equations of motion. For the nonlinear equations of motion, there are 11 state variables since the control surface deflections are also independent variables (Ψ and z have no effect on the integration). Thus an equilibrium point is more precisely defined as a local minimum in 11-space. The values of the state variables at the equilibrium point then describe a nominal point, about which high order terms can be neglected. A set of linear differential equations can then be produced, and the $\underline{A}$ and $\underline{B}$ matrices calculated, to provide a state space description of the submarine.

For each nominal point thus determined, the resulting linear model must be validated by perturbing the nominal point to form a set of initial conditions, and then comparing the results of integrating both the nonlinear and the linear equations of motion. Provided the perturbations are not too large, the nonlinear model will always return to the equilibrium point values, while the linear model will never reach steady state due to the non-zero forcing term

imposed by the control surfaces. The comparison of the two time histories, therefore, is limited to checking initial derivatives, apparent natural frequencies, and the damping rate.

Four linear models were developed, corresponding to forward velocities of 5, 10, 20, and 25 knots. Control surface deflections were maintained at the values previously mentioned. The models are designated S5R5, S10R5, S20R5, and S25R5, reflecting the speed and rudder deflection. Figures 2.3 and 2.4 show results of the comparisons for selected state variables for the 5 and 20 knot models. The perturbations applied to the nominal point were identical in all cases (see table 2.3). The comparisons show excellent correlation between the linear and nonlinear models and serve to validate the linear models. In particular, the initial derivatives, the apparent natural frequency of response, and the damping factors match almost exactly for the linear and nonlinear models. Notice that the pitch rate q(t) (figure 2.3 (c) and (d) and 2.4 (c) and (d)) contains two oscillatory modes, reflecting the cross coupling between the rudders and stern planes when the submarine has a non-zero roll angle. The roll angle for the 5 knot model is -0.6 degrees and for the 20 knot model, -8 degrees. The $\underline{A}$ and $\underline{B}$ matrices for the four models are presented in appendix A.

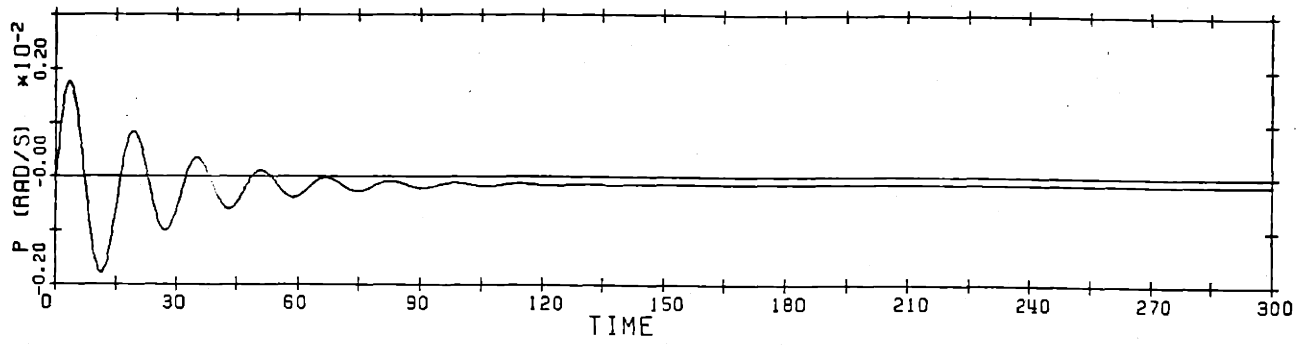

(a) Roll rate p(t) for the linear model

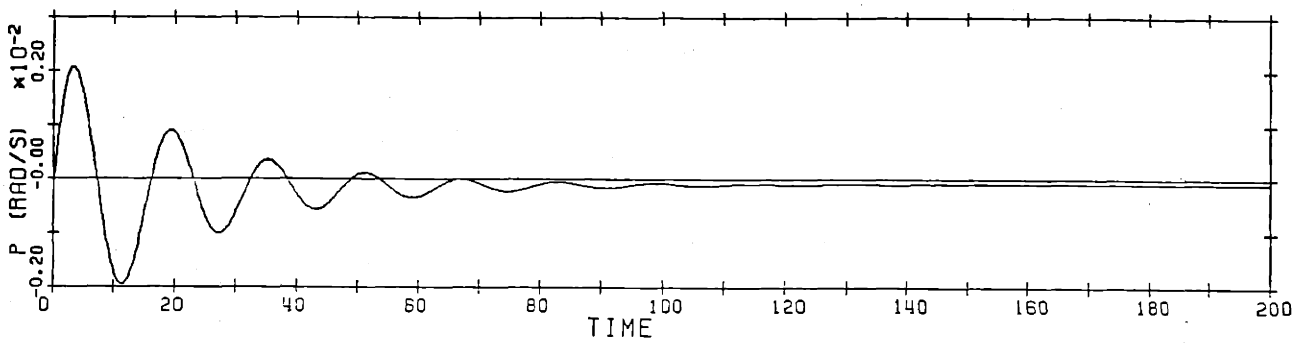

(b) Roll rate p(t) for the nonlinear model

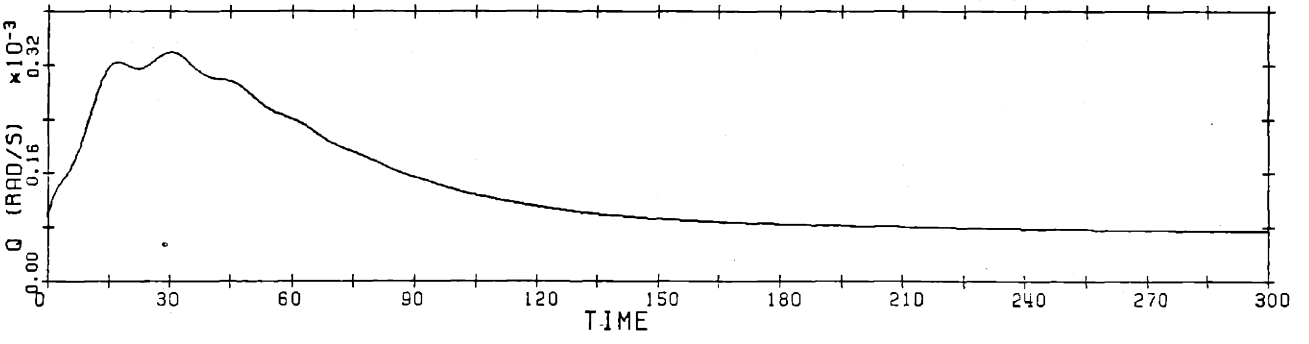

(c) Pitch rate q(t) for the linear model

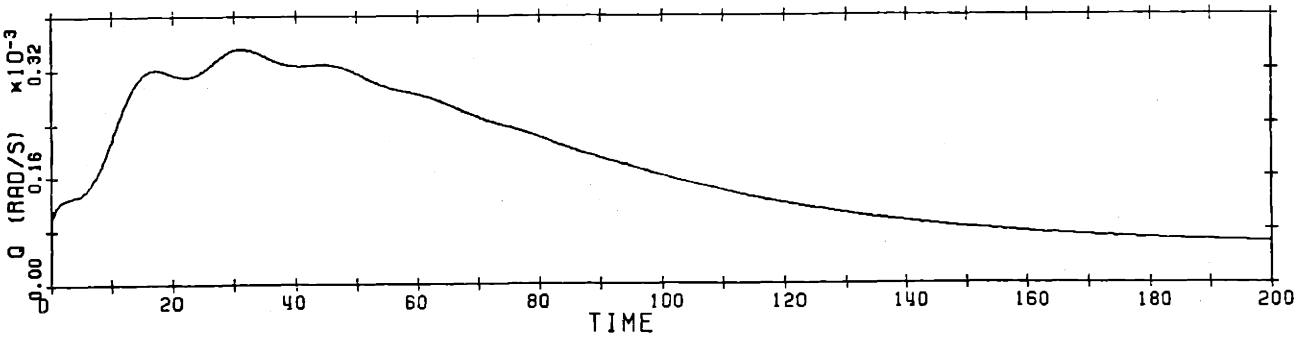

(d) Pitch rate q(t) for the nonlinear model

Figure 2.3. Comparison of Linear and Nonlinear 5 Knot Models

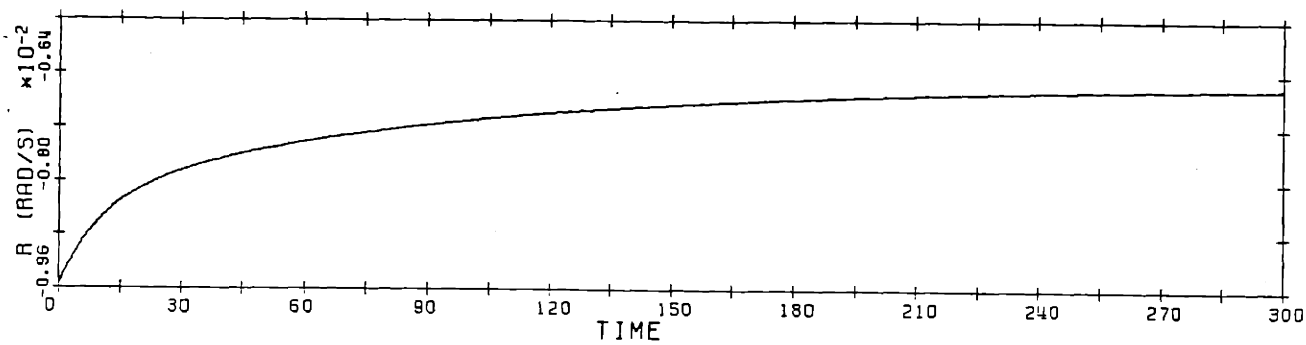

(e) Yaw rate r(t) for the linear model

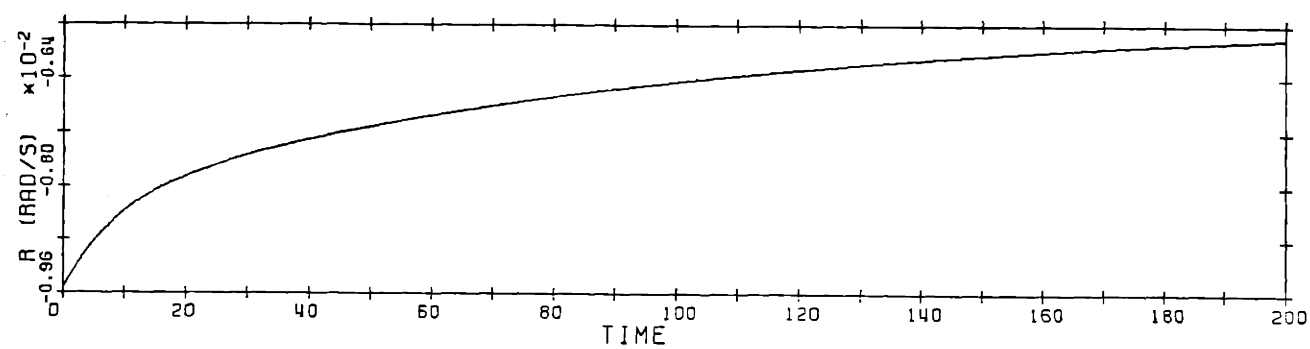

(f) Yaw rate r(t) for the nonlinear model

Figure 2.3. Comparison of Linear and Nonlinear 5 Knot Models

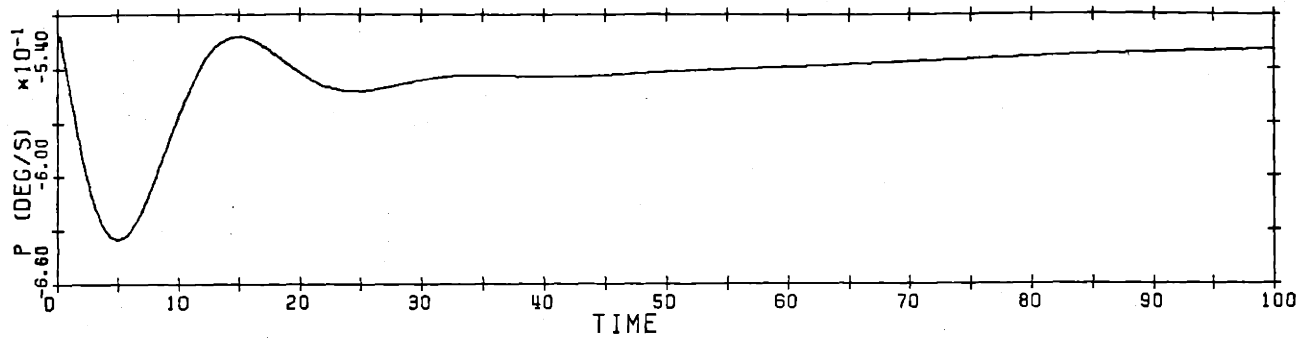

(a) Roll rate p(t) for the linear model

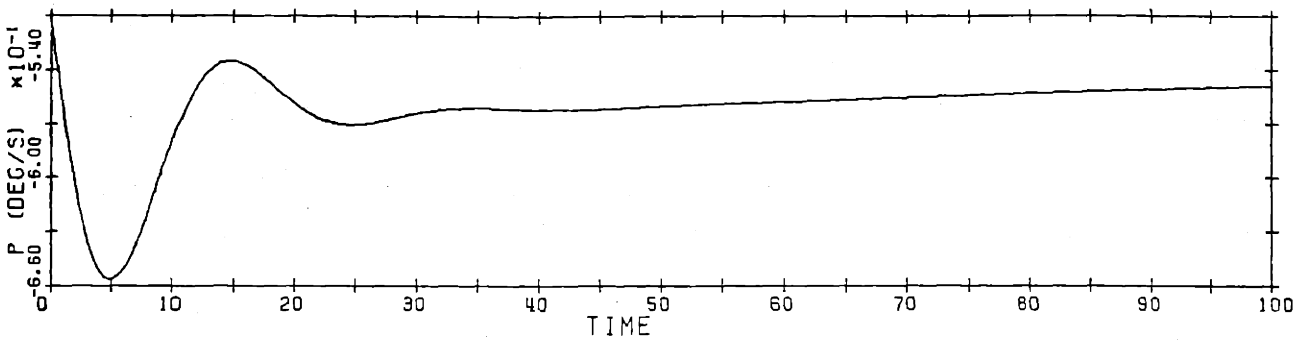

(b) Roll rate p(t) for the nonlinear model

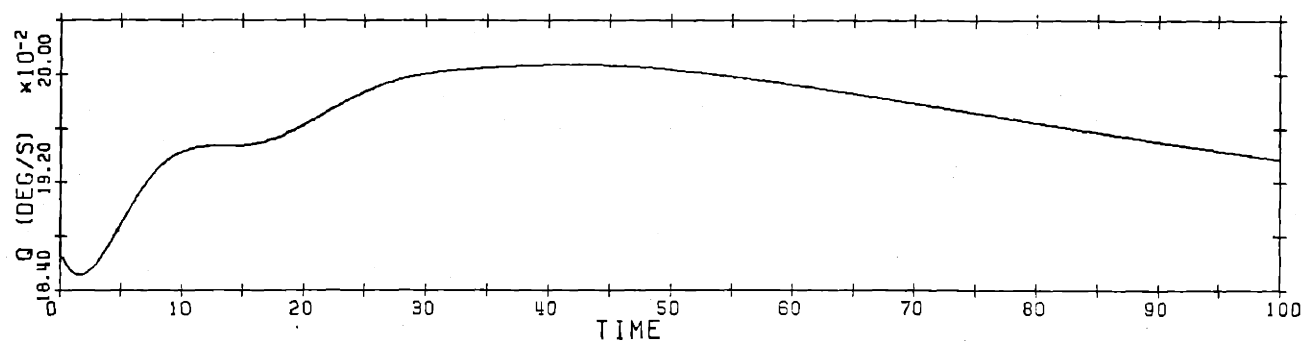

(c) Pitch rate q(t) for the linear model

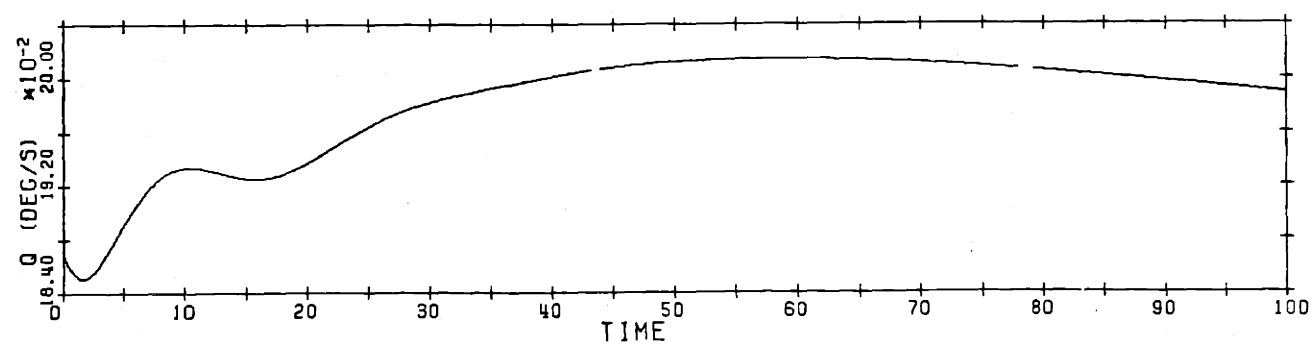

(d) Pitch rate q(t) for the nonlinear model

Figure 2.4. Comparison of Linear and Nonlinear 20 Knot Models

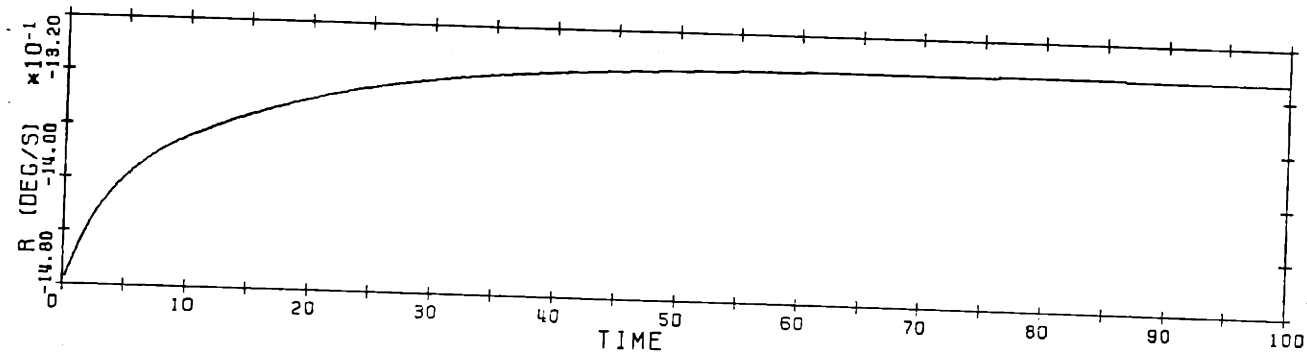

(e) Yaw rate r(t) for the linear model

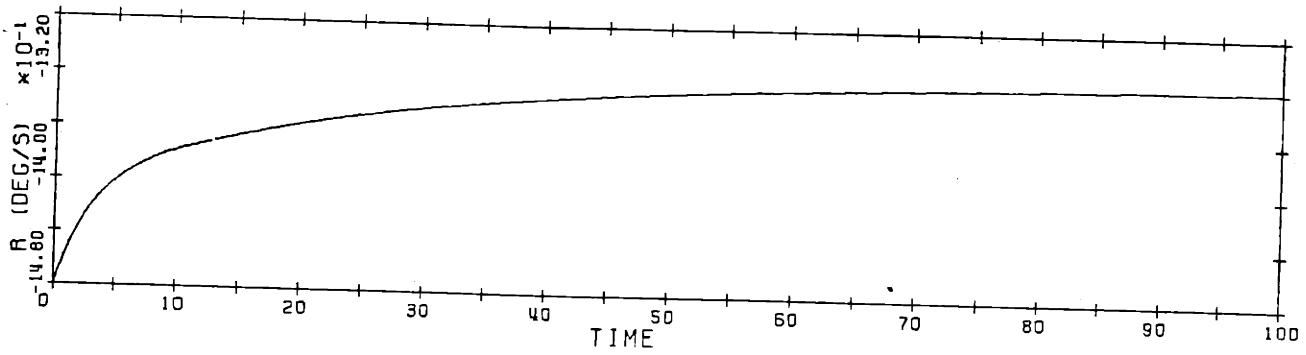

(f) Yaw rate r(t) for the nonlinear model

Figure 2.4. Comparison of Linear and Nonlinear 20 Knot Models

Table 2.3

Perturbations Applied to Nominal Points

State Variable	Perturbation
u	+ 2.0 ft/sec
v	+ 0.2 ft/sec
w	- 0.02 ft/sec
p	- 0.00003 rad/sec
q	+ 0.00003 rad/sec
r	- 0.003 rad/sec
ϕ	- 0.5 degrees
θ	- 1.0 degrees

2.5 Selection of the Output Variables

Selection of the output variables requires both a careful study of the $\underline{A}$ and $\underline{B}$ matrices and determination of the intent of the controller design. Three control variables are available so that three output variables can be chosen. An autopilot could be designed, using the position variables Ψ and z, or a rate controller could be designed, using the rate variables u, v, w, p, q, or r. The attitude variables ϕ and θ could be included in either design, depending on the importance of these variables to the control system designer.

The philosophy taken in this thesis is that a rate controller be designed to control the submarine during various maneuvers. As previously mentioned, the submarine

model was linearized about a nonconventional operating point to ensure that the cross coupling of the control surfaces would be captured in the $\underline{A}$ and $\underline{B}$ matrices. The simplifying assumption is made that the rate commands are presented in the form of commands for w and r. If this assumption were not made, the coordinate transformation effect of the Euler angles would require a C matrix that was dependent on the real time values of ϕ, θ, and Ψ, making the C matrix state dependent. The third output variable is taken to be θ, the pitch angle, permitting the controller to accomplish depth changes without imparting a pitch angle on the submarine. The reader should note that w(t) is not an inertial reference plane variable, and represents the true vertical rate only when the submarine has zero pitch and roll angles. Unfortunately, $\dot{z}(t)$ is not available as a state variable and this discrepancy must be tolerated.

With the output variables determined, and the $\underline{A}$ and $\underline{B}$ matrices calculated, the state space description of the submarine model is now complete and takes the form

$$\dot{\underline{x}}(t) = \underline{A}\,\underline{x}(t) + \underline{B}\,\underline{u}(t)$$

$$\underline{y}(t) = \underline{C}\,\underline{x}(t), \qquad (2.1)$$

where $\underline{y}(t) = [\ w(t) \quad r(t) \quad \theta(t)\ ]'$.

2.6 Performance Requirements

Two performance requirements are imposed on the controller design. First, the maximum crossover frequency is limited to that of the submarine's ability to respond and, second, the steady state error to step commands and step disturbances is to be zero.

The maximum crossover frequency is based on the perturbed response of the non-linear model. Inspection of figure 2.5 reveals an average settling time to within 90% of steady state of 60-65 seconds, leading to a desired crossover frequency of 0.10 radians/sec.

Inspection of the perturbed response of all four models confirms an intuitive feeling that the settling time increases as the submarine slows, requiring that a different performance requirement be levied on each design.

The value of 0.10 rad/sec was declared to be the maximum for the fastest model (25 knots), and a least squares curve was fitted to the approximate time constants indicated by the plots. A linear fit proved satisfactory, giving a correlation coefficient of 0.9983 and, when transformed to yield maximum crossover frequencies, produced the results in

table 2.4.

Table 2.4

Crossover Frequencies for the Linear Models

Model	Crossover Frequency (rad/sec)
5 Knot	0.05
10 Knot	0.06
20 Knot	0.08
25 Knot	0.10

The zero steady state error requirement is met by placing integrators in each of the three input channels. The integrators are placed at the input to the plant because this is where the error signal appears. The integrators will then become a part of the compensator which is before the plant in the feedback loop. As will be seen, the use of integral control does not prevent the maximum crossover frequency specification from being met.

2.7 Summary

This chapter has described the origins of the submarine model, briefly described the process of producing a linear model, and presented the reasoning by which the output variables were chosen. Additionally, performance constraints were imposed on the controller design, thus setting the stage for analysis of the open loop dynamics of

the plant.

The next chapter will analyze the plant using the method of modal decomposition, and present data showing the eigenstructure of the submarine linear models.

Chapter 3

ANALYSIS OF THE LINEAR MODEL

3.1 Introduction

In this chapter, the eigenstructure of the unaugmented 20 knot model will be investigated. As previously stated, the 20 knot model was the first to be developed and the only one to have a detailed analysis performed on it.

For each of the other three linear models (at 5, 10, and 25 knots) analysis was limited to inspection of the poles and zeros, and producing singular value plots of the open loop plant. Several consistency checks were also performed in an effort to avoid any numerical errors.

In the previous chapter, a state space description of the submarine linear model was developed in the form

$$\dot{\underline{x}}(t) = \underline{A}\,\underline{x}(t) + \underline{B}\,\underline{u}(t) \qquad (3.1)$$

$$\underline{y}(t) = \underline{C}\,\underline{u}(t). \qquad (3.2)$$

Prior to the actual analysis of the linear model, it will be shown that the order of the model can be reduced, based on

the zero entries present in the $\underline{A}$ and $\underline{B}$ matrices.

The eigenstructure of the 20 knot model is revealed by the method of modal analysis [13]. This method involves the implicit application of similarity transformations to the $\underline{A}$ matrix, reducing it to a diagonal matrix whose entries are the poles of the open loop system. The similarity transformations provide a means of describing the state space of the linear system in separate decoupled modes, thereby yielding information as to the controllability and observability of the system.

This information, coupled with the pole-zero structure, provides the basis and validity for the LQG/LTR designs of the next chapter.

3.2 Reduction of the Model

Inspection of the $\underline{A}$ matrix for the 20 knot model (refer to Appendix A, model S20R5) reveals zero entries in all elements of the last two columns. This indicates that the present values of the states Ψ and z can have no influence on any other state. In other words, the present depth and heading angle are irrelavent to the dynamic response of the linear system.

Zeros in the last two rows of $\underline{B}$ (Appendix A) further indicate that the controls exert no direct influence on the derivatives of Ψ and z.

Therefore, since the purpose of the controller is not concerned with controlling either of these variables, they are removed from the linear model. This is accomplished by deleting the last two rows and columns of $\underline{A}$, and the last two rows of $\underline{B}$, leaving an 8 state system.

3.3 The Natural Modes of the System

Determination of the natural modes of the 20 knot linear model is accomplished by diagonalizing the state space description. For any linear dynamic system without input to output direct coupling, we have

$$\dot{\underline{x}}(t) = \underline{A}\,\underline{x}(t) + \underline{B}\,\underline{u}(t) \qquad (3.3)$$

$$\underline{y}(t) = \underline{C}\,\underline{x}(t). \qquad (3.4)$$

Now define a new state vector $\underline{z}(t)$ by the relation

$$\underline{x}(t) = \underline{T}\,\underline{z}(t), \qquad (3.5)$$

where $\underline{T}$ is an as yet unspecified, n x n, invertible matrix. Then we have

$$\underline{T}\,\dot{\underline{z}}(t) = \underline{A}\,\underline{T}\,\underline{z}(t) + \underline{B}\,\underline{u}(t) \qquad (3.6)$$

$$\underline{y}(t) = \underline{C}\,\underline{T}\,\underline{z}(t). \qquad (3.7)$$

Multiplying (3.6) on the left by $\underline{T}^{-1}$, we are left with

$$\dot{\underline{z}}(t) = \underline{T}^{-1}\,\underline{A}\,\underline{T}\,\underline{z}(t) + \underline{T}^{-1}\,\underline{B}\,\underline{u}(t) \qquad (3.8)$$

$$\underline{y}(t) = \underline{C}\,\underline{T}\,\underline{z}(t). \qquad (3.9)$$

If $\underline{T}$ is such that $\underline{T}^{-1}\,\underline{A}\,\underline{T}$ is diagonal, then the state vector $\underline{z}(t)$ defines a new state space in which the modes are decoupled and the entries of $\underline{T}^{-1}\,\underline{A}\,\underline{T}$ are the eigenvalues of $\underline{A}$. Let

$$\underline{\Lambda} = \underline{T}^{-1}\,\underline{A}\,\underline{T}. \qquad (3.10)$$

Then we have $$\underline{A}\,\underline{T} = \underline{T}\,\underline{\Lambda}. \qquad (3.11)$$

Now, represent the $\underline{T}$ matrix by its n column vectors $\underline{v}_1$, $\underline{v}_2$, ..., $\underline{v}_n$, so that equation 3.11 can be expressed as

$$\underline{A}\,\underline{v}_i = \underline{v}_i\lambda_i \quad \text{for } i = 1 \text{ to } n \quad (\Lambda = [\lambda_i]). \qquad (3.12)$$

Thus the columns of $\underline{T}$ are the eigenvectors of $\underline{A}$ and the diagonalization is possible only when the $\underline{A}$ matrix has distinct eigenvalues.

The $\underline{T}$ matrix is called the modal matrix, with each column of $\underline{T}$ describing the motion of the submarine along the coordinate axes of the state vector components u, v, w, p, q, r, ϕ, and θ, for a particular mode. Since every possible dynamic response of the submarine must consist of a linear combination of the decoupled modes, analysis of the columns of $\underline{T}$ should provide the designer with very useful information regarding the submarine's dynamic response.

Unfortunately, it is not a simple matter to visualize or characterize motions in 8-space, especially when the

magnitude of the motions are complex numbers expressed in various units.

Analysis of the modes of the system is accomplished in two steps. First, the $\underline{A}$ and $\underline{B}$ matrices of the linear model are transformed so that all angular components of the state vector will have units of degrees or degrees/sec, as appropriate. Details of the transformations applied are in appendix B1.

Secondly, the columns of the resulting modal matrix are graphed in bar chart form by taking absolute values of each element of the normalized column vectors. The loss of phase information resulting from taking absolute values is considered to be of less importance than the magnitude of the motion along a particular state component.

The bar charts (figure 3.1) have a vertical scale of 0 to 100%, reflecting the intent of displaying the relative magnitude of the response, and the eigenvalue corresponding to a particular mode is noted below each graph. Note that the two columns corresponding to a complex eigenvalue do not produce unique modes when graphed in this manner. Complex, or oscillatory modes are indicated by the labeling and the presence of a complex eigenvalue.

It should be noted at this point that the modes shown

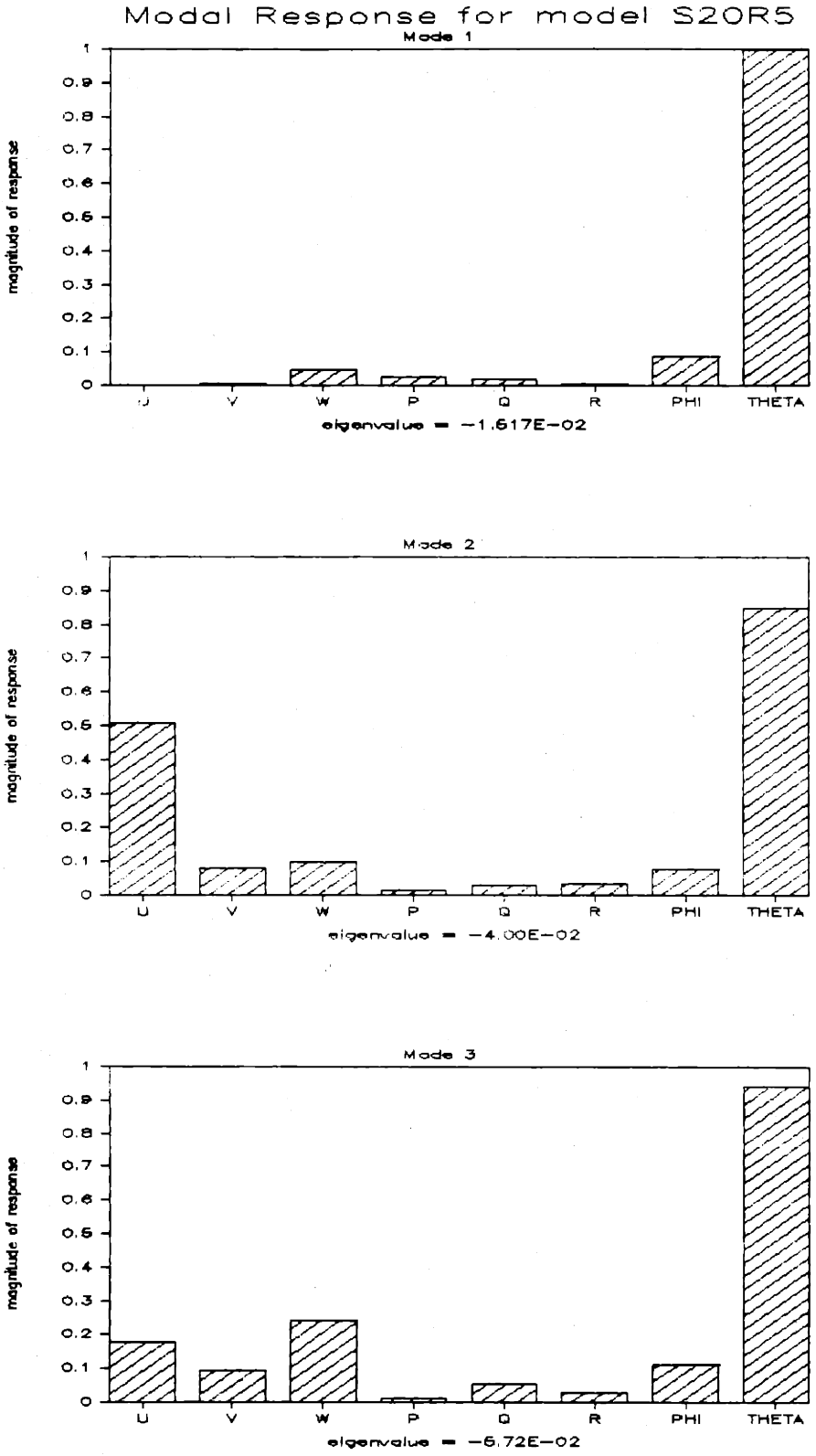

Figure 3.1(a) Modes 1, 2, and 3 for Model S20R5

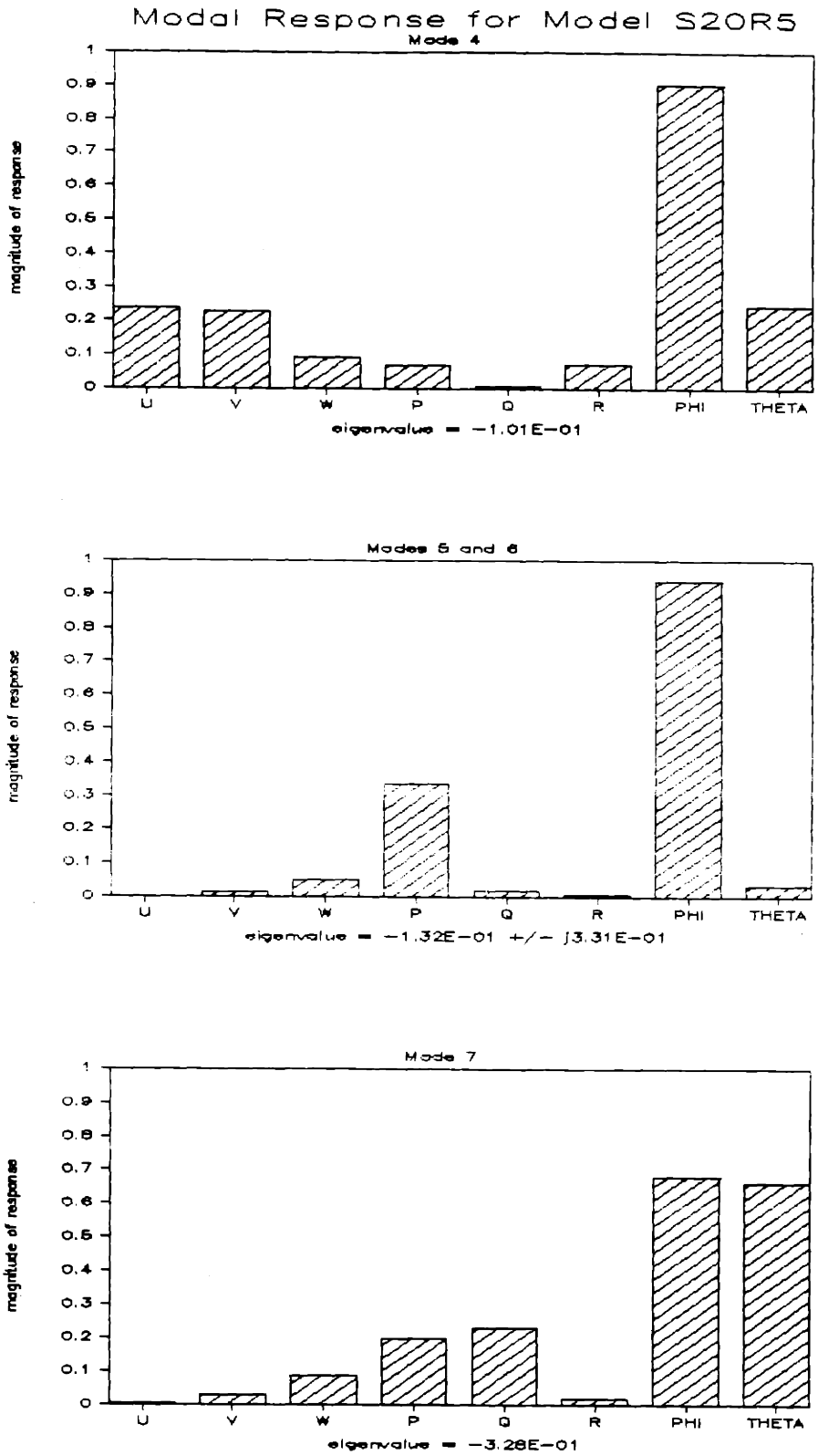

Figure 3.1(b) Modes 4, 5, 6, and 7 for Model S20R5

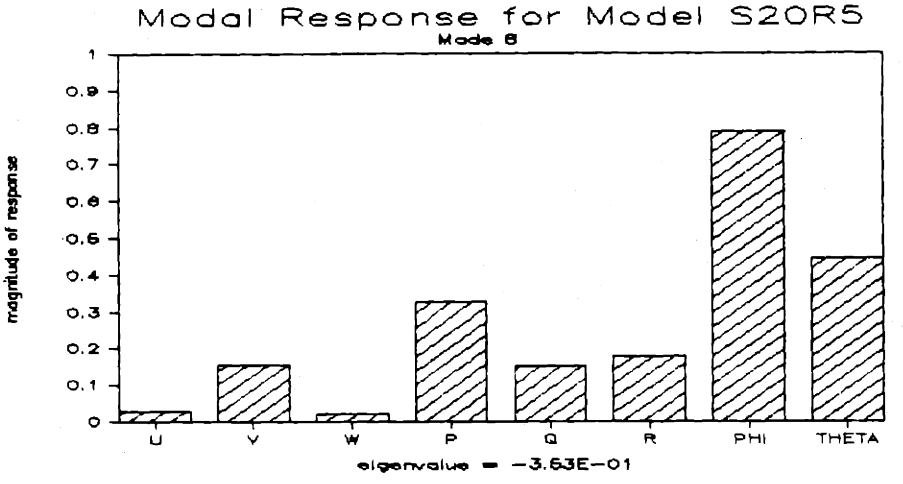

Figure 3.1(c) Mode 8 for Model S20R5

represent the natural modes of a linear model of a submarine proceeding downward, in a port turn, at 20 knots. (Recall that the nominal point specifies 5 degrees of rudder and 1 degree on the planes). Thus, although the bar charts provide a convenient means of displaying the modes of a linear system, in this particular case they are displaying the modes of a system linearized about a nominal point that serves to further obscure any physical interpretation. For this reason, interpretation of the modes is limited to the following observations:

1. All eigenvalues, and hence the open loop poles, are in the left half plane.

2. Mode 1 appears to represent the steady state response of the submarine in a diving turn with constant control surface deflections.

3. Modes 1, 2, and 3 are relatively lightly damped compared to the other modes. They also have less roll response and higher pitch response than the others, and tend to indicate that the sail of the submarine acts as a damper in side to side motions of the submarine.

4. Modes 5 and 6 represent a nearly pure roll mode in that almost the entire response is concentrated in

roll and roll rate. The inability to directly control roll and roll rate is reflected in the oscillatory behavior of these modes.

5. Comparison of the magnitudes for roll, pitch, and yaw rates for modes 4 and 8 appears to indicate that as more yaw rate is introduced, some of the roll response is converted to pitch response. This is indicative of the cross coupling that exists between the stern planes and the rudder when the submarine is rolling and turning at the same time.

The eigenvalues and modal matrices for all models are contained in appendices B2 through B5.

3.4 Controllability and Observability

The LQG/LTR design methodology provides, under certain conditions, guarantees to the control system designer concerning gain and phase margins [8]. It should be noted that the guarantees are not absolute, and exist only in the sense that the LTR phase of the design process recovers a loop shape that approaches that of the Kalman Filter design, which does have the robustness guarantees.

The linear system must meet certain requirements, however,

before the validity of the results are assured. Specifically, the system must have no unstable modes which are not controllable, and no unstable modes which are not observable. If controllability and observability of the system can be established, then the weaker conditions of stabilizability and detectability are assured.

When a linear system can be diagonalized, as in the present case, determination of controllability and observability becomes a very simple matter. Additionally, even when a system does not meet the criteria for being controllable or observable, the weaker conditions of stabilizability and detectability are also readily determined.

Recall that the new state vector $\underline{z}$ (equation 3.5) defines a non-physical state space in which the natural modes of the system are decoupled. Thus a particular row of the $\underline{T}^{-1}\ \underline{B}$ matrix links the input vector $\underline{u}$ to a particular mode. Each element in the row then links a particular input (in our case a control surface) to a mode. Therefore, a zero entry in the (i,j) position of the $\underline{T}^{-1}\ \underline{B}$ matrix would indicate that the ith mode is not controllable by the jth input.

Similarly, the matrix $\underline{C}\ \underline{T}$ in equation 3.9 indicates whether a particular mode is visible in the output.

The 20 knot linear model has non-zero entries in the $\underline{T}^{-1}\ \underline{B}$ and $\underline{C}\ \underline{T}$ matrices (refer to appendix B4) and is therefore both controllable and observable, providing us with assurances that the LQG design method to be applied in the next chapter will have no difficulties.

3.5 Poles, Zeros, and Singular Values

The poles of the open loop plant are the eigenvalues of the $\underline{A}$ matrix presented in the previous section. As was indicated, the plant is open loop stable, having all left half plane poles.

Multivariable transmission zeros appearing in the right half plane may present difficulties in an LQG/LTR design [8]. Fortunately, the 20 knot linear model has no non-minimum phase zeros, nor do any of the other models (refer to Appendix B6).

The open loop poles for all four models are presented with the modal information in appendices B2 through B5, and the transmission zeros for each model in Appendix B6.

Singular value plots of the open loop models are shown in figure 3.2. It will be noticed that integral control is yet to be added, and that satisfactory command following

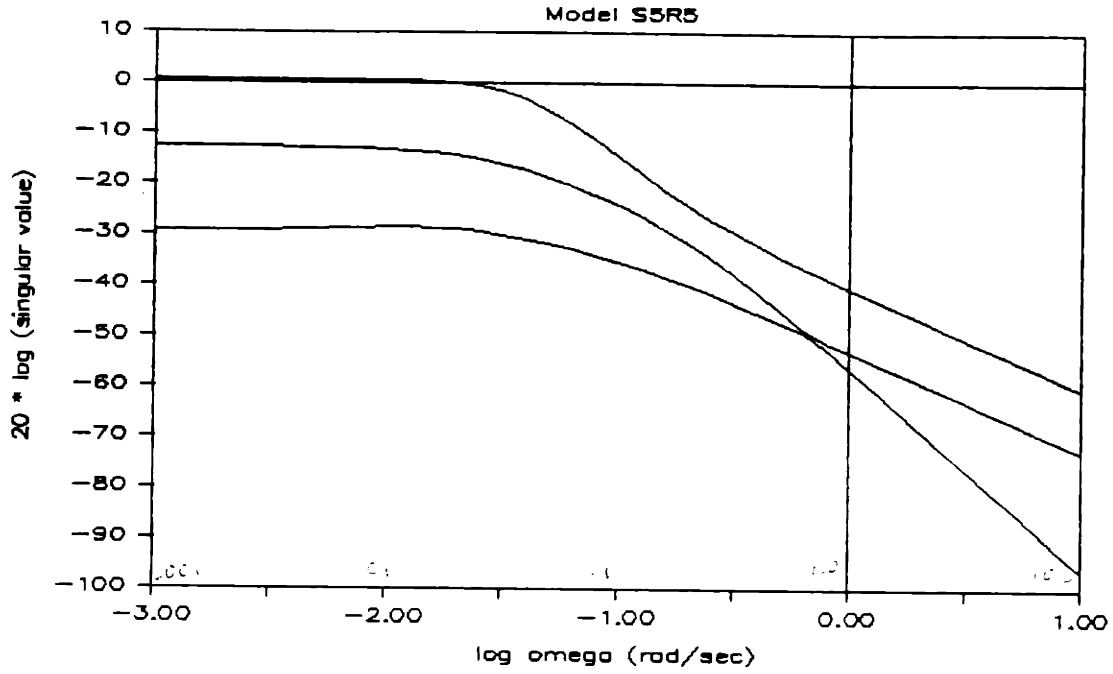

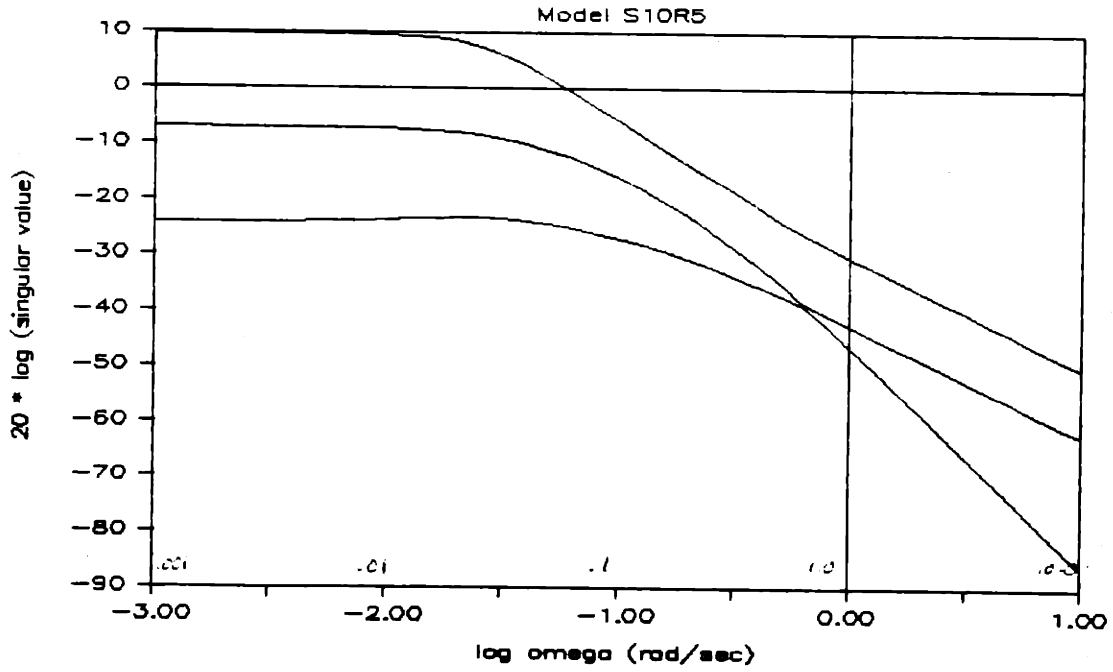

Figure 3.2(a) Open Loop Singular Values for the 5 and 10 Knot Linear Models

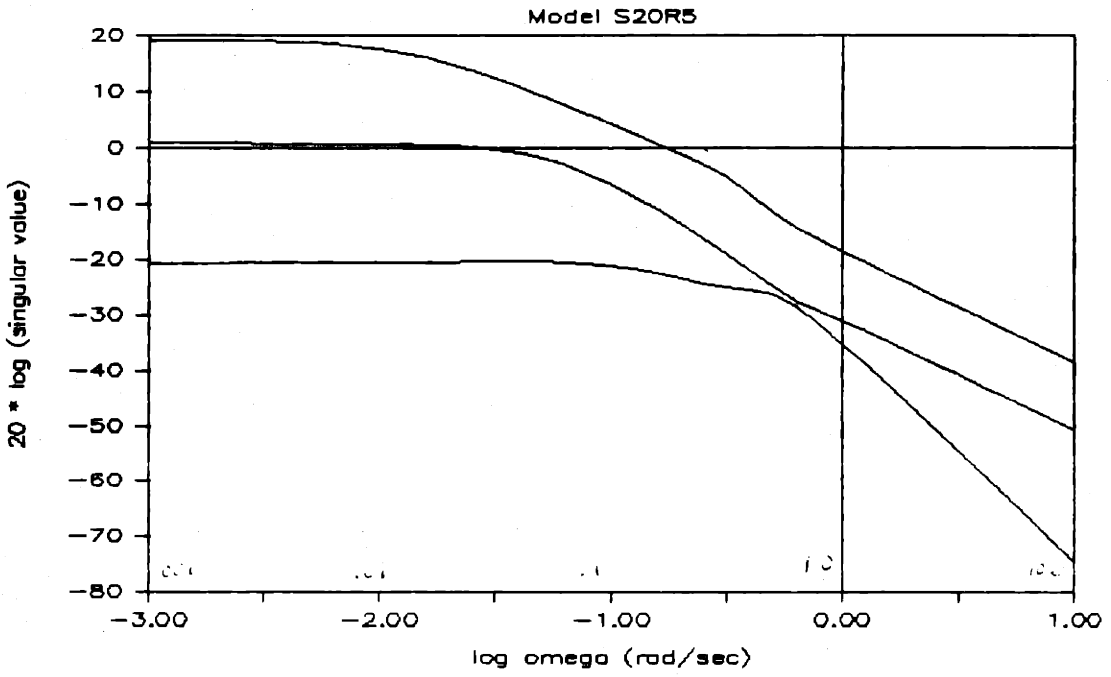

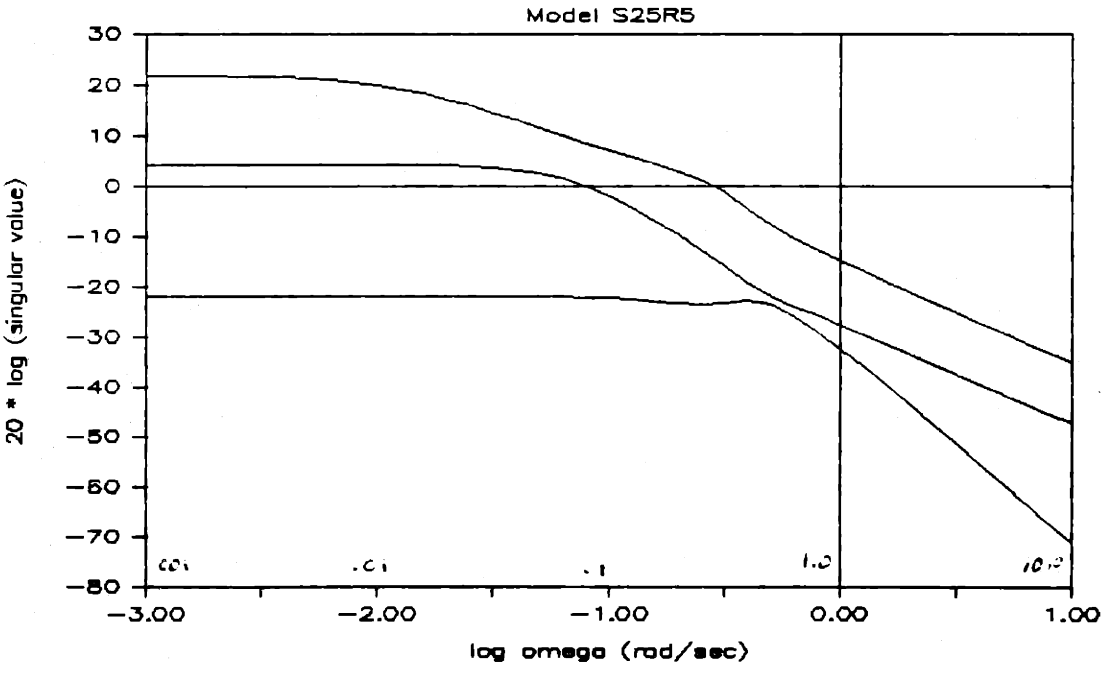

Figure 3.2(b) Open Loop Singular Values for the 20 and 25 Knot Linear Models

performance will indeed require the addition of integrators in the loop transfer function matrix. The increased effect of the control surfaces as speed increases can be seen by noting the increased dc gain for each sucessive model.

As a further indication of the effect of the control surfaces on the outputs, the dc gains of the open loop transfer function matrix for the 20 knot model are listed in table 3.1. By reading across for each output variable, the relative effect of the control surfaces can be determined. The results are as expected, with the sail planes having the most effect on w, the rudder on r, and the stern planes on θ. The gains for w are significantly higher than for the other two outputs, indicating a need for scaling, which is done in the next chapter.

Table 3.1. Input to Output Coupling

	ds	db	dr
w	11 db	19 db	16 db
r	-56 db	-49 db	-18 db
θ	19 db	-8.1 db	-3.0 db

3.6 A Further Example of the Usefulness of Modal Analysis

This chapter on analysis of the linear model would be incomplete without demonstrating the extreme usefulness of modal analysis in detecting inconsistencies in a model.

The initial linear model of the submarine on the CSDL computer contained an 11th state known as η. The purpose of this state was to include the propulsion plant dynamics and was defined as u(actual)/u(commanded).

Modal analysis of the model with η included resulted in eight modes essentially the same as those depicted in figure 3.1, and a ninth mode with all response concentrated in u and η. Furthermore, this ninth mode had a near-zero eigenvalue and zeros in the corresponding row of the $\underline{T}^{-1}\ \underline{B}$ matrix.

From the previous discussion of modal analysis, we can see that this situation is indicative of an uncontrollable and unstable mode, thus rendering the LQG design methodology invalid. If, however, the near-zero eigenvalue is taken to be the digital representation of a true zero eigenvalue, and the reasoning is applied that the actual submarine must be stable in forward velocity, then the facts imply an

inconsistency in the model.

To further refine this conclusion, both the linear and the nonlinear equations of motion were integrated over time, using the scaled magnitudes of the eigenvector corresponding to the unstable mode. The nonlinear plot decayed back to the local equilibrium point whereas the linear plot displayed an unforced response that remained at the perturbed values.

This last information clearly indicated a dependency among the states of the linear model, and the problem was then quickly traced to the treatment of the propulsion plant as a constant rpm source for the propeller. Thus the commanded u was being taken as constant for any run, and n represented a constant multiple of u, producing the dependent state.

Application of the chain rule to the system of 11 equations in 11 unknowns (used to calculate the $\underline{A}$ and $\underline{B}$ matrices) reduced the order of the system to 10, and eliminated the unstable state.

It is hoped that this example may serve to aid the reader in the methodical elimination of similar problems in a linear model.

3.7 Summary

This chapter has described the technique of modal analysis and its use in determining the eigenstructure and modal composition of the state space description of a linear model.

Application of this technique has enabled us to establish the prerequisites required to pursue the LQG/LTR design procedure to be covered in the next chapter. These are that the open loop linear model be detectable and stabilizable, and that the location of any non-minimum phase zeros be determined.

Finally, an example of the usefulness of modal analysis in tracking down an error in the linearization of the nonlinear model was presented.

Chapter 4

LINEAR MIMO DESIGNS

4.1 Introduction

This chapter presents the linear portion of the design process, utilizing the LQG/LTR design methodology as the MIMO design tool.

The design section begins with an overview of the complete step by step LQG/LTR procedure, as tailored to conform to the main focus of this thesis.

Augmentation of the submarine model dynamics with integrators will then be discussed, along with a comparison of open loop singular value plots for the augmented and unaugmented 20 knot model.

Finally, the methods used to ensure the identical behavior of the singular values of the open loop plant at both the high and low ends of the frequency spectrum will be presented.

Testing of the compensator begins with a comparison of the step responses of both the linear and nonlinear models, and concludes with simulations of evasive maneuvers and control surface saturation tests.

All parameters used in the design process and many of the design products for all four models are contained in the appendices.

4.2 The LQG/LTR Design Methodology

The multivariable LQG/LTR design methodology consists of a four step process [8].

Step one involves the development of a low frequency model of the nominal plant and determination of the uncertainties present in the model. It is assumed that the frequency range of interest for purposes of command following and disturbance rejection is at low frequencies.

The uncertainty in the nominal model, including sensor noise, unmodeled dynamics, and certain actuator dynamics, is similarly assumed to be concentrated at high frequencies. The determination of what constitutes high and low frequencies consists of fixing the maximum allowable crossover frequency for the nominal design.

In this thesis, the actual linear time invariant plant and the low frequency nominal model are taken to be identical, and no attempt is made to establish the modeling uncertainty. Therefore, step one is restricted to producing the linear model, as was discussed in chapter 2, and determination of the maximum allowable crossover frequency for each model, also discussed in chapter 2.

Step two of the design process establishes the low frequency performance requirements. The frequency domain block representation of the compensated plant is shown in figure 4.1.

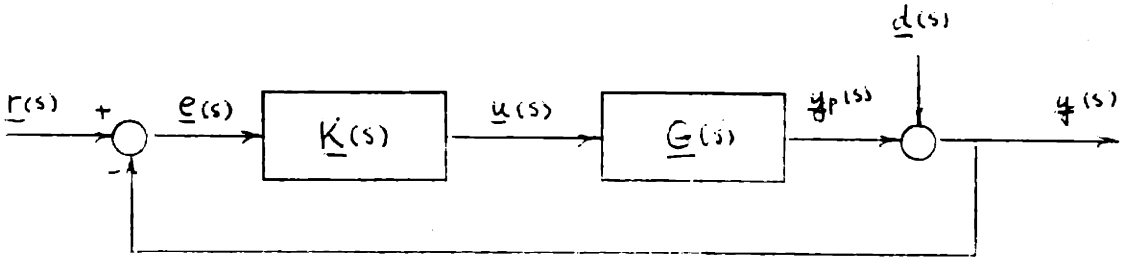

Figure 4.1. Block Diagram of a MIMO Compensated Plant

$\underline{r}(s)$ = reference signal or command input vector

$\underline{e}(s)$ = error signal vector

$\underline{u}(s)$ = control input vector to the plant

$\underline{y}_p(s)$ = output vector of the plant

$\underline{d}(s)$ = disturbance vector reflected at the plant output

$\underline{K}(s)$ = compensator transfer function matrix

$\underline{G}(s)$ = (augmented) plant transfer matrix

The transfer matrix $\underline{G}(s)$ is assumed to contain the nominal low frequency model of the submarine $\underline{G}_p(s)$ plus any augmented dynamics $\underline{G}_a(s)$ and is termed the nominal design model. Thus $\underline{G}(s) = \underline{G}_p(s)\ \underline{G}_a(s)$. To determine the requirements to be imposed on the compensator transfer matrix $\underline{K}(s)$, the overall transfer function of the closed loop system is calculated

$$\underline{y}(s)=[\underline{I}+\underline{G}(s)\underline{K}(s)]^{-1}\underline{d}(s)+[\underline{I}+\underline{G}(s)\underline{K}(s)]^{-1}\underline{G}(s)\underline{K}(s)\underline{r}(s). \quad (4.1)$$

Good command following requires that $\underline{y}(s) \approx \underline{r}(s)$ and good disturbance rejection will result if the contribution of $\underline{d}(s)$ can be kept small. Here, $s = j\omega$ is in the low end of the frequency spectrum.

Both of these requirements can be met if the minimum singular values of the matrix product $\underline{G}(s)\underline{K}(s)$ are large with respect to unity at frequencies below crossover.

Similarly, the response of the outputs to high frequency effects can be minimized if the maximum singular values of $\underline{G}(s)\underline{K}(s)$ are small compared with unity at frequencies above crossover.

The combined effect of steps 1 and 2 is to place barriers on the singular value plot for $\underline{G}(j\omega)\underline{K}(j\omega)$ as indicated in figure 4.2. The high frequency barrier places a robustness requirement on the compensator and the low frequency barrier

is a result of the command following and disturbance rejection requirements.

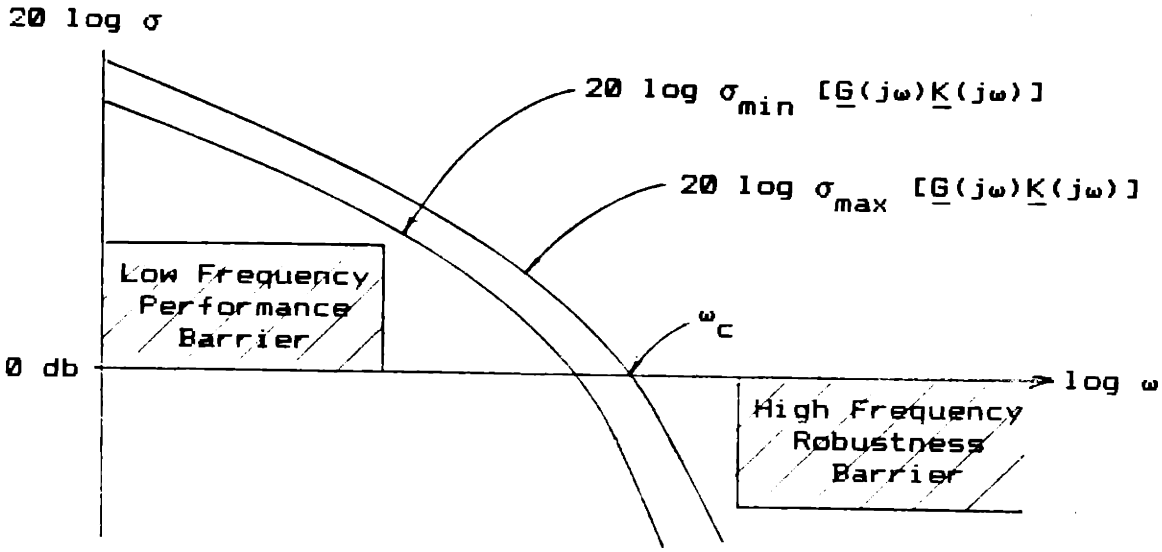

Figure 4.2 Desired Singular Value Relationships

The remainder of the design process is concerned with determining the transfer matrix $\underline{K}(s)$ so that the singular values of the open loop transfer matrix $\underline{G}(j\omega)\underline{K}(j\omega)$ will have the shapes shown in figure 4.2. This process is known as loop shaping and is at the heart of the LQG/LTR design procedure.

Initially, the Kalman Filter methodology is applied to the state space description of the nominal design model (nominal model plus augmentation) to produce a transfer matrix $\underline{G}_{KF}(s)$ that has the desired loop shapes. The Kalman Filter theory is applied in a very specific manner and should not be

confused with optimal state estimation applications.

To solve the Kalman Filter problem, the nominal design model state space description,

$$\dot{\underline{x}}(t) = \underline{A}\,\underline{x}(t) + \underline{B}\,\underline{u}(t) \qquad (4.2)$$

$$\underline{y}(t) = \underline{C}\,\underline{x}(t), \qquad (4.3)$$

is reformulated to produce the somewhat modified dynamics

$$\dot{\underline{x}}(t) = \underline{A}\,\underline{x}(t) + \underline{L}\,\underline{\xi}(t) \qquad (4.4)$$

$$\underline{y}(t) = \underline{C}\,\underline{x}(t) + \underline{\theta}(t). \qquad (4.5)$$

where $\underline{\xi}(t)$ represents the process white noise,

and $\underline{\theta}(t)$ represents the measurement white noise.

The covariance of these two Gaussian signals is

$$\mathrm{cov}[\underline{\xi}(t);\underline{\xi}(\tau)] = \underline{I}\delta(t-\tau), \qquad (4.6)$$

and

$$\mathrm{cov}[\underline{\theta}(t);\underline{\theta}(\tau)] = \mu\underline{I}\delta(t-\tau) \quad (\mu > 0). \qquad (4.7)$$

The design parameters μ and $\underline{L}$ are then used to produce the desired loop shapes of the transfer matrix $\underline{G}_{KF}(s)$ where

$$\underline{G}_{KF}(s) = \underline{C}(s\underline{I}-\underline{A})^{-1}\underline{H}, \quad \text{and} \qquad (4.8)$$

$$\underline{H} = (1/\sqrt{\mu})\ \underline{\Sigma}\ \underline{C}'. \qquad (4.9)$$

The matrix $\underline{\Sigma}$ is the solution to the Filter Algebraic Riccati Equation (FARE)

$$\underline{0} = \underline{A}\,\underline{\Sigma} + \underline{\Sigma}\,\underline{A}' + \underline{L}\,\underline{L}' - (1/\sqrt{\mu})\ \underline{\Sigma}\,\underline{C}'\underline{C}\,\underline{\Sigma}. \qquad (4.10)$$

Fortunately, the transfer matrix $\underline{G}_{KF}(s)$ can be approximated quite readily, providing that the parameter $\mu << 1$, and the FARE need not be evaluated for each choice of μ and $\underline{L}$. It

can be shown [8] that

$$\sigma_i[\underline{G}_{KF}(j\omega)] \approx (1/\sqrt{\mu})\ \sigma_i[\underline{G}_{FOL}(j\omega)], \quad \text{for } \mu << 1, \tag{4.11}$$

$$\text{where } \underline{G}_{FOL}(j\omega) = \underline{C}(s\underline{I}-\underline{A})^{-1}\underline{L}. \tag{4.12}$$

Thus the $\underline{L}$ matrix can be chosen in such a way as to produce the desired loop shape and μ used to adjust the singular values up and down to meet the required crossover frequency criteria.

Providing that $[\underline{A},\underline{L}]$ is stabilizable, and that $[\underline{A},\underline{C}]$ is detectable, any choice of μ and $\underline{L}$ will produce the following guaranteed properties for $\underline{G}_{KF}(s)$:

1. Closed loop stable

2. Robustness:

$$\sigma_i[\underline{I}+\underline{G}_{KF}(j\omega)] \geq 1 \tag{4.13}$$

$$\sigma_i[\underline{I}+\underline{G}_{KF}^{-1}(j\omega)] \geq 1/2 \tag{4.14}$$

3. Infinite upward gain margin

4. 6 db downward gain margin

5. Phase margins of ± 60°

The final step in the LQG/LTR design procedure involves the "recovery" of the loop shapes of $\underline{G}_{KF}(s)$ by the compensated plant transfer matrix $\underline{G}(s)\underline{K}(s)$. This is accomplished by solving the Control Algebraic Riccati Equation (CARE)

$$\underline{0} = -\underline{K}\,\underline{A} - \underline{A}'\underline{K} - q\underline{C}'\underline{C} + \underline{K}\,\underline{B}\,\underline{B}'\underline{K}\ ;\quad q > 0 \qquad (4.15)$$

using the design parameter q, and defining the control gain matrix $\underline{G}$ by

$$\underline{G} = \underline{B}'\underline{K}. \qquad (4.16)$$

For the solution to the CARE to be valid, we must have $[\underline{A},\underline{B}]$ stabilizable and $[\underline{A},\underline{C}]$ detectable. Furthermore, the nominal design plant must not have any non-minimum phase zeros.

The control gain matrix $\underline{G}$ and the filter gain matrix $\underline{H}$ (4.9), when calculated using the above procedures, define a special type of compensator $\underline{K}_{MBC}(s)$ known as a Model Based Compensator (figure 4.3). This type of compensator differs from other LQG/LTR compensators only in the manner in which the control and filter gain matrices are calculated.

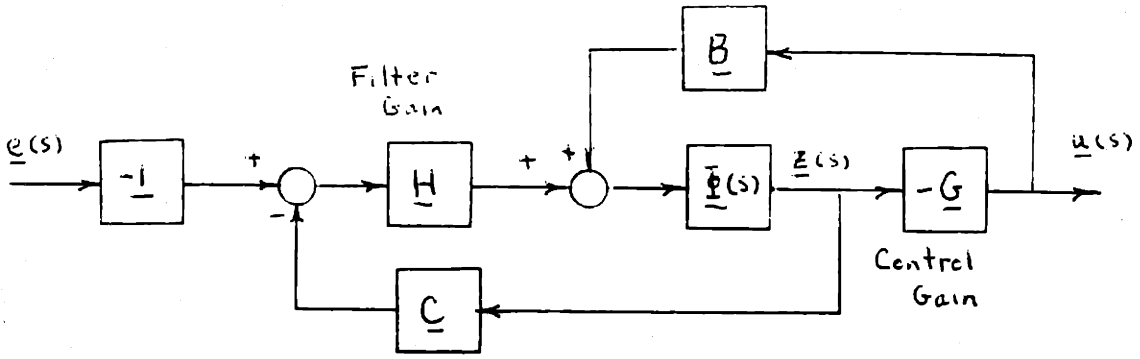

Figure 4.3. The Model Based Compensator

The state space description of the (model based) compensator is then given by

$$\dot{\underline{z}}(t) = (\underline{A}-\underline{B}\ \underline{G}-\underline{H}\ \underline{C})\ \underline{z}(t) - \underline{H}\ \underline{e}(t) \qquad (4.17)$$

$$\underline{u}(t) = -\underline{G}\ \underline{z}(t), \qquad (4.18)$$

It can be shown that the singular values of $\underline{G}(s)\underline{K}_{MBC}(s)$ at frequencies below crossover converge to those of $\underline{G}_{KF}(s)$ as the design parameter $q \to \infty$, providing that the plant is minimum phase [8]. At frequencies above crossover, an extra pole of roll-off is produced by the recovery phase, further enhancing the high frequency robustness. Thus the loop shape of $\underline{G}_{KF}(s)$ is recovered and the resulting controller will have the desired performance characteristics described earlier.

4.3 Augmented Dynamics

The dynamics of the submarine model are augmented by placing integrators in each of the three control channels. This is accomplished by defining an augmentation plant $\underline{G}_a(s)$ whose state space description is simply

$$\underline{A}_a = \underline{0},\ \underline{B}_a = \underline{C}_a = \underline{I},$$

with all matrices being 3 x 3.

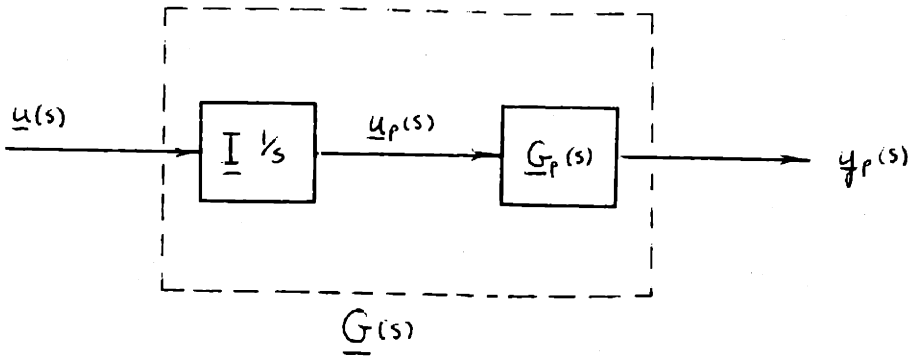

Figure 4.4. Inclusion of the Augmented Dynamics

Then the nominal low frequency model and the augmentation dynamics are combined by performing a state space multiplication, forming $\underline{G}(s)$ as shown in figure 4.4. Note that the physical input to the plant is now labeled $\underline{u}_p(s)$ to distinguish it from the output of the compensator $\underline{u}(s)$. Although the augmentation dynamics $\underline{G}_a(s)$ will eventually be lumped with the compensator, they are kept separate until the LQG/LTR design procedure is complete. Figure 4.5 shows a comparison of the singular values of the unaugmented and augmented 20 knot model. As can be seen, adding the integrators at the plant input produces a 60 db gain increase at .001 rad/sec.

2.4 Kalman Filter Design

In the overview of the LQG/LTR design methodology, it was

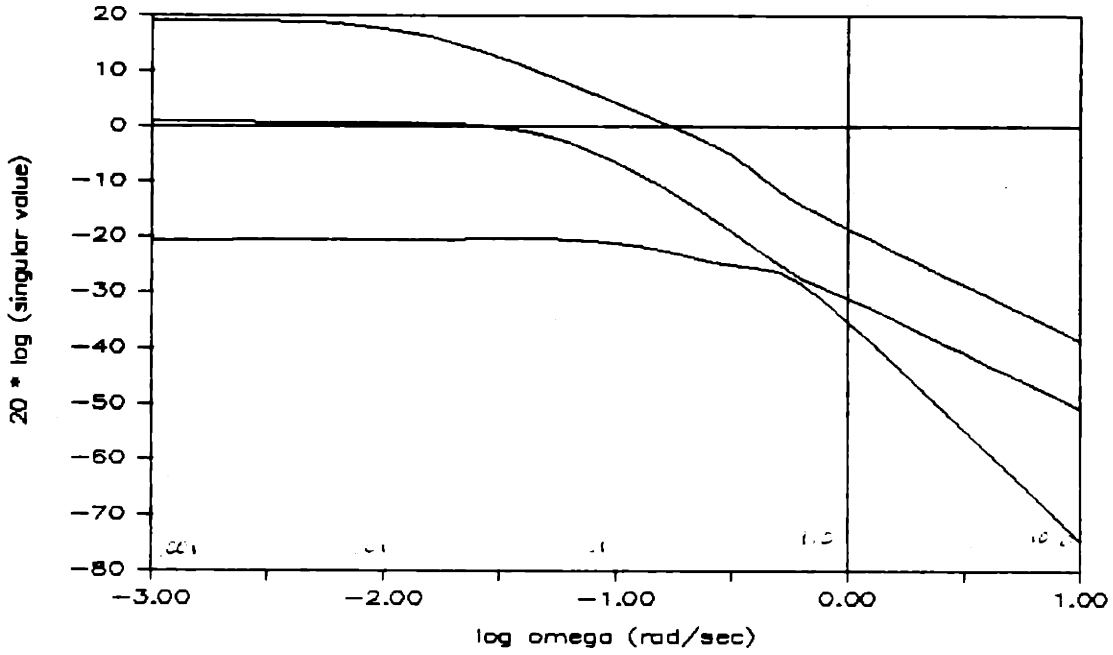

(a) Unaugmented plant

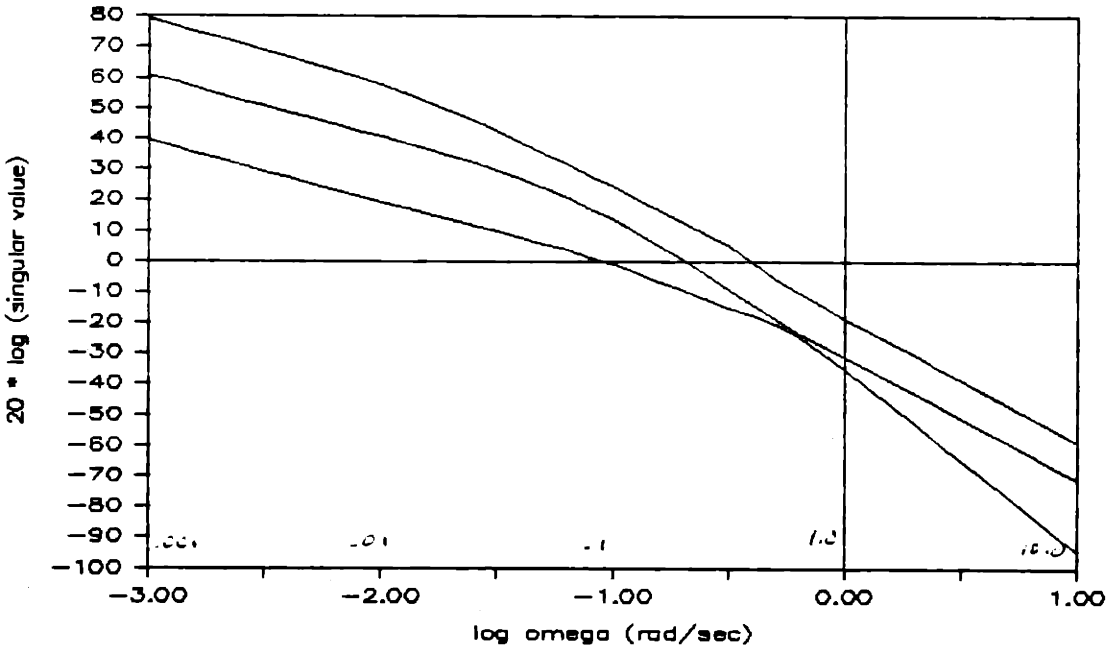

(b) Plant augmented with integral control

Figure 4.5. Singular Values for the Unaugmented and Augmented 20 Knot Model

stated that the singular values of the Kalman Filter transfer function matrix are closely approximated by the singular values of $(1/\sqrt{\mu})\underline{G}_{FOL}(j\omega)$. Furthermore, $\underline{G}_{FOL}(j\omega)$ can be easily calculated for each choice of $\underline{L}$, simplifying the iterative nature of the design process.

To satisfy the loop shaping requirements represented by the low and high frequency barriers shown in figure 4.2, it is helpful if the maximum and minimum singular values of $\underline{G}_{KF}(j\omega)$ are identical at low and high frequencies. Therefore, the choice of $\underline{L}$ is based on this philosophy.

Recall that $\underline{G}(s) = \underline{G}_a(s)\underline{G}_p(s)$ (section 4.3) and define a state space representation for $\underline{G}(s)$ by the relation

$$\underline{G}(s) = \underline{C}(s\underline{I}-\underline{A})^{-1}\underline{B}. \qquad (4.19)$$

Then the matrices $\underline{A}$ and $\underline{C}$ can be partitioned into

$$\underline{A} = \begin{bmatrix} \underline{0} & \underline{0} \\ \underline{B}_p & \underline{A}_p \end{bmatrix} \qquad \underline{C} = [\ \underline{0} \quad \underline{C}_p\ ], \qquad (4.20)$$

and similarly for $s\underline{I}-\underline{A}$ and its inverse

$$s\underline{I}-\underline{A} = \begin{bmatrix} s\underline{I} & \underline{0} \\ -\underline{B}_p & s\underline{I}-\underline{A}_p \end{bmatrix} \quad (s\underline{I}-\underline{A})^{-1} = \begin{bmatrix} \underline{I}/s & \underline{0} \\ (s\underline{I}-\underline{A}_p)^{-1}\underline{B}_p/s & (s\underline{I}-\underline{A})^{-1} \end{bmatrix} \qquad (4.21)$$

At low frequencies, $s\underline{I}-\underline{A}_p \approx -\underline{A}_p$ and $(s\underline{I}-\underline{A}_p)^{-1} \approx -\underline{A}_p^{-1}$. Recall that $\underline{A}_p^{-1}$ exists since $\underline{A}_p$ has distinct and non-zero eigenvalues. We now partition the $\underline{L}$ matrix into $\underline{L}_1$ and $\underline{L}_2$

and form $\underline{G}_{FOL}(s)$ for low frequencies

$$\underline{G}_{FOL}(s) = \underline{C}(s\underline{I}-\underline{A})^{-1}\underline{L} \approx [\underline{0} \quad \underline{C}] \begin{bmatrix} \underline{I}/s & \underline{0} \\ -\underline{A}_p^{-1}\underline{B}_p/s & -\underline{A}_p^{-1} \end{bmatrix} \begin{bmatrix} \underline{L}_1 \\ \underline{L}_2 \end{bmatrix} \tag{4.22}$$

$$\approx -\underline{C}_p\underline{A}_p^{-1}\underline{B}_p\underline{L}_1/s - \underline{C}_p\underline{A}_p^{-1}\underline{L}_2.$$

From this, it is seen that we can match the singular values at low frequency by choosing

$$\underline{L}_1 = -(\underline{C}_p\underline{A}_p^{-1}\underline{B}_p)^{-1}, \tag{4.23}$$

if it exists, and leaving $\underline{L}_2$ unspecified. Then, as $\omega \to 0$,

$$\underline{G}_{FOL}(j\omega) \approx \underline{I}/j\omega + \underline{M}, \tag{4.24}$$

where $\underline{M}$ is a 3x3 constant matrix. Although $\underline{M}$ will have an impact at frequencies approaching crossover, the first term will dominate for ω small enough.

At high frequencies, $s\underline{I}-\underline{A}_p \approx s\underline{I}$ and $(s\underline{I}-\underline{A}_p)^{-1} \approx I/s$. Thus, at high frequencies, we have

$$\underline{G}_{FOL}(s) = \begin{bmatrix} \underline{0} & \underline{C}_p \end{bmatrix} \begin{bmatrix} \underline{I}/s & \underline{0} \\ \underline{B}_p/s^2 & \underline{I}/s \end{bmatrix} \begin{bmatrix} \underline{L}_1 \\ \underline{L}_2 \end{bmatrix} \tag{4.25}$$

$$= \underline{C}_p\underline{B}_p\underline{L}_1/s^2 + \underline{C}_p\underline{L}_2/s.$$

Since $1/s > 1/s^2$ as $s \to \infty$, then the second term will dominate the maximum singular value at high frequencies. Thus we can match the singular values at high frequency by choosing

$$\underline{L}_2 = \underline{C}_p'(\underline{C}_p\underline{C}_p')^{-1} \tag{4.26}$$

so that, as $\omega \to \infty$,

$$\underline{G}_{FOL}(j\omega) = -\underline{C}_p\underline{B}_p\underline{L}_1/\omega^2 + \underline{I}/\omega. \tag{4.27}$$

The required inverses can be shown to exist for the models used via numerical means. Additionally, whenever $\underline{C}_p$ is such that distinct states are extracted from the state vector, the matrix $\underline{C}_p\underline{C}_p'$ is always diagonal and hence invertible.

The above method of constructing the $\underline{L}$ matrix provides the designer with a guarantee of identical behavior of the singular values of the Kalman Filter transfer matrix for low and high frequencies. Unfortunately, the shape of the singular values at frequencies near crossover is not controlled, and significant differences may exist between the maximum and minimum singular values in the crossover region. Figure 4.6 is a plot of the singular values of $\underline{G}_{FOL}(s)$ for the $\underline{L}$ matrix constructed as in equations 4.23 and 4.26. Although the singular values match at high and low frequencies, a large separation exists between the maximum and minimum crossover frequencies.

To control the separation of the singular values at frequencies near crossover, it is necessary to investigate the magnitudes of the elements of the matrix transfer

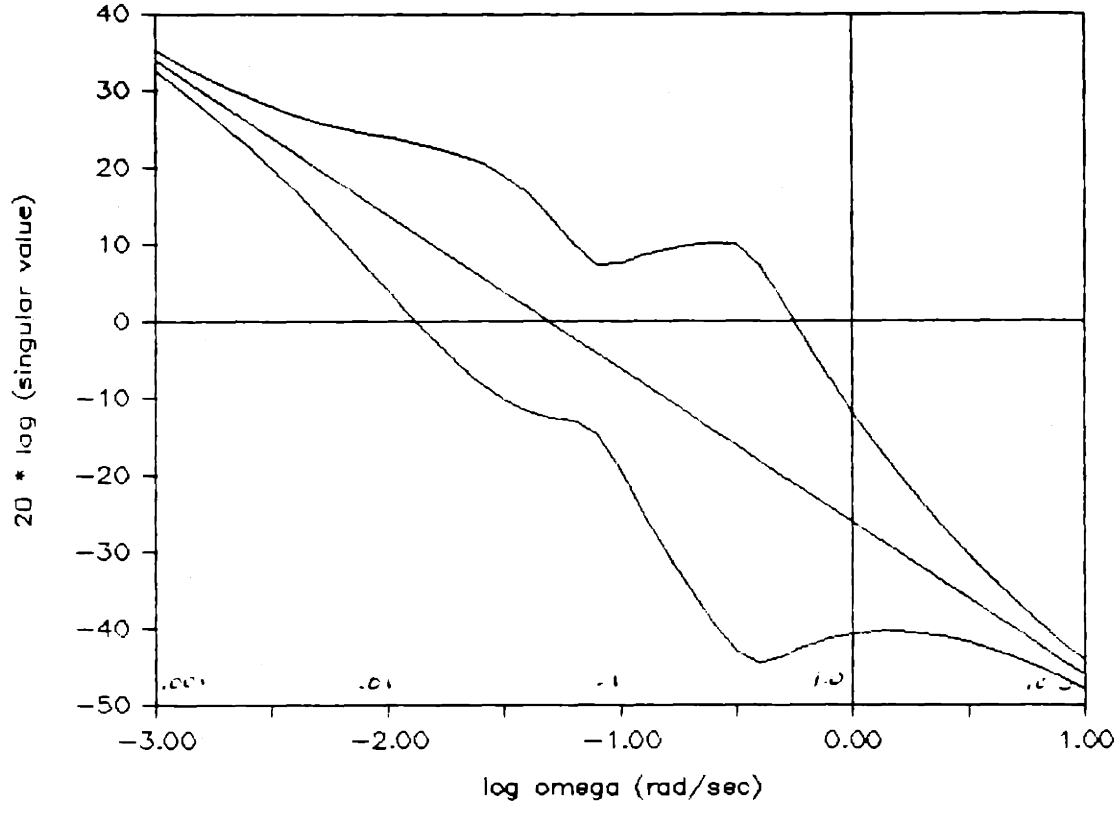

Figure 4.6. Singular Values for G(fol) for the 20 Knot Model Before Scaling

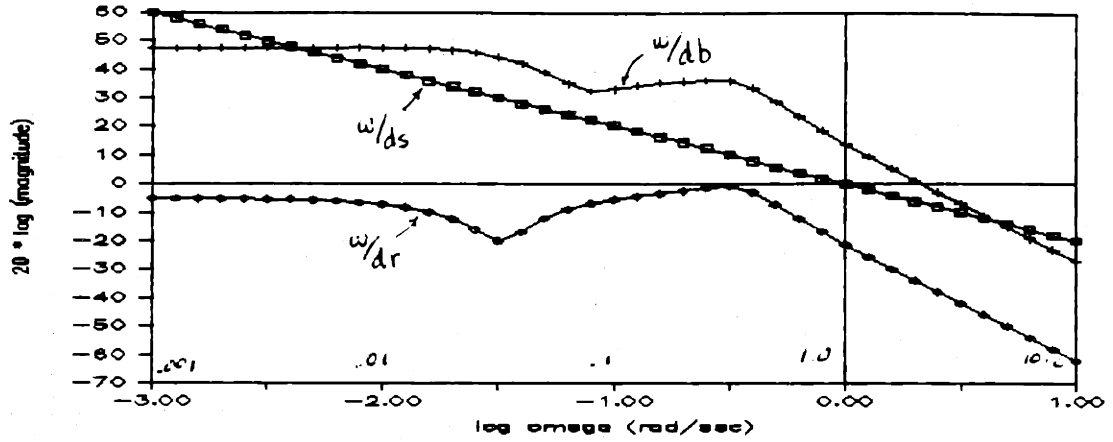

(a) w as a function of ds, db, and dr

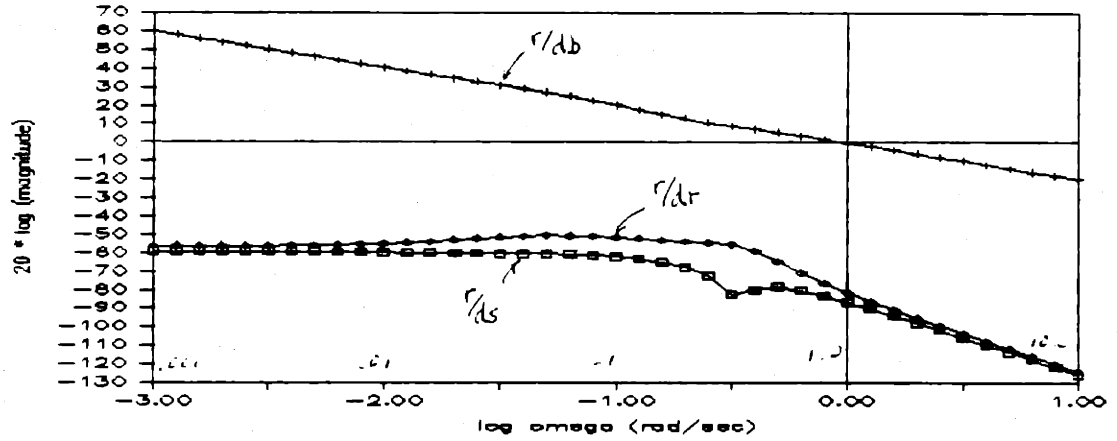

(b) r as a function of ds, db, and dr

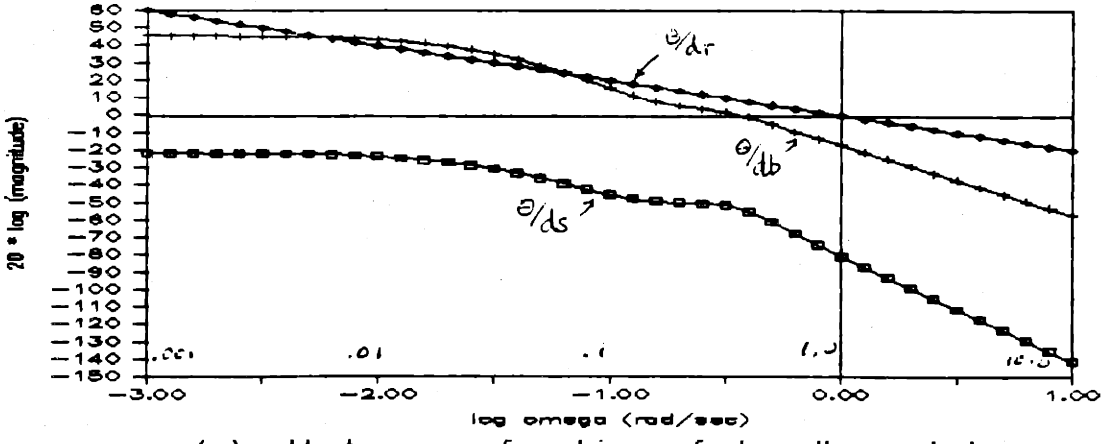

(c) theta as a function of ds, db, and dr

Figure 4.7. Magnitudes of the Elements of G(fol) for the 20 Knot Model

function $\underline{G}_{FOL}(j\omega)$ over a frequency range including the crossover frequency, and apply scaling to the $\underline{C}_p$ matrix to achieve a tight crossover pattern. The magnitudes of the elements of the matrix transfer function are plotted in figure 4.7 for each input to output function. Each of the plots represents the coupling from the three controls to a single output. The curves are fairly smooth except for figure 4.7(a), which shows the coupling from the controls ds, db, and dr to the output w. The desired crossover is at $\omega = 0.100$, or $\log \omega = -1.00$, and figure 4.7(a) displays both an increase in coupling from dr and a decrease in coupling from db in this area. Referring back to table 3.1, it was observed that the dc gains for w were significantly higher than for r and θ. Both of these facts tend to indicate that the $\underline{C}_p$ matrix entry corresponding to w should be scaled down. A comparison of the magnitudes of the transfer matrices in this manner for all four submarine models resulted in the following choice for the $\underline{C}_p$ matrix.

$$\underline{C}_p = \begin{bmatrix} 0 & 0 & .1 & 0 & 0 & 0 & 0 & 0 \\ 0 & 0 & 0 & 0 & 0 & 1 & 0 & 0 \\ 0 & 0 & 0 & 0 & 0 & 0 & 0 & 1 \end{bmatrix} \qquad (4.28)$$

The vast improvement in the behavior of the singular values near crossover can be seen in figure 4.10(a), a plot of the singular values of $\underline{G}_{FOL}(s)$ for the 20 knot model using the new $\underline{C}_p$ matrix.

A more detailed discussion of output variable scaling for the purpose of shaping the singular values at frequencies near crossover can be found in [14] and [15].

Once the $\underline{L}$ matrix has been determined, the choice of the parameter μ becomes a simple matter of moving the singular value plots up or down until the desired crossover frequency is obtained. Refer to table 4.1 for a listing of the particular values used for μ for each of the models during the Kalman Filter design process. The Kalman Filter gain matrices are contained in appendix C1.

Table 4.1. Values used for μ

Model	μ
S5R5	.04
S10R5	.05
S20R5	.05
S25R5	.04

4.5 Completing the LQG/LTR Design

As was indicated in the overview of the LQG/LTR design procedure, once the Kalman Filter design is complete, the remainder of the design process is quite straightforward, requiring only a choice of the parameter q. Recall that our

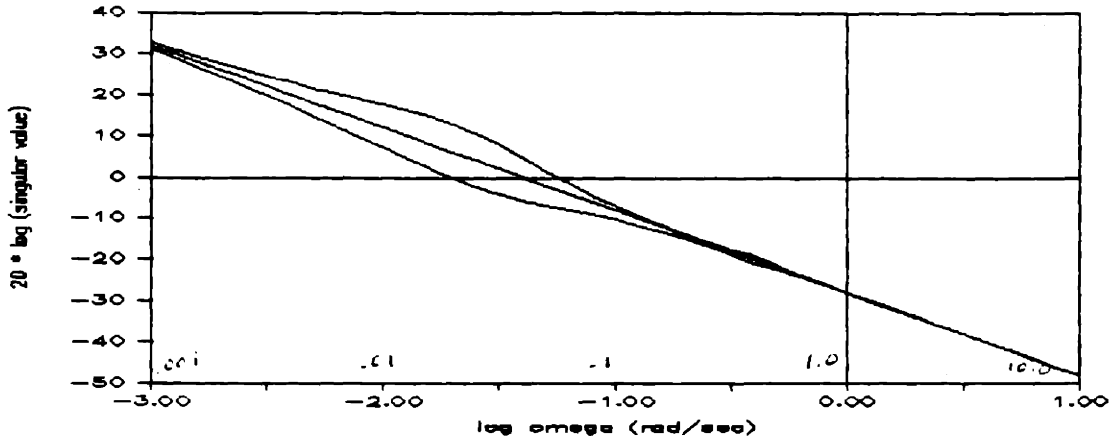

(a) Kalman filter open loop G(fol)

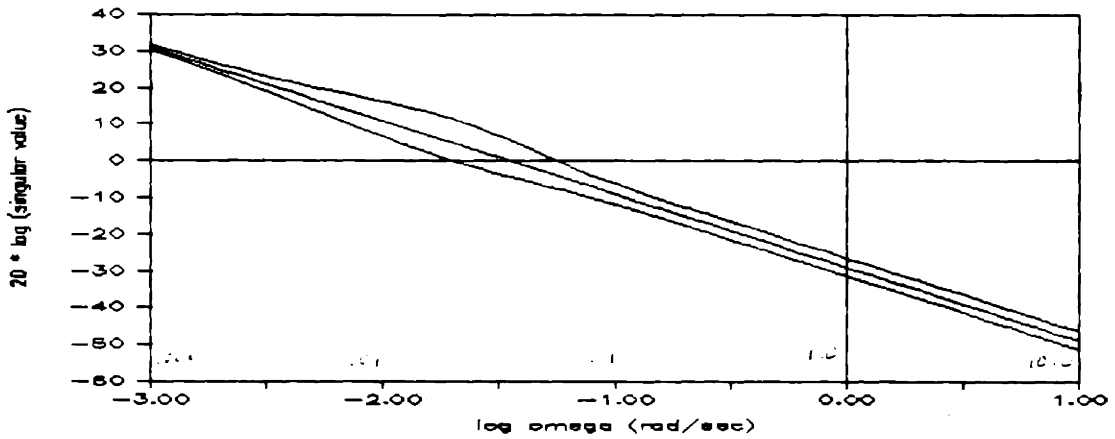

(b) Kalman filter open loop G(kf)

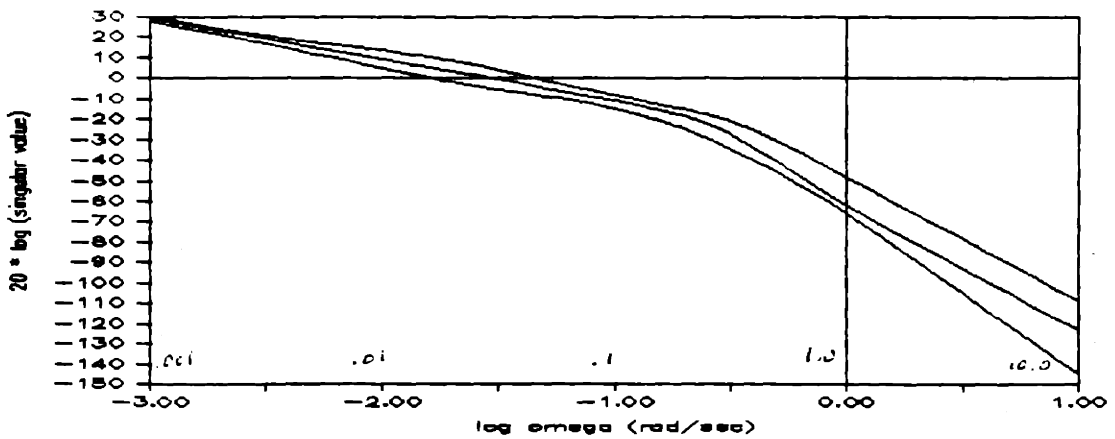

(c) Recovered open loop transfer function

Figure 4.8. Design Summary for the 5 Knot Model

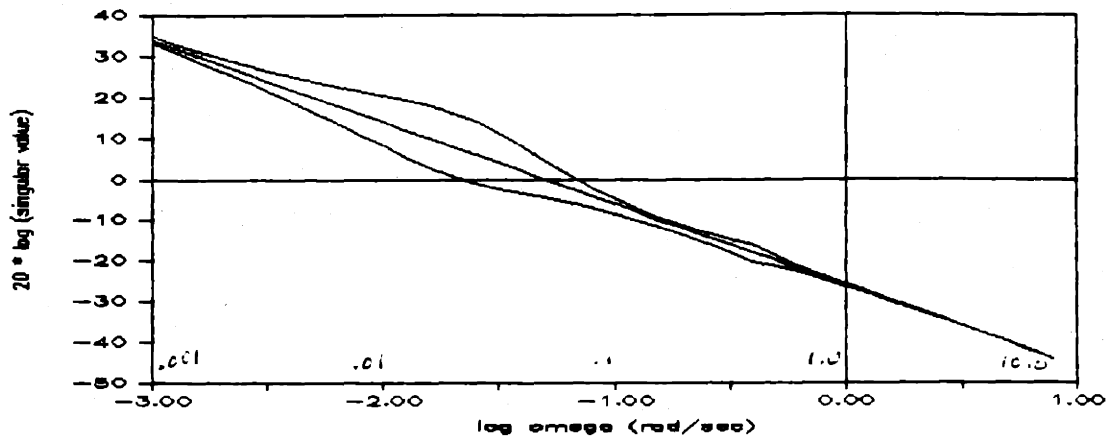

(a) Kalman filter open loop G(fol)

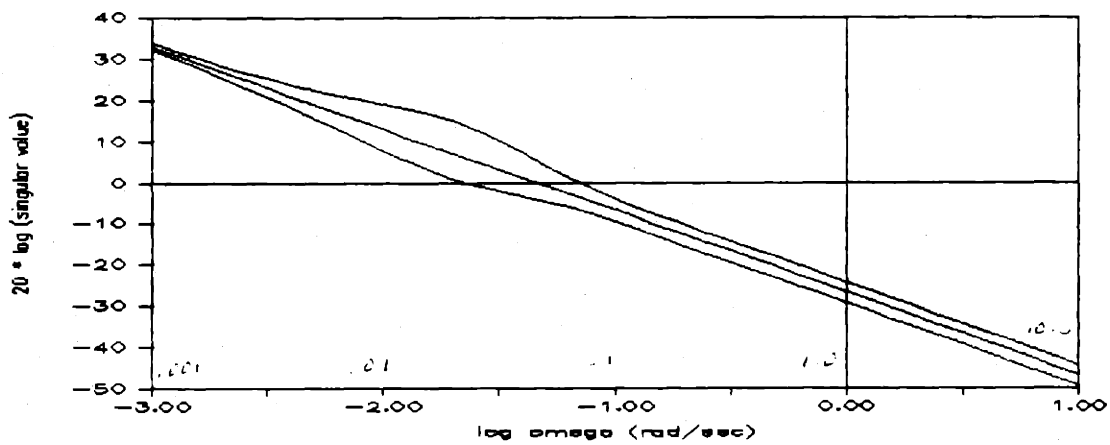

(b) Kalman filter open loop G(kf)

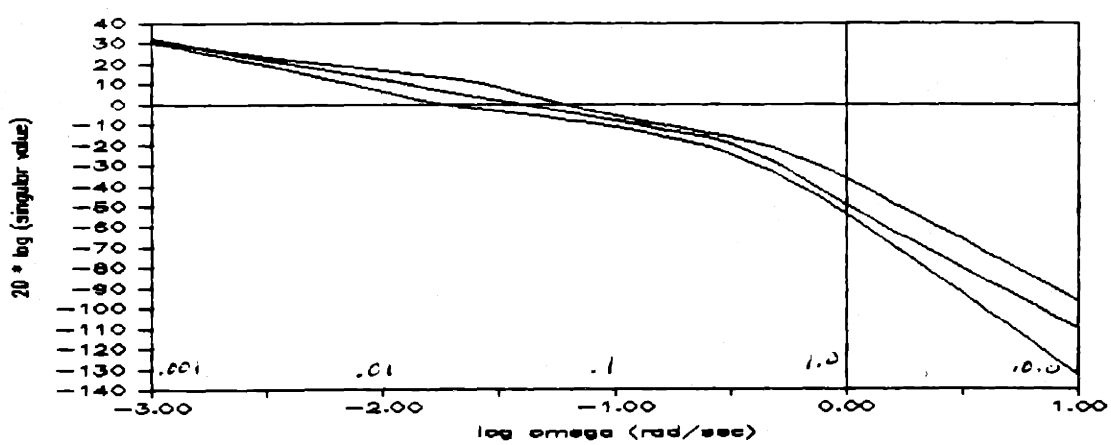

(c) Recovered open loop transfer function

Figure 4.9. Design Summary for the 10 Knot Model

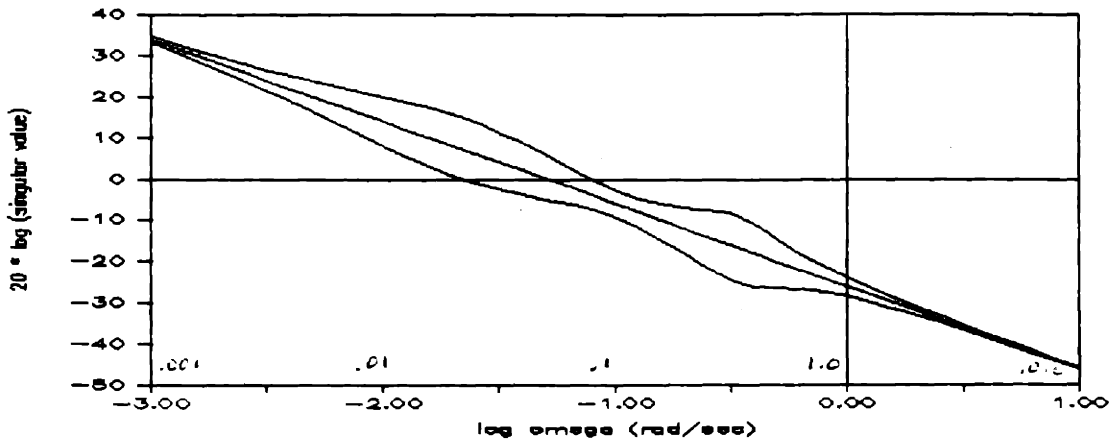

(a) Kalman filter open loop G(fol)

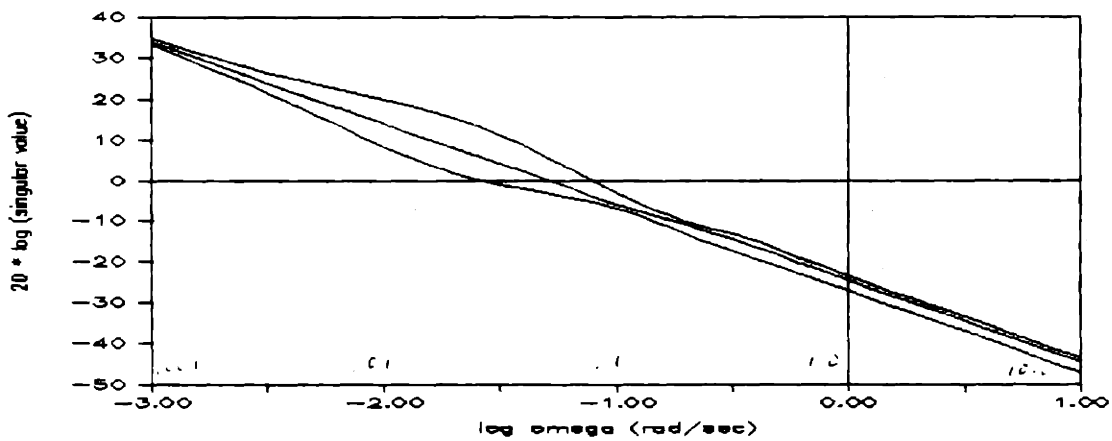

(b) Kalman filter open loop G(kf)

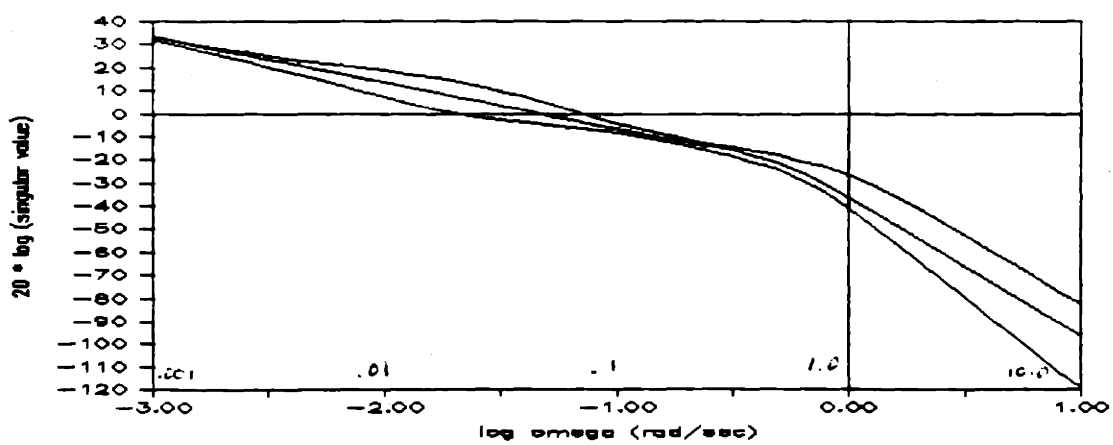

(c) Recovered open loop transfer function

Figure 4.10. Design Summary for the 20 Knot Model

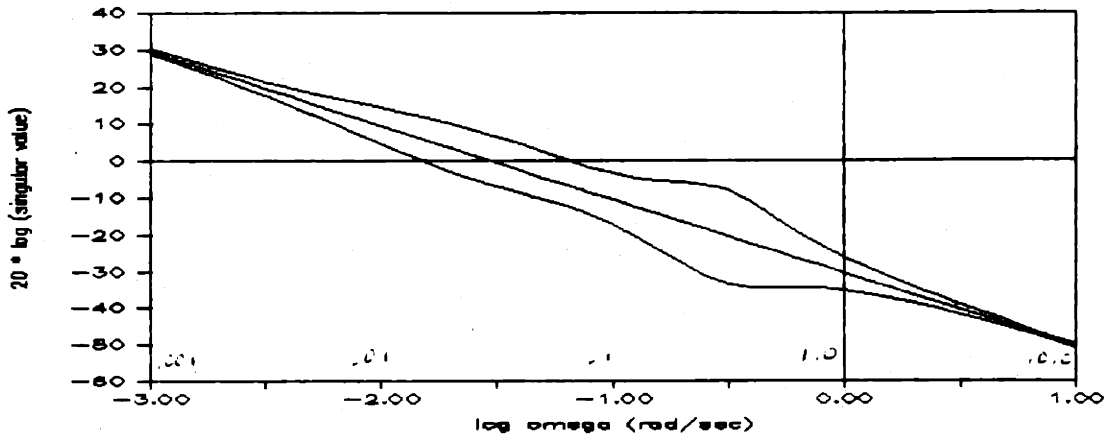

(a) Kalman filter open loop G(fol)

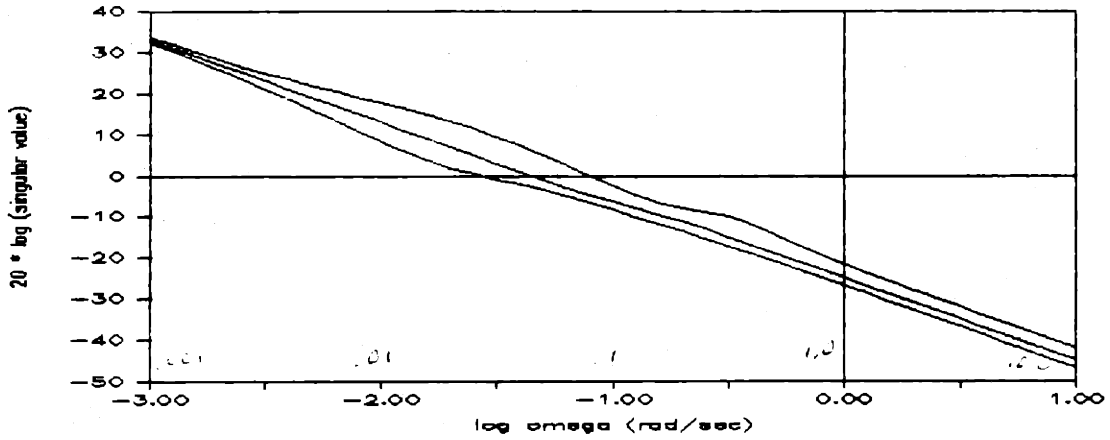

(b) Kalman filter open loop G(kf)

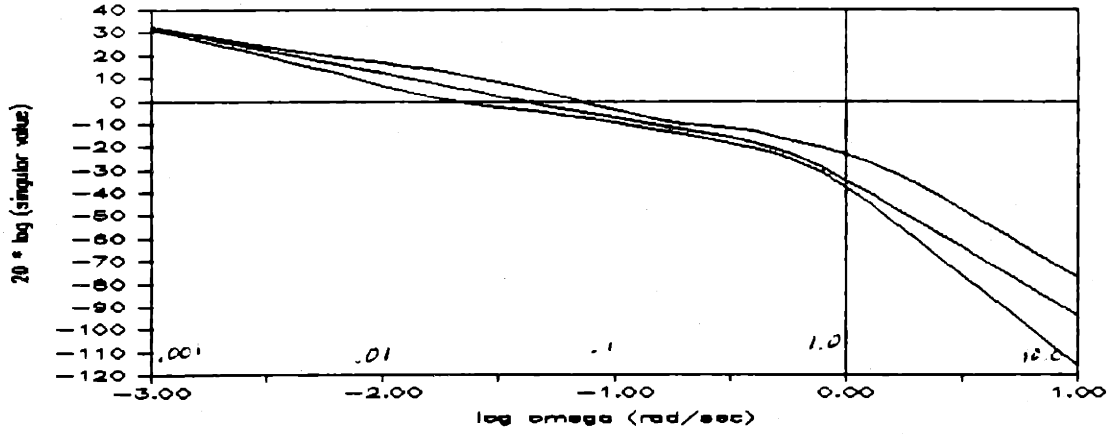

(c) Recovered open loop transfer function

Figure 4.11. Design Summary for the 25 Knot Model

submarine models did not have any low frequency transmission zeros. A value of q = 100.0 was used for all models, producing the control gain matrices in appendix C2.

The complete design sequence is summarized in figures 4.8 through 4.11, the singular value plots of $\underline{G}_{FOL}(s)$, $\underline{G}_{KF}(s)$, and $\underline{G}(s)\underline{K}(s)$ for each of the four models. The maximum and minimum crossover frequencies for the final loop transfer function matrix $[\underline{G}(s)\underline{K}(s)]$ are summarized in table 4.2.

Table 4.2. Final Crossover Frequencies for $\underline{G}(s)\underline{K}(s)$

Model	ω_{min}	ω_{max}
S5R5	.016	.050
S10R5	.020	.068
S20R5	.029	.078
S25R5	.024	.079

4.6 The Closed Loop System

Prior to beginning the testing phase of the compensator design, properties of the closed loop plant will be investigated.

The state space representation of the closed loop system can be written down by inspecting figures 4.1 and 4.3. Let

$\underline{x}(t)$ represent the state of the nominal design model and $\underline{z}(t)$ the state of the compensator. Then the closed loop system can be described by

$$\begin{bmatrix} \dot{\underline{x}}(t) \\ \dot{\underline{z}}(t) \end{bmatrix} = \begin{bmatrix} \underline{A} & -\underline{B}\,\underline{G} \\ \underline{H}\,\underline{C} & \underline{A}-\underline{B}\,\underline{G}-\underline{H}\,\underline{C} \end{bmatrix} \begin{bmatrix} \underline{x}(t) \\ \underline{z}(t) \end{bmatrix} + \begin{bmatrix} \underline{0} \\ -\underline{H}\,\underline{C} \end{bmatrix} \underline{r}(t)$$

$$\underline{y}(t) = \begin{bmatrix} \underline{C} & \underline{0} \end{bmatrix} \begin{bmatrix} \underline{x}(t) \\ \underline{z}(t) \end{bmatrix}. \qquad (4.29)$$

The poles and zeros for the closed loop system are contained in appendix C3. All poles are in the left-half plane so that the system is in fact closed loop stable.

By setting $\underline{d}(s)$ equal to zero in equation 4.1, it is seen that the singular values of the closed loop plant should be very near unity (zero db on a log plot) from dc up to the crossover frequency, and then fall off above crossover. This is depicted in figures 4.12 and 4.13, the closed loop singular value plots for all four models.

4.7 Testing of the Compensated Submarine Model

Testing of the LQG/LTR model based compensator design was accomplished by providing the computer program with a data file containing time sequenced command inputs and then integrating either the linear or nonlinear equations of

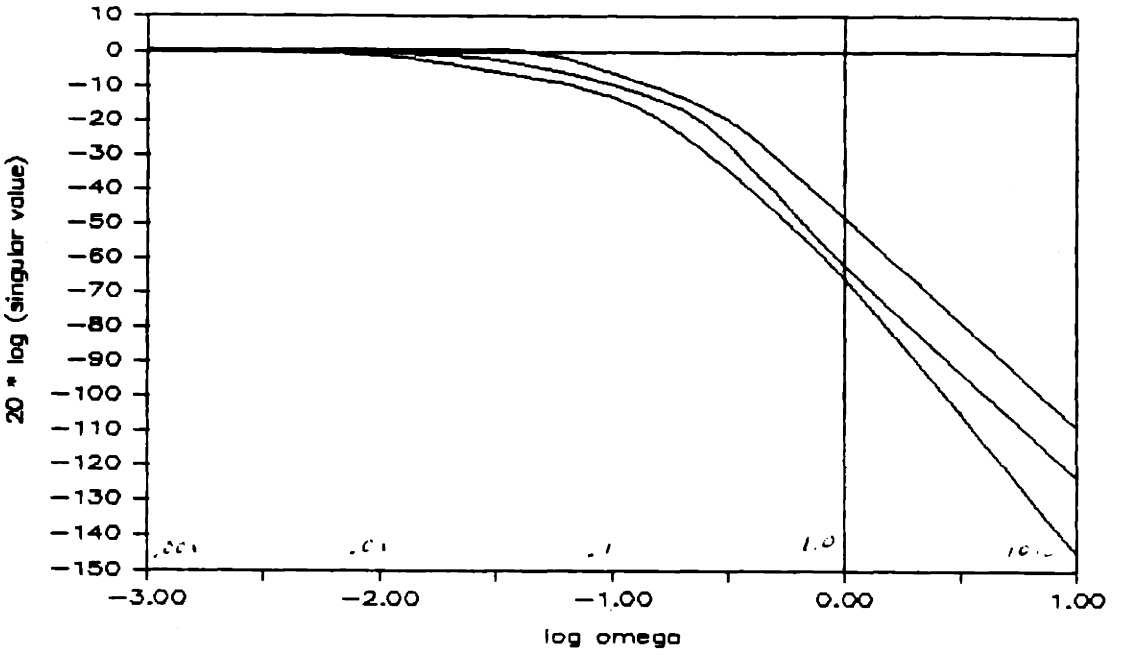

(a) The 5 knot model

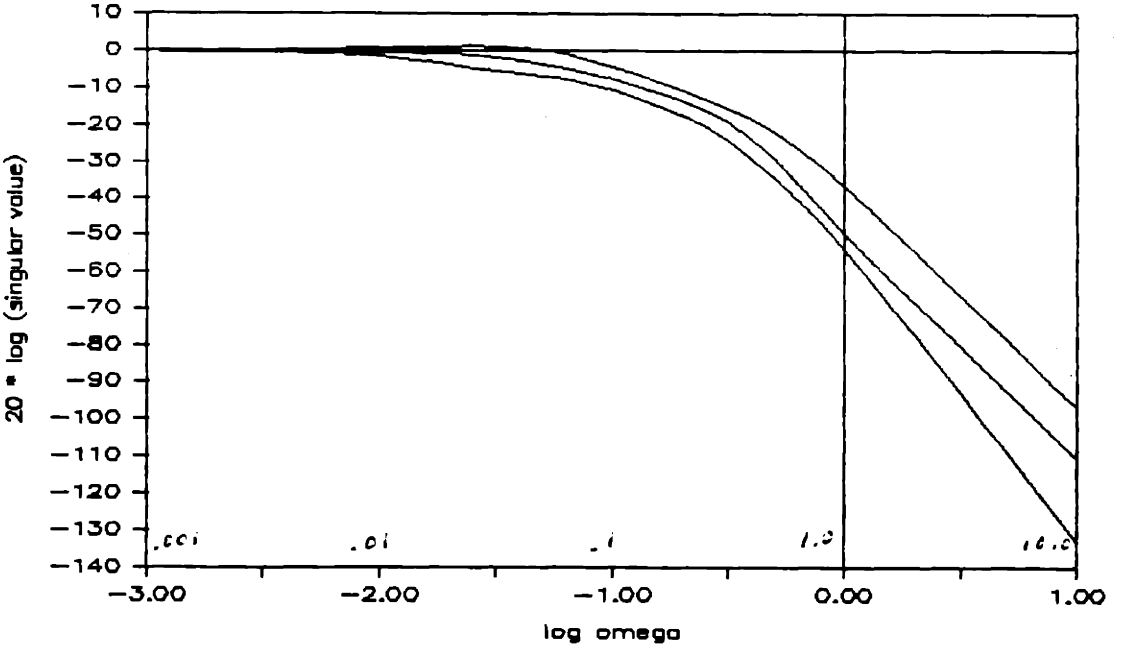

(b) The 10 knot model

Figure 4.12. Closed Loop Singular Values for the 5 and 10 Knot Compensated Designs

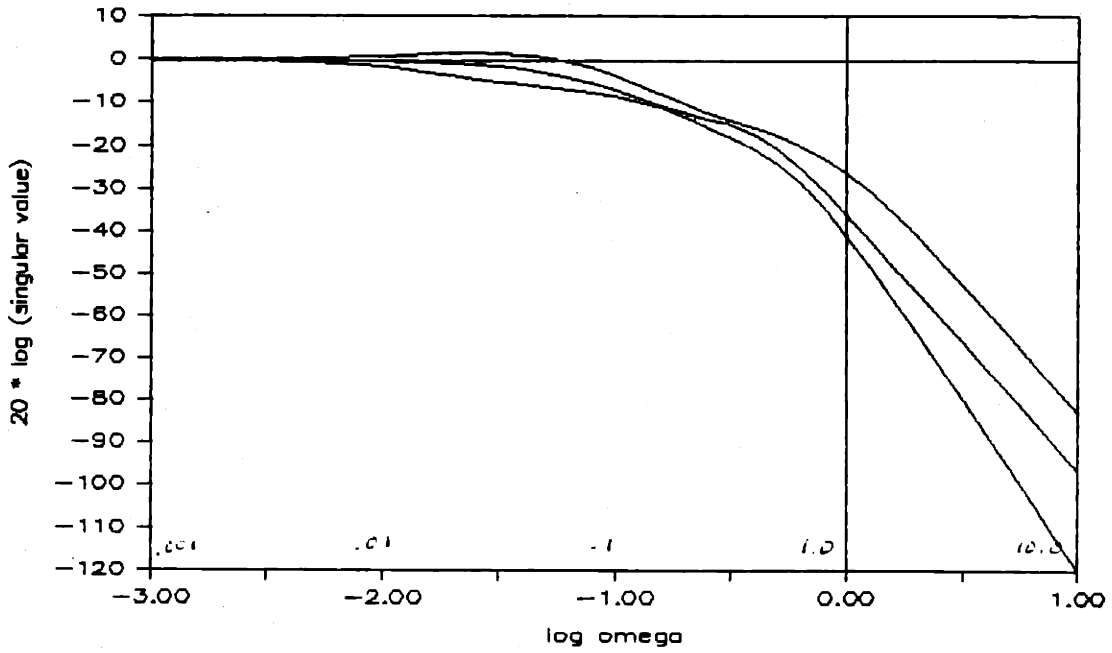

(a) The 20 knot model

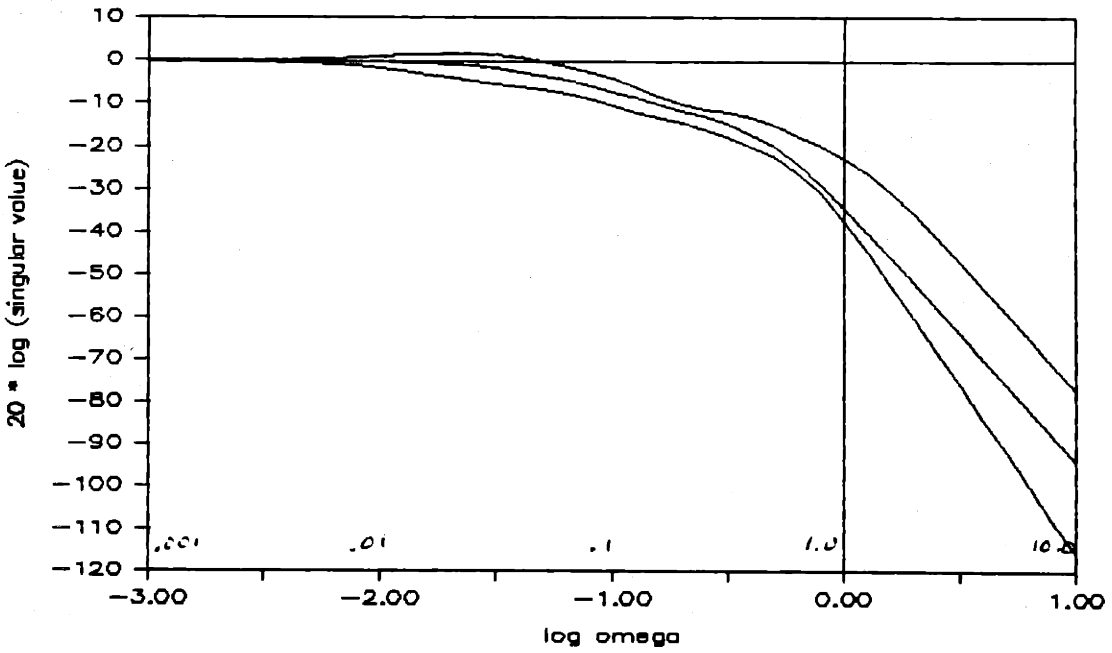

(b) The 25 knot model

Figure 4.13. Closed Loop Singular Values for the 20 and 25 Knot Compensated Designs

motion. The command inputs for each test are superimposed on the output variable time histories to indicate the time that the command was applied and also to provide an implicit error history.

Results are shown for the 20 knot model only as it enjoyed the most exhaustive testing. Check runs were made for the other models and displayed similar results.

4.8 Comparison of Linear and Nonlinear Simulations

The initial testing consisted of a comparison of the responses of the linear and nonlinear equations of motion to step inputs. Figure 4.14 is representative of this stage of testing and shows the time histories of the three output variables (w, r, and θ) and the three control surfaces when the submarine model is subjected to step inputs in w and θ. For this plot, the initial values of the command inputs were set to the nominal values for the 20 knot model, with the step changes being applied at t = 50 seconds, and removed at t = 100 seconds.

The reader should note the coupling that exists between the stern and fairwater planes as they deflect in opposite directions (as they should) in response to the pitch command

(figure 4.14 j and l). Additionally, the pitch command completely dominates the response initially and the command in w has no effect until the pitch error decreases. This should not be the case if the inertial variable ż was used in place of w, although any demonstration of this supposition will have to wait until the computer model is changed.

Figure 4.14 also displays the effects of the cross coupling that exists between yaw rate and pitch, as indicated by the variation in yaw rate (r) (figure 4.14 (e) and (f)) and the rudder deflection (figure 4.14 (m) and (n)) at the time when the step command is applied in θ (figure 4.14 (g) and (h)). This is a result of both the unconventional operating point that the model was linearized about and the non-zero roll angle. Recall that the nominal point reflects a diving turn so that a roll angle is present for this maneuver.

The main objective of this test was to determine the extent of agreement between the linear and nonlinear compensated models in order to establish the validity of both the compensator design and the computer software being used for the simulations. The extremely close agreement between the time histories for the linear and nonlinear models displayed by figure 4.14 thus establishes the

validity and permits further. All further simulations are performed using the nonlinear computer model.

4.9 Further Simulation of the Nonlinear Model

Having established the validity of the compensator design by successful comparison of the linear and nonlinear simulations, the next step is to examine such factors as symmetry, multiple commands, and control surface saturation.

The degree of symmetry present in the submarine model was evaluated by commanding a turn first in one direction and then in the opposite direction. The results are shown in figure 4.15 and reveal that even with the unconventional operating point used in producing the linear model, remarkable symmetry exists in the expected state variables. The roll angle (ϕ) time history is included in this figure to display the submarine's tendency to lean into a turn. A rather curious phenomenon is also displayed in that the submarine pitches up initially when commanded to turn. This trait reportedly exists in an actual submarine and was also observed on the real time simulation facility mentioned in the introduction to chapter 2. Finally, notice that the performance of the controller begins to degrade at about 135

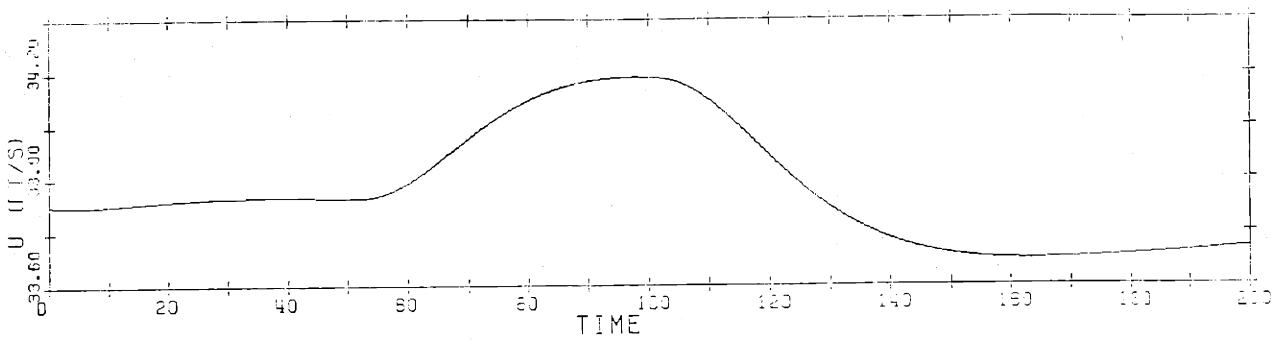

(a) Forward velocity u(t) for the linear model

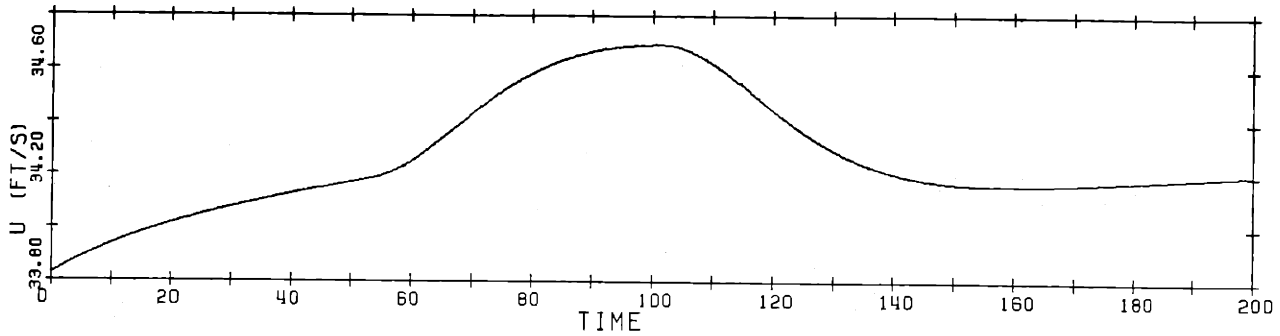

(b) Forward velocity u(t) for the nonlinear model

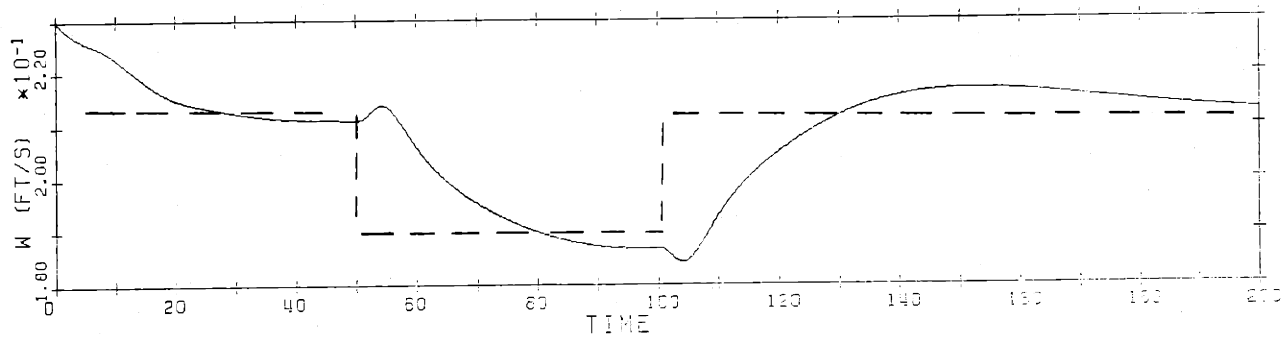

(c) Vertical rate w(t) for the linear model

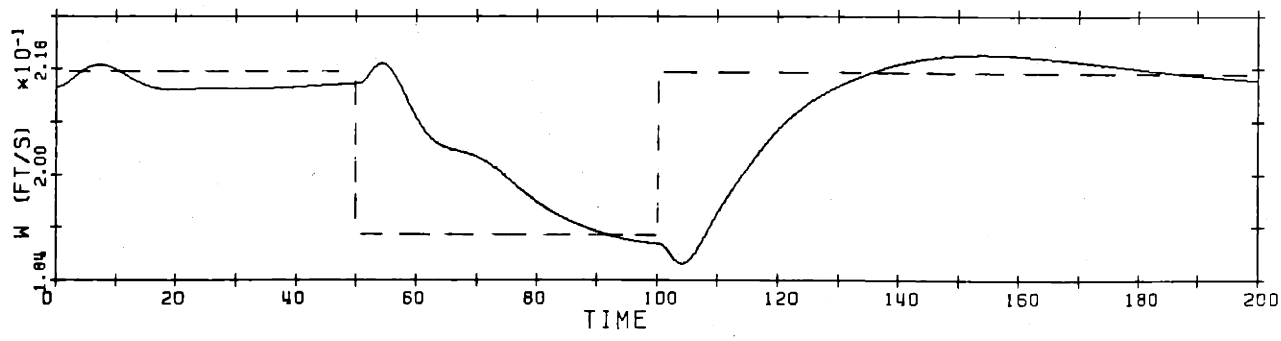

(d) Vertical rate w(t) for the nonlinear model

Figure 4.14. Comparison of the Linear and Nonlinear Simulations

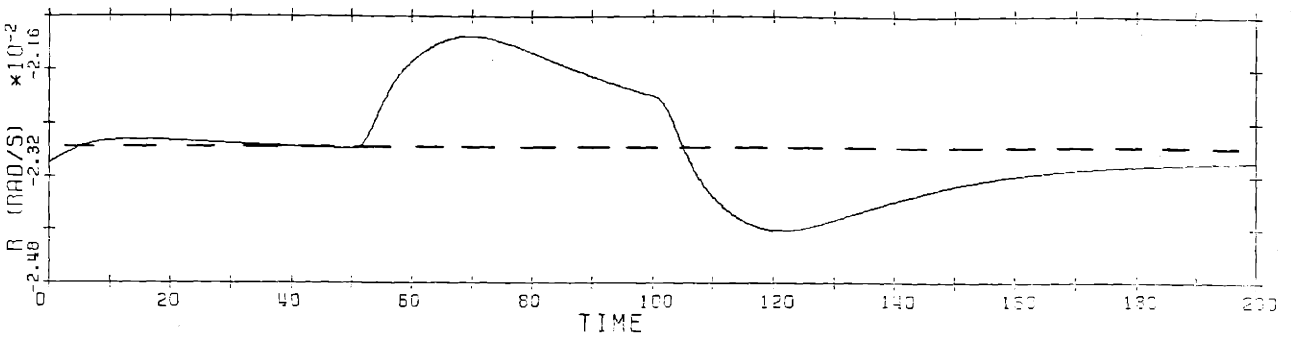

(e) Yaw rate r(t) for the linear model

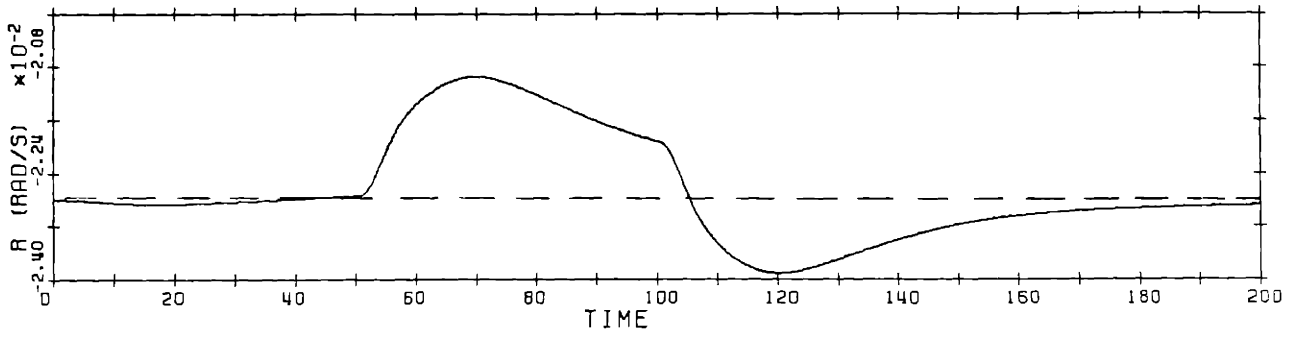

(f) Yaw rate r(t) for the nonlinear model

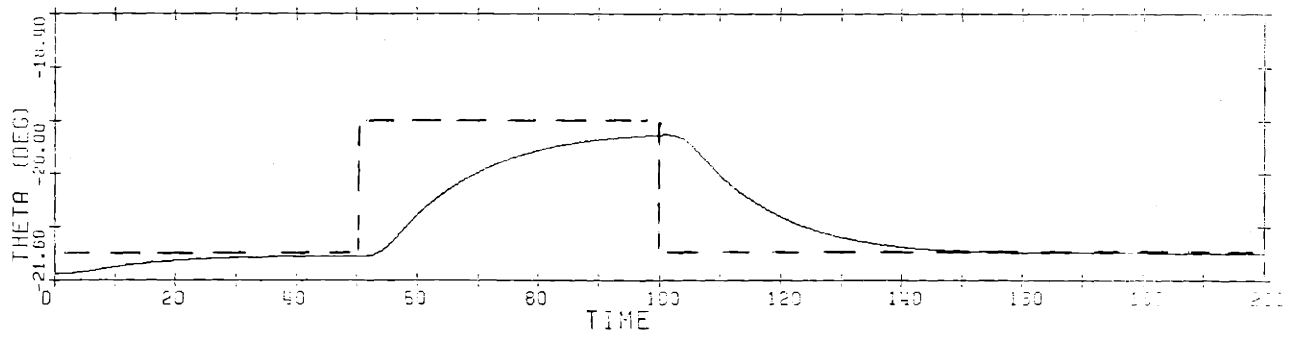

(g) Pitch angle theta(t) for the linear model

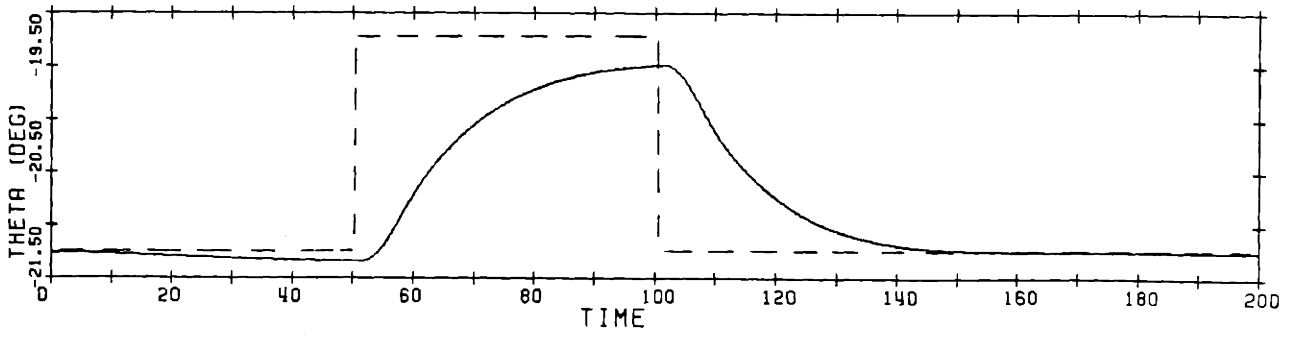

(h) Pitch angle theta(t) for the nonlinear model

Figure 4.14. (Cont'd)

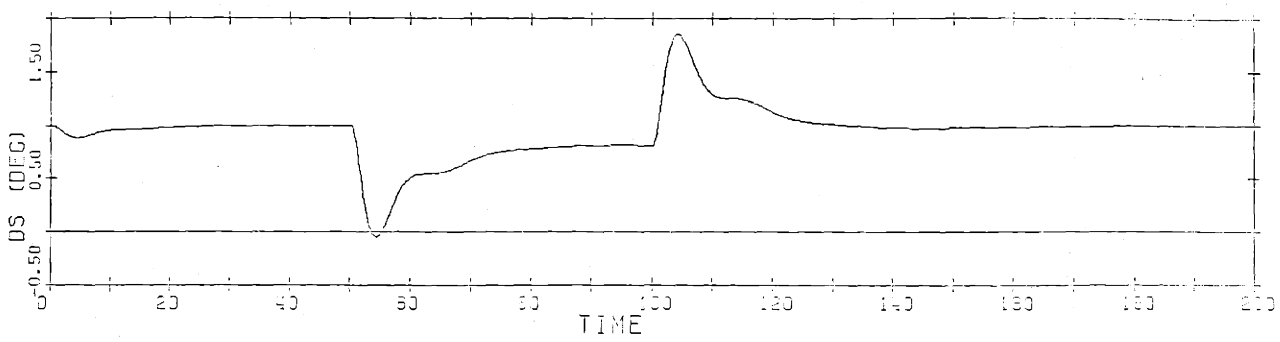

(i) Stern plane deflection for the linear model

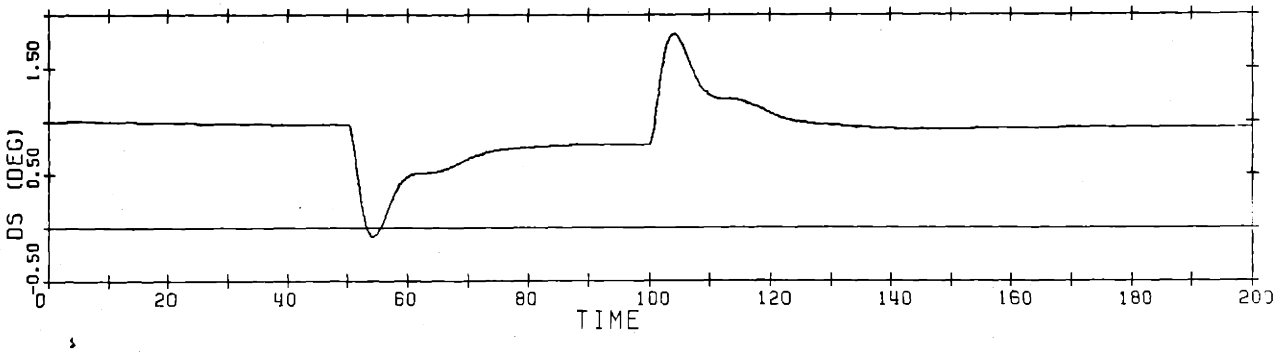

(j) Stern plane deflection for the nonlinear model

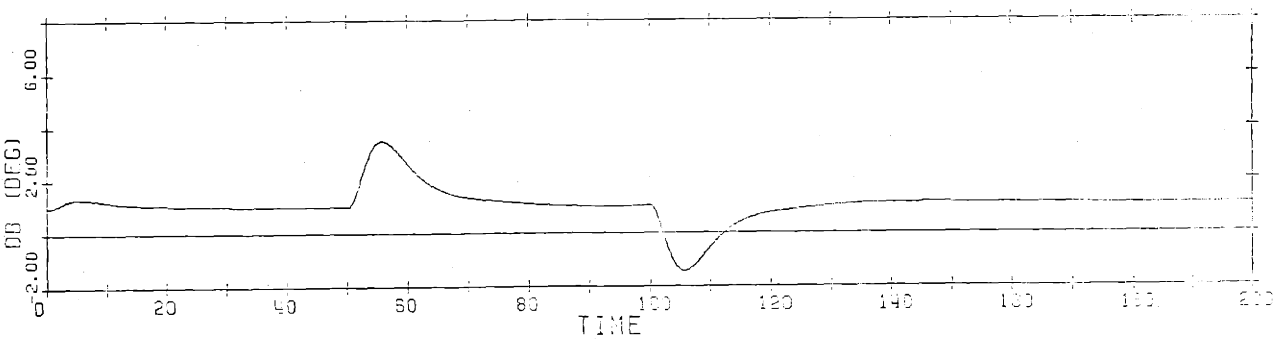

(k) Fairwater plane deflection for the linear model

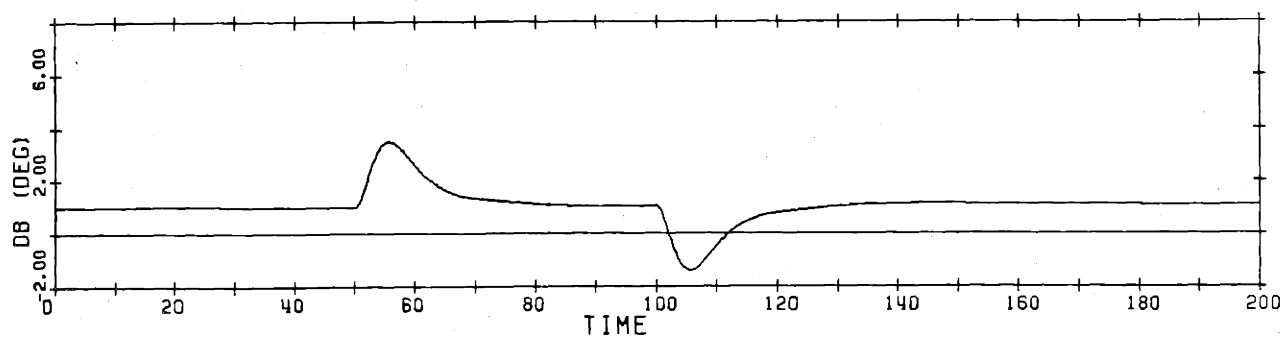

(l) Fairwater plane deflection for the nonlinear model

Figure 4.14. (Cont'd)

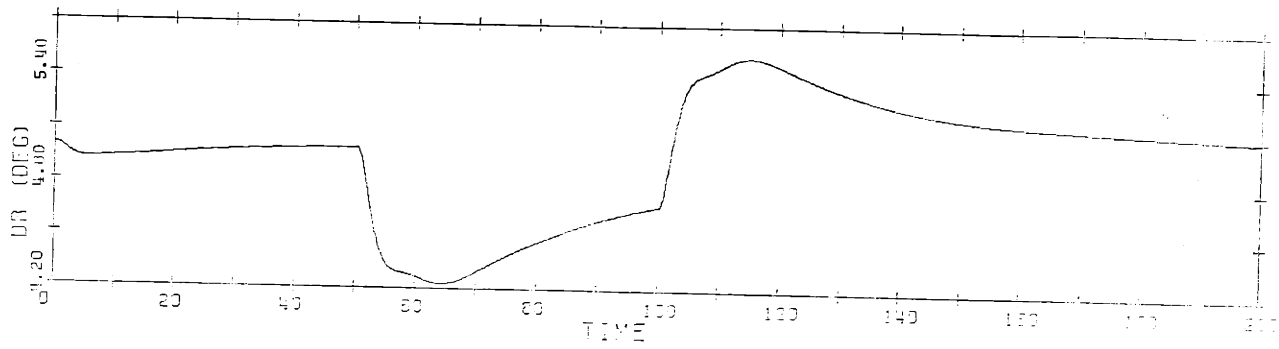

(m) Rudder deflection for the linear model

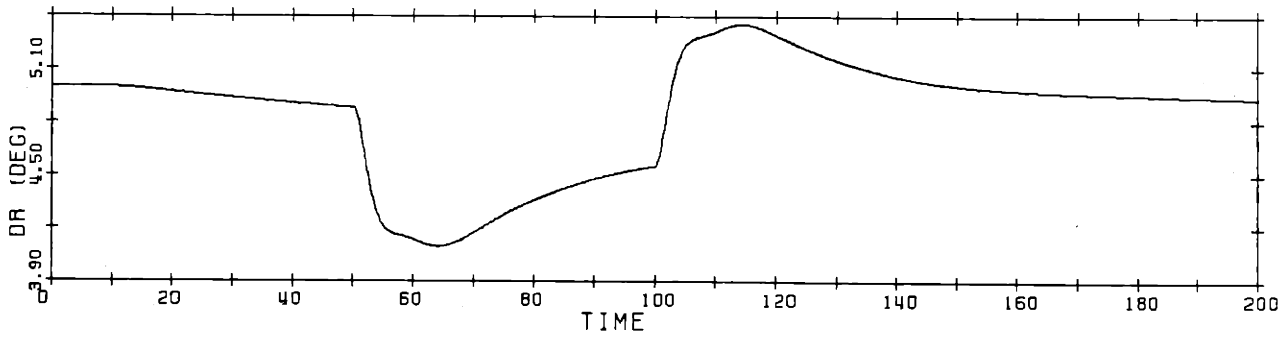

(n) Rudder deflection for the nonlinear model

Figure 4.14. (Cont'd)

seconds as the forward velocity reaches 33% below the nominal point, indicating that gain scheduling is necessary.

The multiple command test was accomplished by simulating an evasive maneuver. The command inputs are applied at different times and simulate first a diving turn followed by a recovery of the initial conditions. The results of this test, shown in figure 4.16, display the ability of the controller to respond to commands in both yaw rate and pitch. Again we see that the pitch command has significant effect on the yaw rate due to the cross coupling. Also displayed is the inability of the sail planes to control w in the presence of pitch commands. The sail planes do, however, aid the stern planes in the initial response to a pitch command by deflecting in the opposite direction, as is desired. Note the loss of control in w at about 75 seconds when the sail planes saturate.

To fully display the behavior of the compensated nonlinear model during periods of control surface saturation, the reference inputs for w and θ used in the previous test were increased significantly in magnitude and the simulation repeated. The results are presented in figure 4.17 and display a loss of control during saturation along with periods of lightly damped oscillatory response. Although

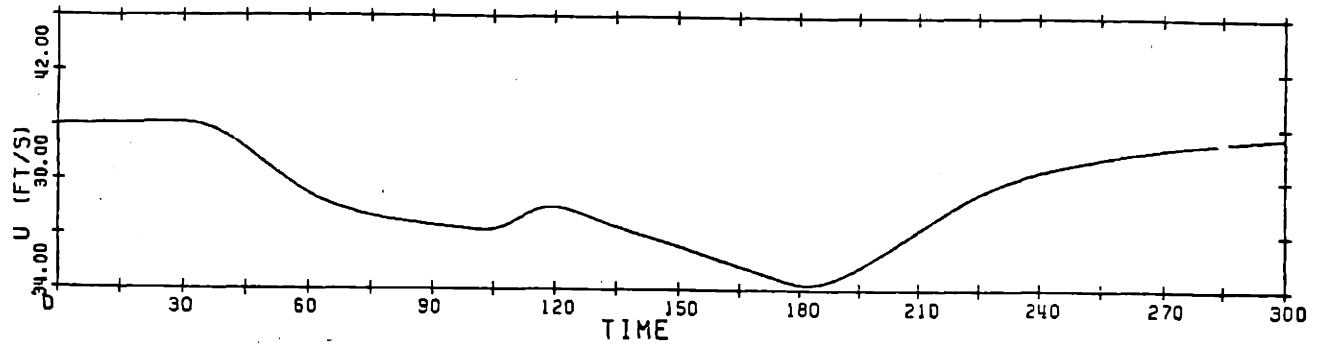

(a) Forward velocity u(t)

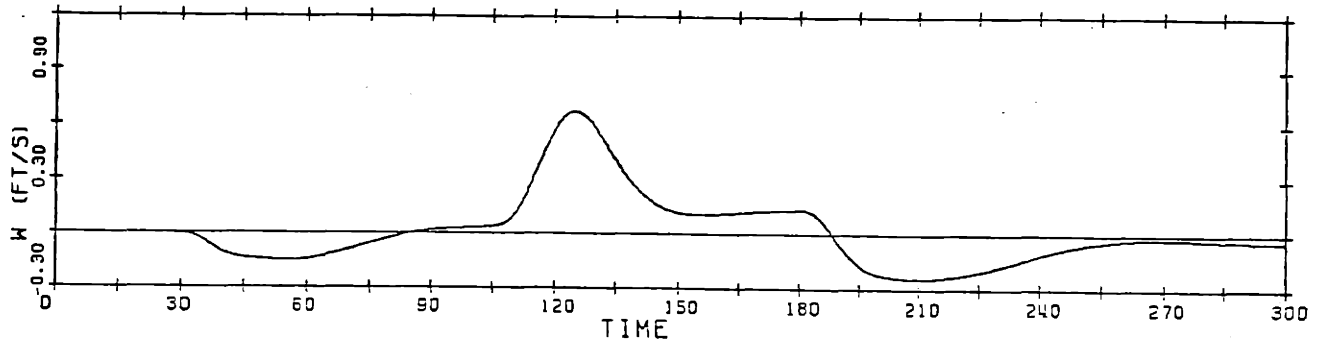

(b) Vertical rate w(t)

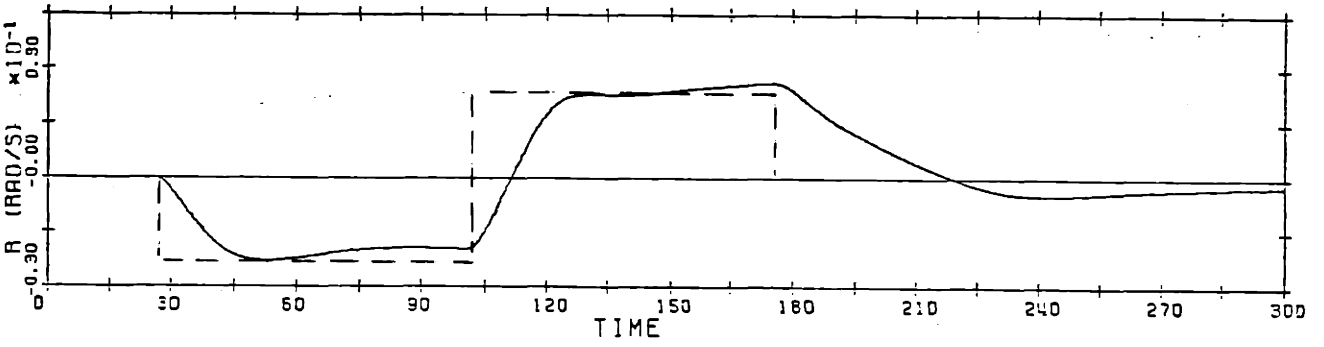

(c) Yaw rate r(t)

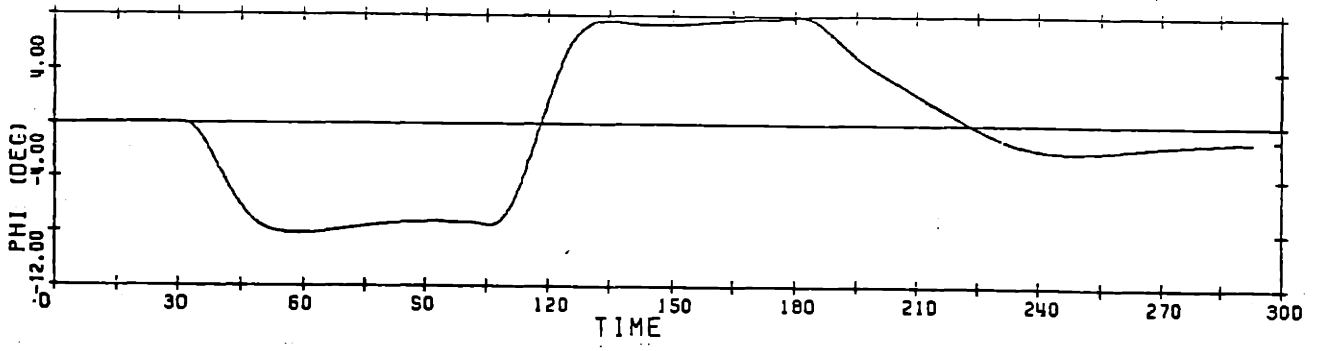

(d) Roll angle phi(t)

Figure 4.15. Yaw Rate Symmetry Test

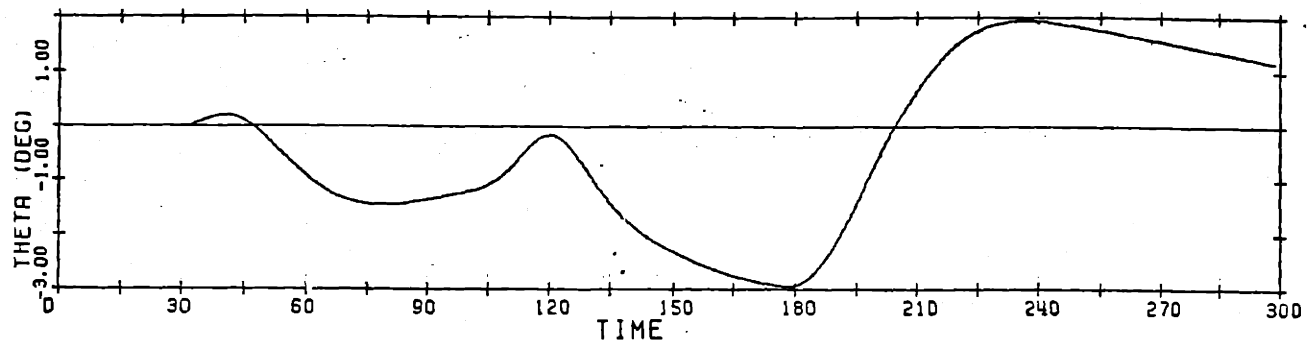

(e) Pitch angle theta(t)

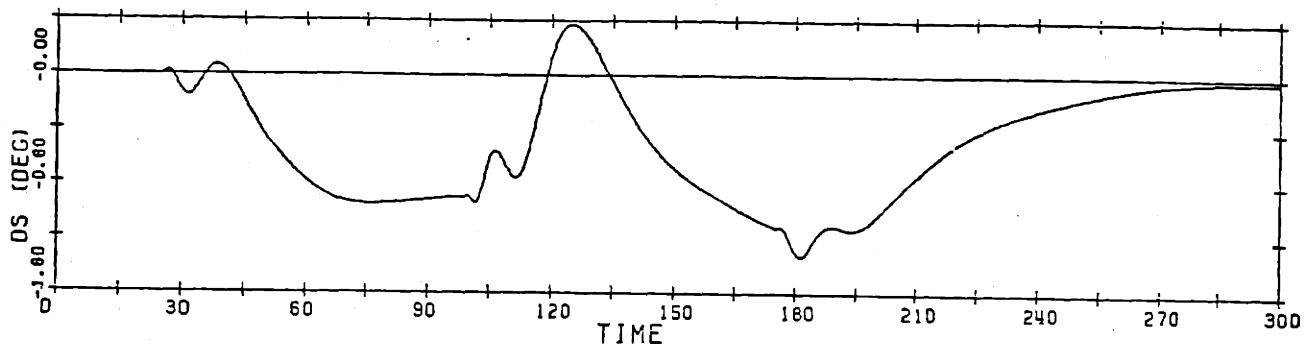

(f) Stern plane deflection

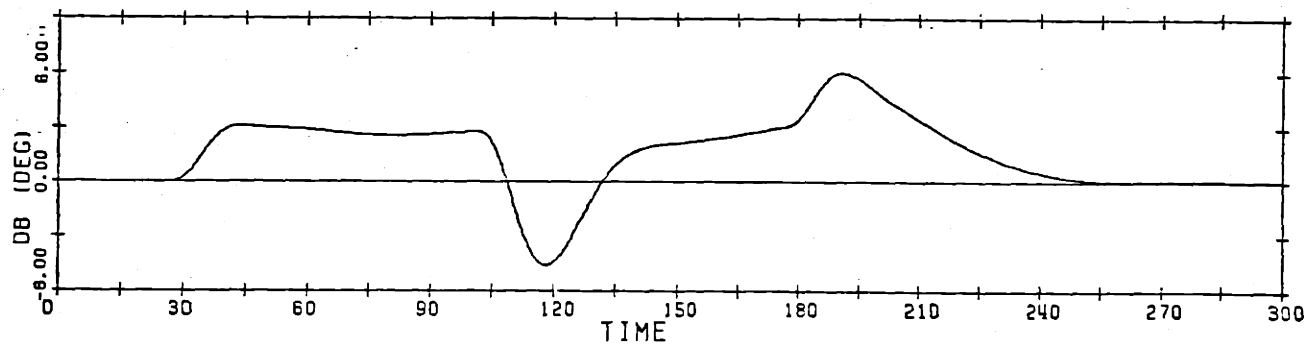

(g) Fairwater plane deflection

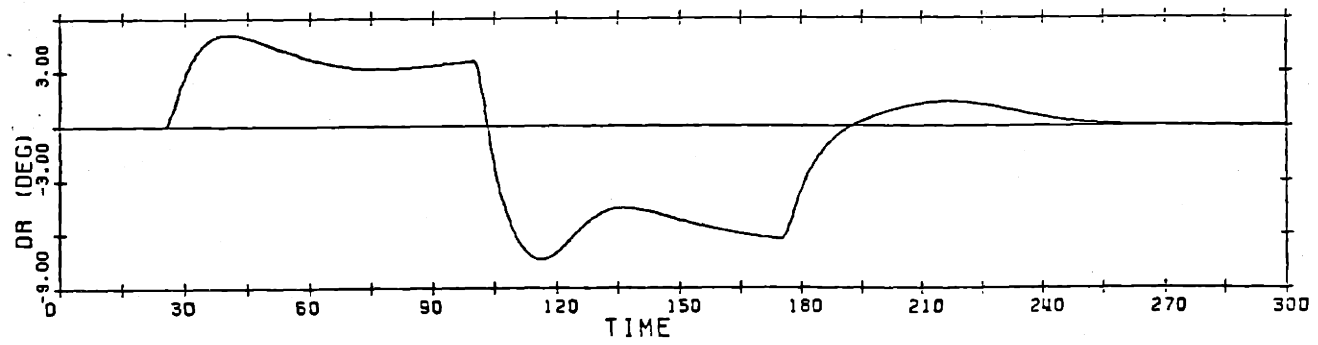

(h) Rudder deflection

Figure 4.15. (Cont'd)

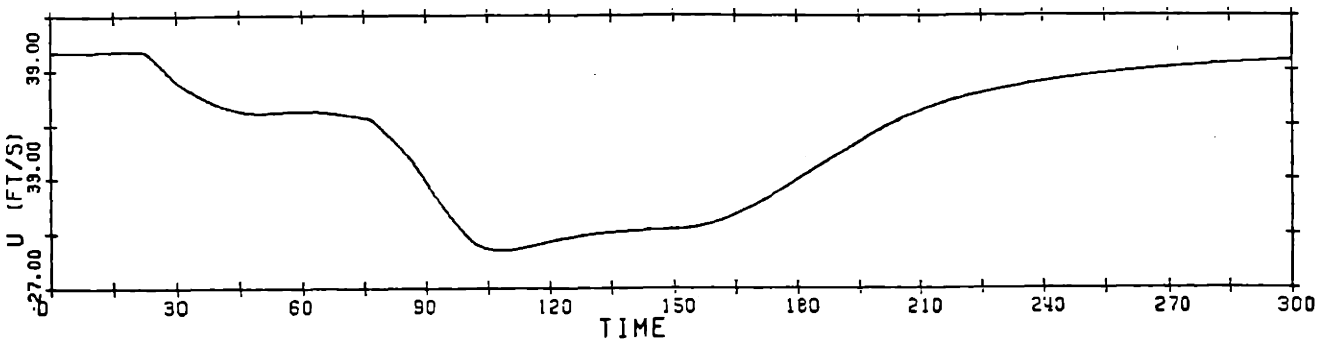

(a) Forward velocity u(t)

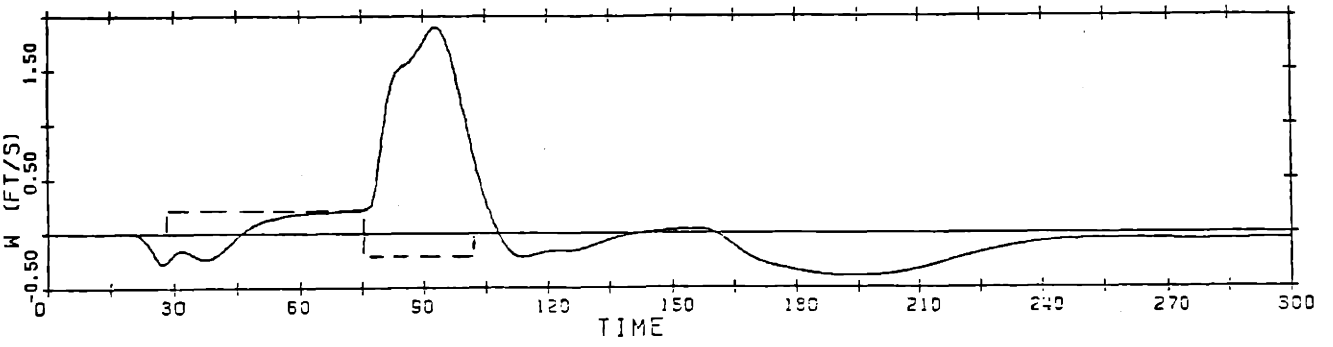

(b) Vertical rate w(t)

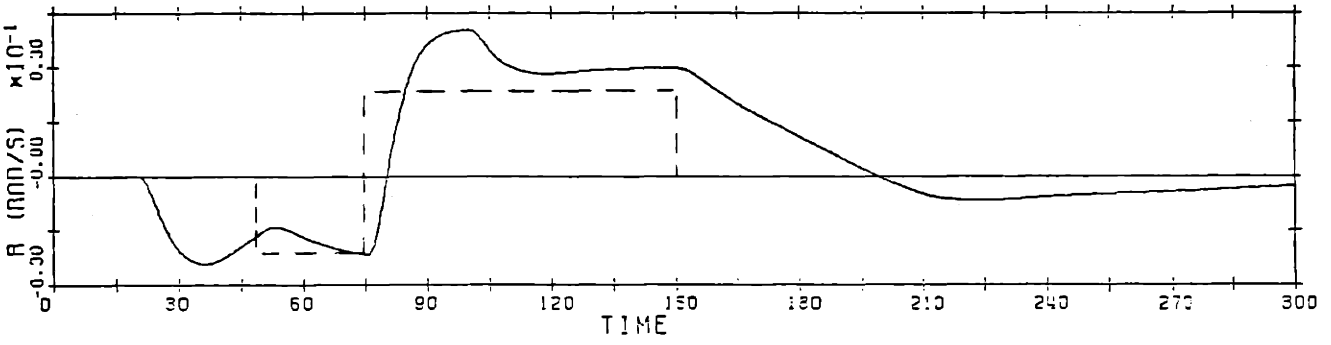

(c) Yaw rate r(t)

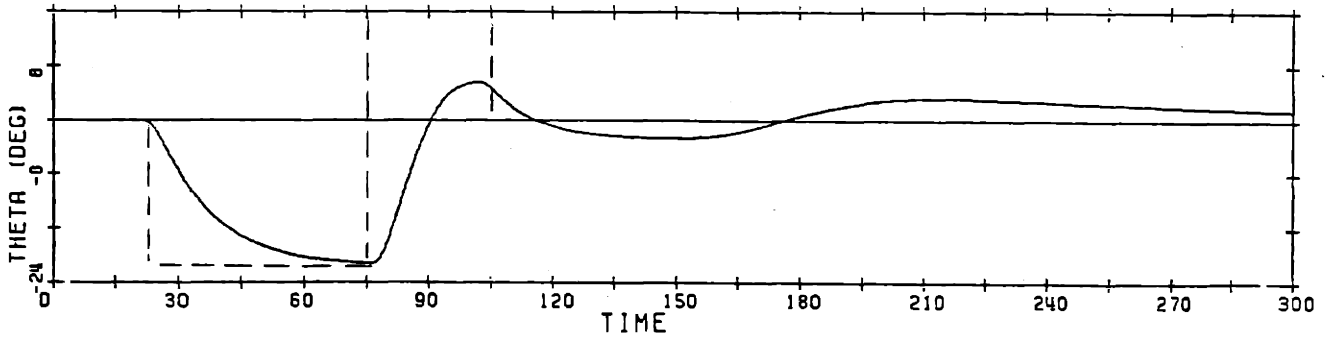

(d) Pitch angle θ(t)

Figure 4.16. Evasive Maneuver Test

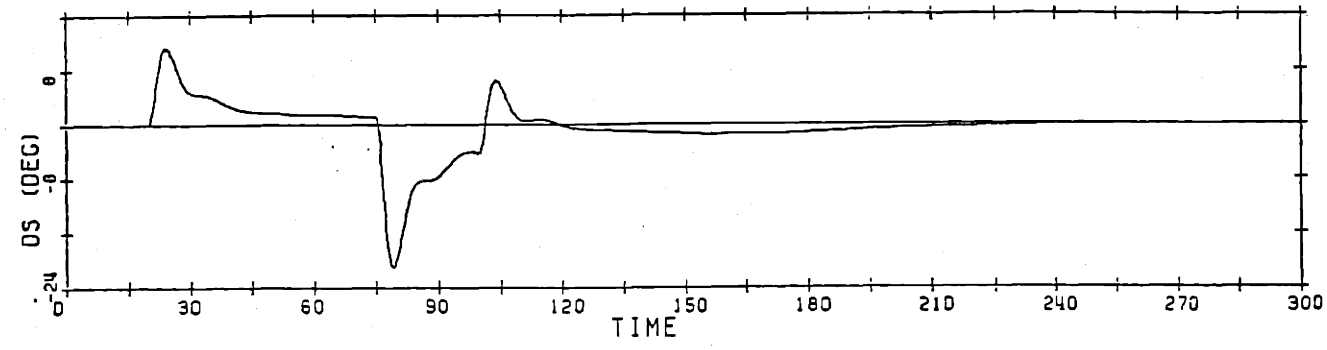

(e) Stern plane deflection

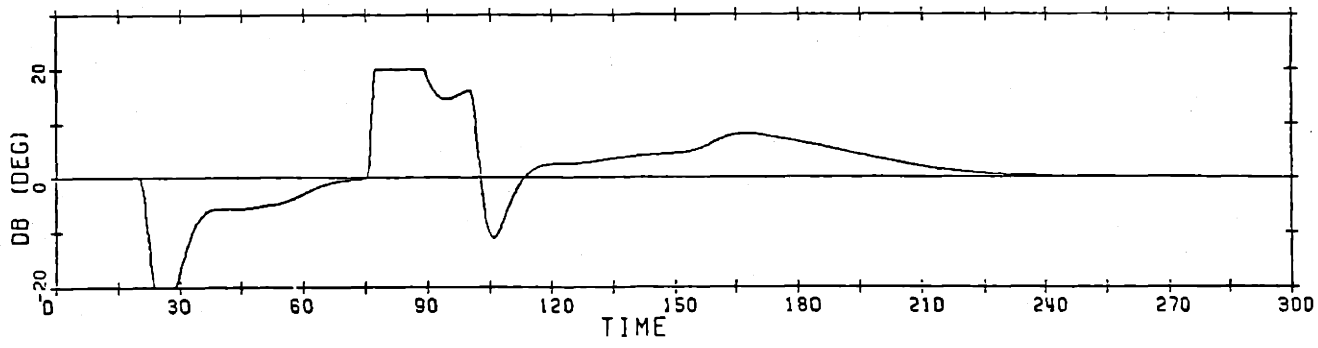

(f) Fairwater plane deflection

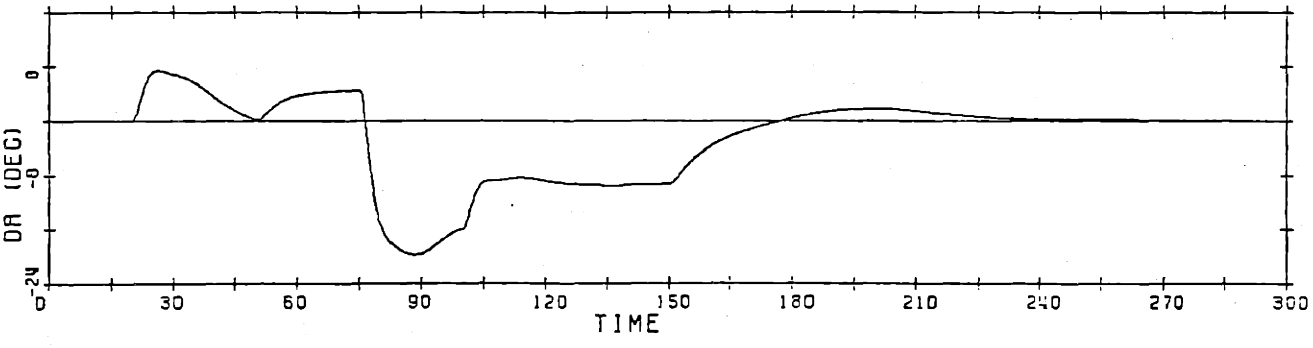

(g) Rudder deflection

Figure 4.16. (Cont'd)

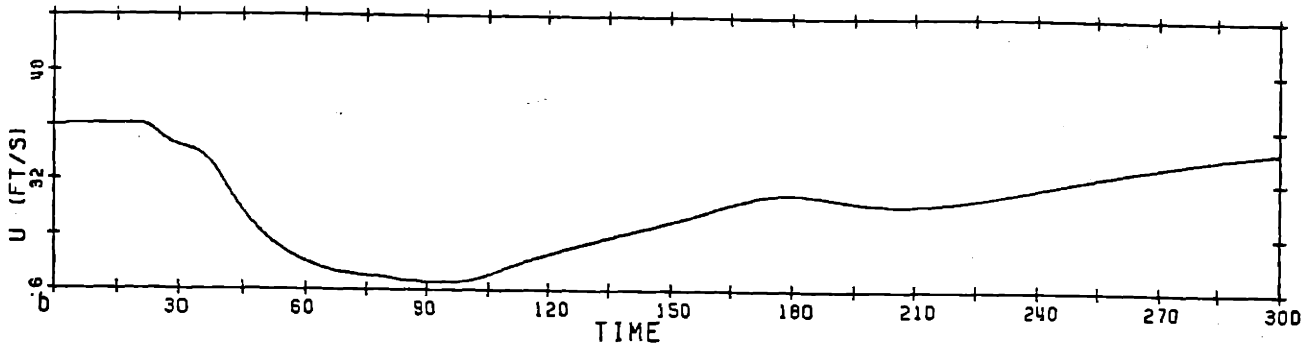

(a) Forward velocity u(t)

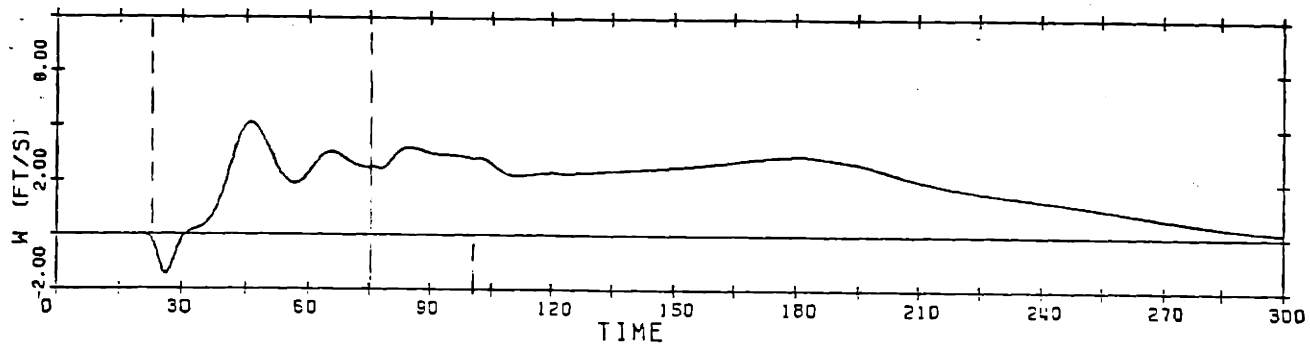

(b) Vertical rate w(t)

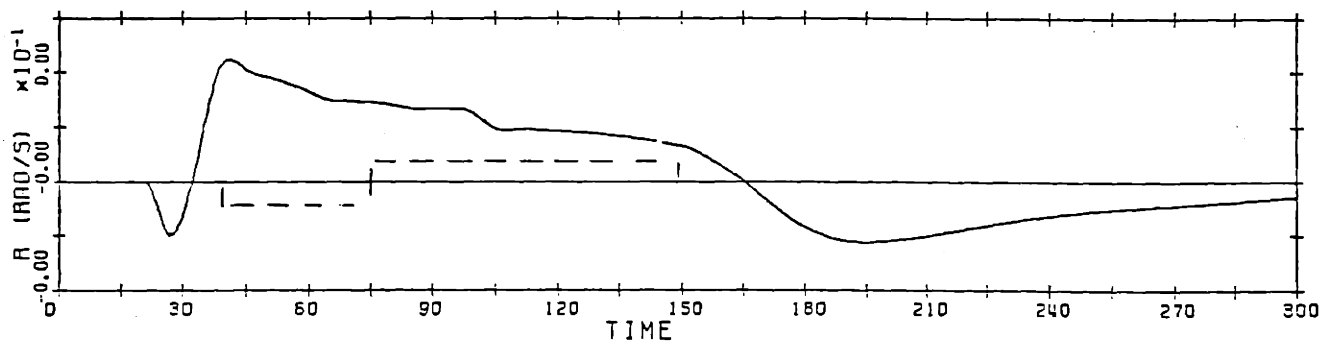

(c) Yaw rate r(t)

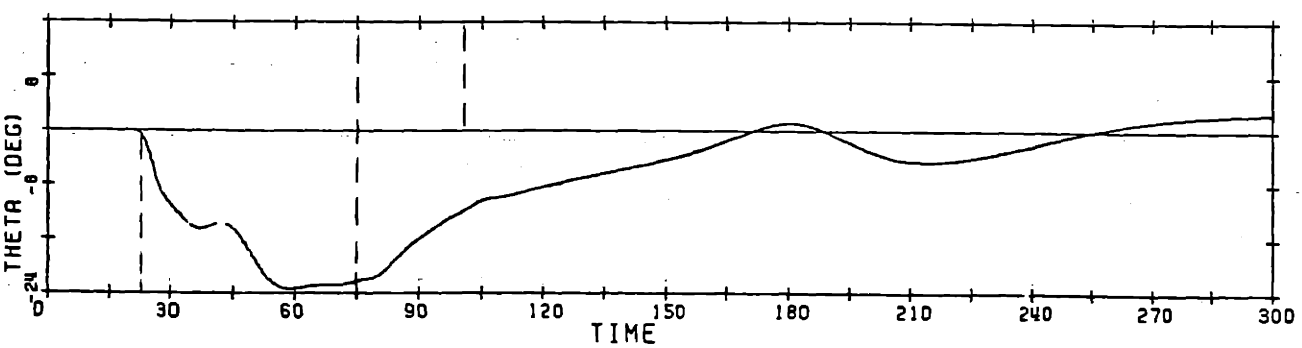

(d) Pitch angle θ(t)

Figure 4.17. Control Surface Saturation Test

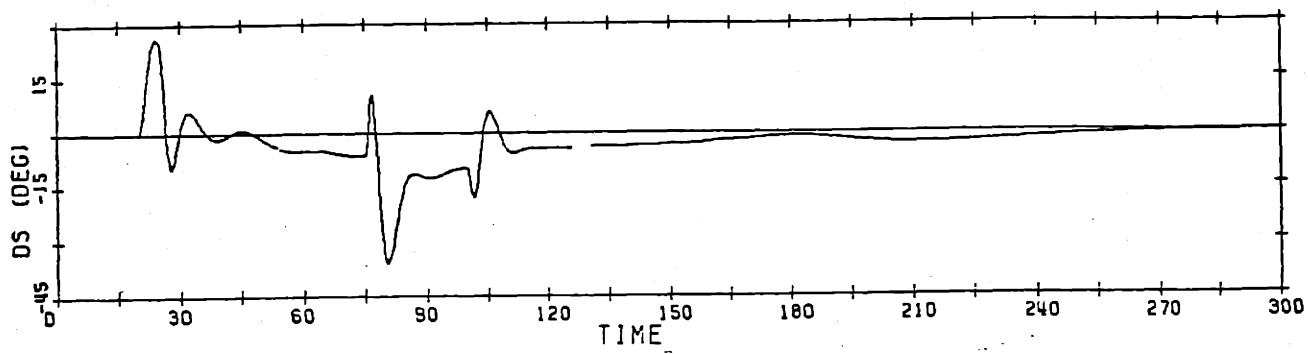

(e) Stern plane deflection

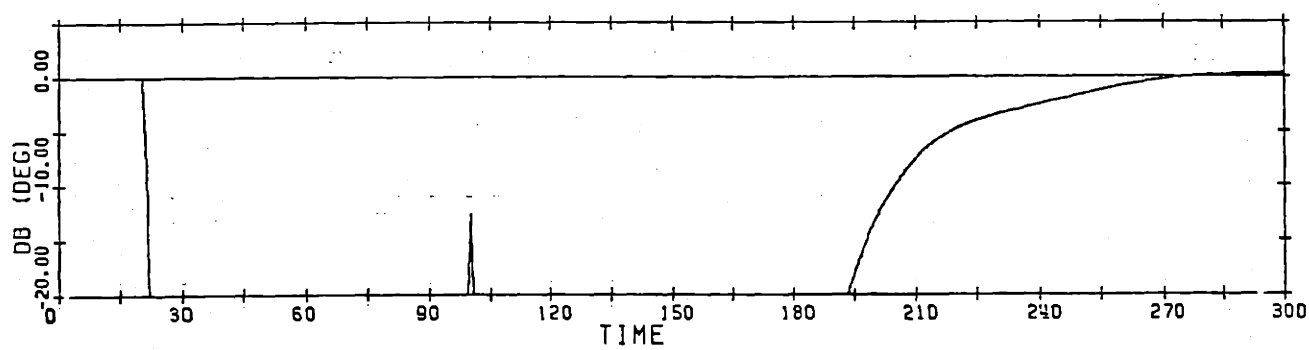

(f) Fairwater plane deflection

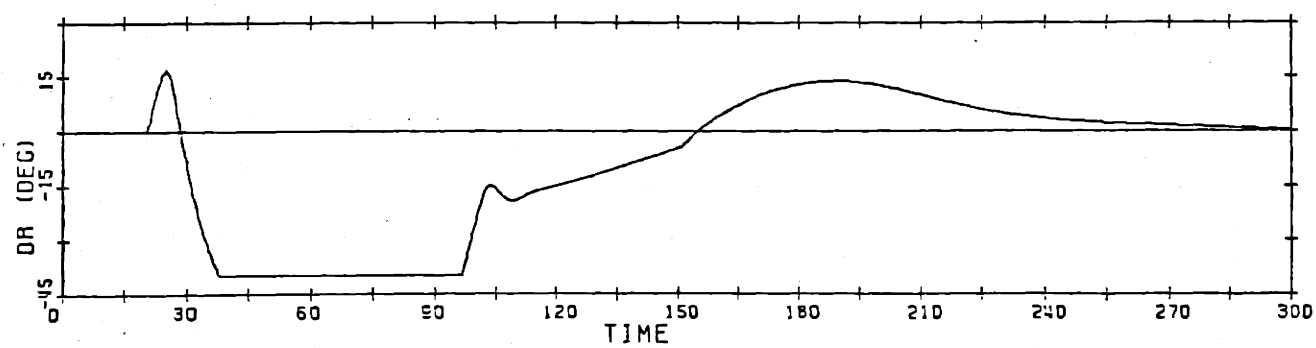

(g) Rudder deflection

Figure 4.17. (Cont'd)

the command inputs are removed at 150 seconds, the errors don't return to zero until nearly 300 seconds. Of particular note is the constant error in w during saturation. This can be seen to be caused by the sail planes since the error in w begins to decrease the instant the sail planes come out of saturation. Also note that although a 25 degree error exists in pitch (the pitch command was -50 degrees) at 60 seconds, the stern planes are only slowing increasing in deflection. The large control surface deflections have slowed the submarine to nearly 9 knots by this time, however, accounting for the decreased control gain. Observe that the submarine speed rapidly decreases when the rudder saturates, but slowly increases in speed past 100 seconds, even though the sail planes saturated.

4.10 Summary

This chapter has presented an overview of the LQG/LTR design methodology and then the application of the methodology to the design of a compensator for the submarine model.

Compensator designs were developed for all four linear models of the submarine, providing the information necessary

to apply a nonlinear curve fit to the compensated parameters, laying the groundwork for the gain scheduling algorithm in the next chapter.

Time histories for the 20 knot model were presented that further validated the linearization of the nonlinear equations of motion and displayed the ability of the compensator design to control the submarine nonlinear model as long as the forward velocity remained close to the nominal point.

Finally, the loss of control that can result from saturation of the control surfaces was demonstrated.

Chapter 5

NONLINEAR MIMO DESIGN

5.1 Introduction

It is well known that drag and lift forces on a body vary as the square of the velocity [16]. Therefore, a compensator designed for a particular speed should not be expected to provide optimum performance over a widely varying speed range.

This chapter demonstrates the technique of gain scheduling as a method of introducing the inherent nonlinearities due to velocity into the compensator design.

The algorithm used to implement the gain scheduling is presented, along with representative nonlinear simulations.

5.2 The Gain Scheduling Algorithm

In the previous chapters, linear models of the submarine

dynamics were developed for four different speeds, and an LQG/LTR design performed on each model. The products of the design effort were the Kalman Filter and Control gain matrices contained in Appendix C1.

The specifics of the computer implementation of the model based compensator require that the compensator be defined by three matrices, $\underline{A}$-$\underline{B}$ $\underline{G}$-$\underline{H}$ $\underline{C}$, $\underline{G}$, and $\underline{H}$ (refer to equations 4.17 and 4.18). As a result, the gain scheduling algorithm must produce the required coefficients to calculate the individual entries for these matrices.

The fact that lift and drag forces vary as the square of the velocity indicates the choice of a polynomial least squares algorithm to produce the required coefficients. Additionally, application of a least squares algorithm to matrices as large as 11 x 11 requires that a computer be used. The fortran program in Appendix D1 is an adaptation of the vector based program developed by A. Miller [17] that will accommodate square and non-square matrices up to order 11.

The program calculates correlation coefficients for each coefficient produced, providing a determination of how good the approximation is. As expected, a linear fit (polynomial of order 1) produced very poor correlation. A second order curve fit produced correlation coefficients averaging 0.98,

with a third order fit only marginally better. Since implementation of gain scheduling would require 187 * n multiplications and 187 * n additions, where n = the order of the polynomial, a minimal order polynomial is desired. Thus a second order polynomial was used to calculate the coefficients. The results, along with the correlation coefficients, are presented in Appendix D2.

The fortran program implementing the submarine model at CSDL was then modified to permit the coefficients for the $\underline{A}$-$\underline{B}$ $\underline{G}$-$\underline{H}$ $\underline{C}$, $\underline{G}$, and $\underline{H}$ matrices to be read in, and new values for these matrices calculated for each iteration during integration of either the linear or nonlinear equations of motion. To calculate a particular entry for one of the matrices, say the (i,j) element of the $\underline{H}$ matrix, the current forward velocity u(t) is first converted to knots (u_k). Then, if $c_{i,j,0}$, $c_{i,j,1}$, and $c_{i,j,2}$ are the coefficients calculated by the gain scheduling algorithm for that element of the $\underline{H}$ matrix, the updated value is given by

$$h_{i,j} = c_{i,j,0} + u_k(c_{i,j,1} + u_k(c_{i,j,2})) \qquad (5.1)$$

Note that the order of multiplication and addition has been arranged to require the minimum amount of calculation.

The fact that the computer implementation of the submarine model did not provide for propeller rpm to be varied was overcome by setting the rpm to the final speed and

introducing the initial speed into the initial conditions.

5.3 Testing of the Nonlinear Compensator

Although the above method of overcoming the constant rpm constraint of the model permitted simulation of gain scheduling, the flexibility of the simulation was somewhat limited. Only one speed excursion could be accomplished during any single run, with the propeller always rotating at a constant rpm.

Figure 5.1 simulates changing depth without imparting a pitch angle to the submarine and provides an excellent example of both the usefulness of w(t) as a state variable and the increase in control surface gain produced by the gain scheduling algorithm. The time history of the sail planes (db) indicates their dominant role in this maneuver. Although the command in w(0.5 ft/sec) is attained quite early at 60 seconds, the submarine is still slowing and the nonlinear compensator increases the sail plane deflection accordingly. The second command in w, at 275 seconds, produces the same magnitude error signal, but results in a much larger initial deflection of the sail planes due to the lower speed. The error in w is seen to stay constant and very near zero during the sail plane movement.

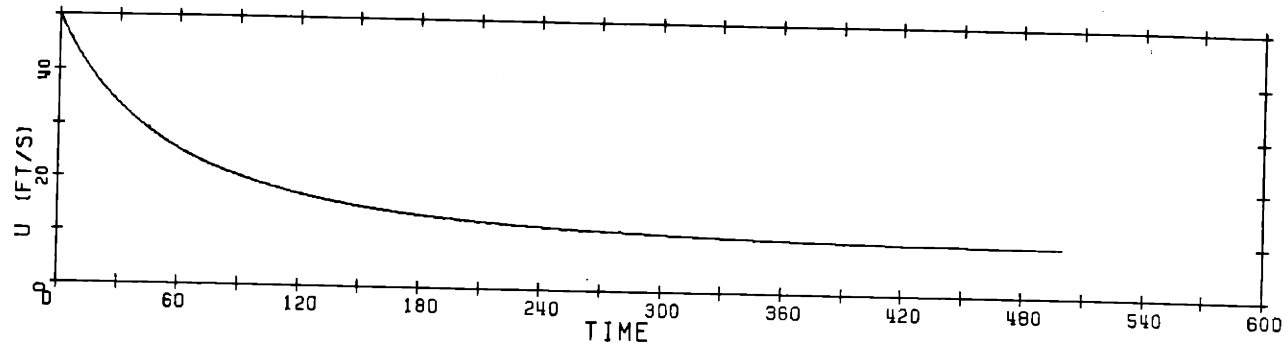

(a) Forward velocity u(t)

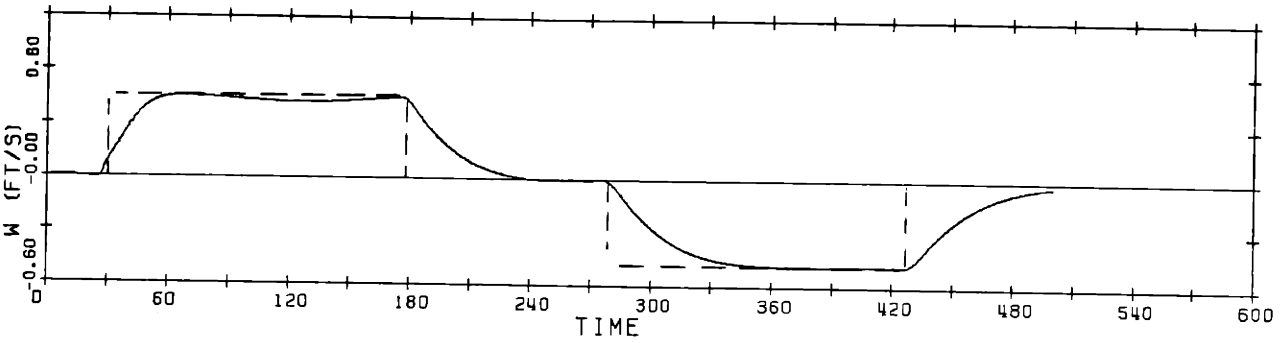

(b) Vertical rate w(t)

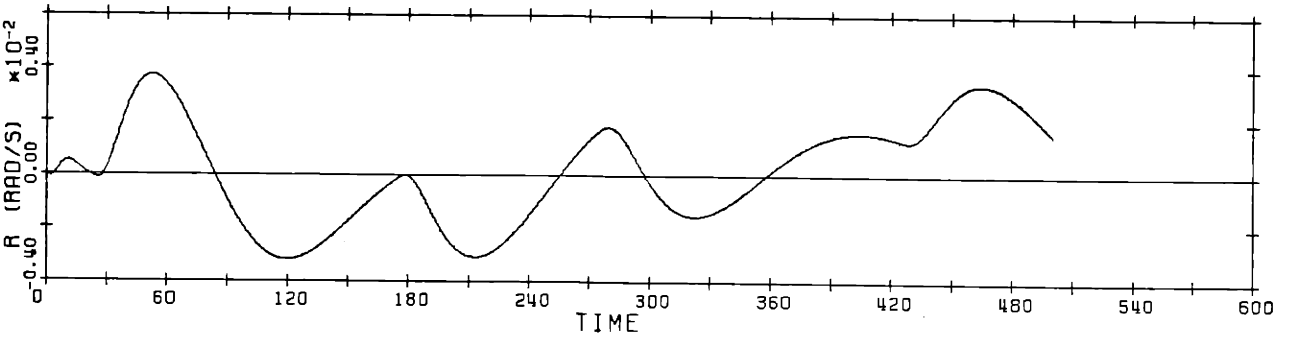

(c) Yaw rate r(t)

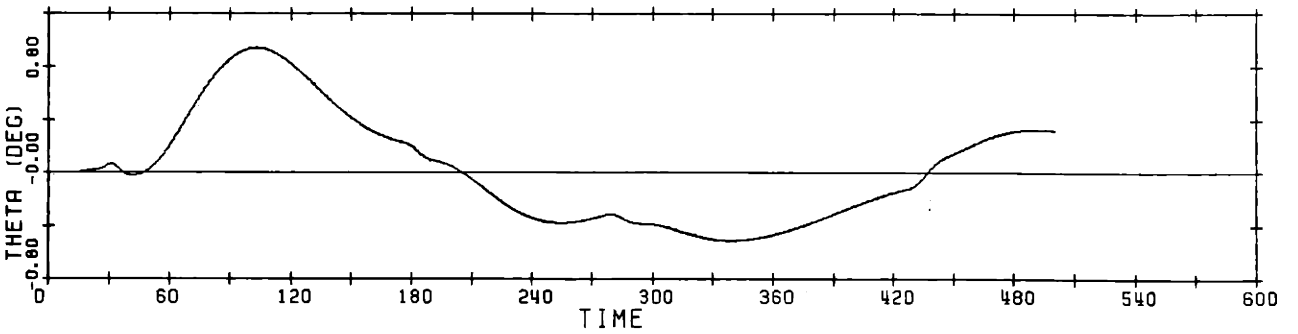

(d) Pitch angle θ(t)

Figure 5.1. Gain Scheduling Demonstration

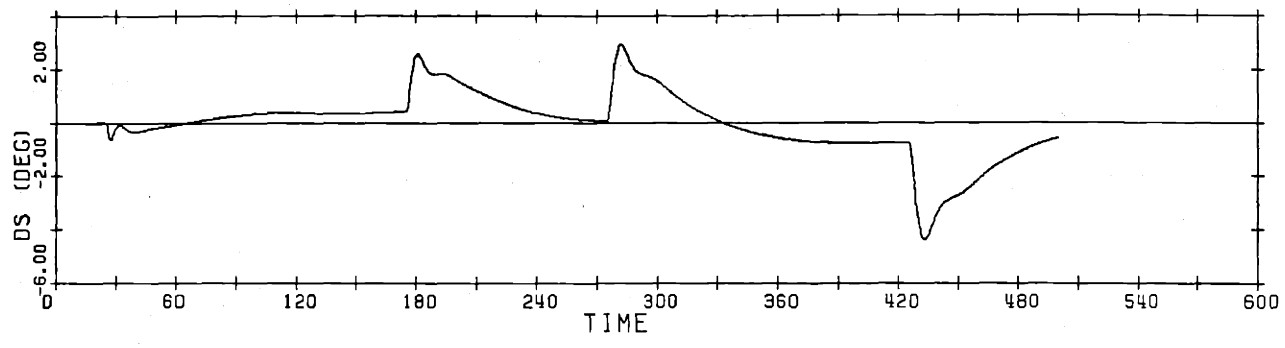

(e) Stern plane deflection

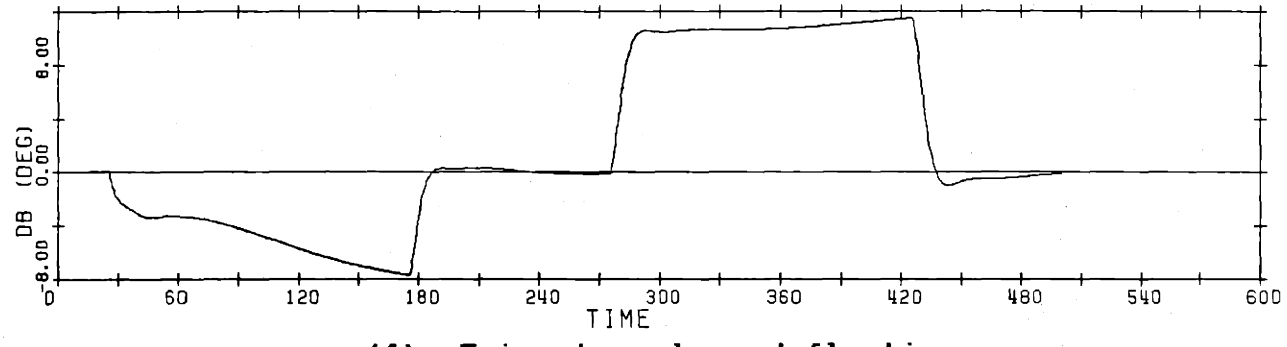

(f) Fairwater plane deflection

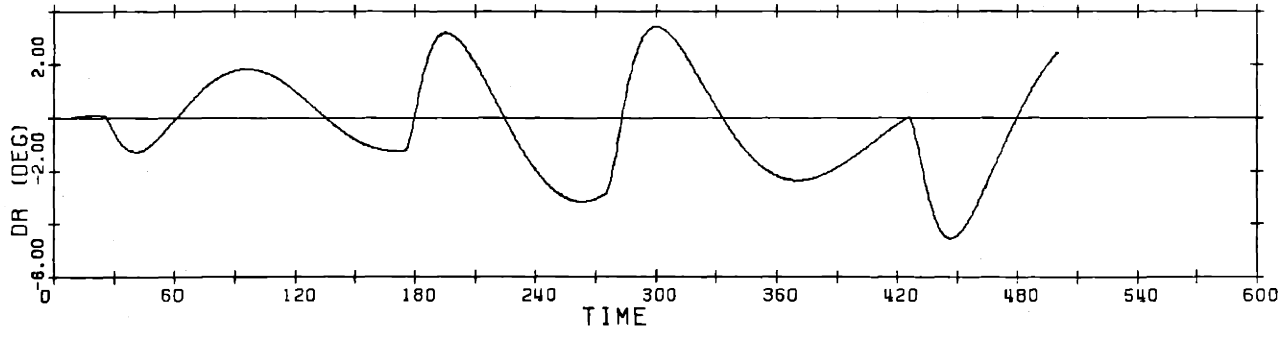

(g) Rudder deflection

Figure 5.1. (Cont'd)

The next two simulations reflect an attempt to further define the nature of the cross coupling that exists between pitch angle θ and yaw rate r. Both tests have initial conditions corresponding to the nominal point for the 5 knot model with the final speed equal to the nominal speed for the 25 knot model. Command inputs were applied as step signals that corresponded to the nominal values for the three output variables for the 10, 20, and 25 knot models. The step inputs for the 10 and 20 knot nominal points were timed so as to occur simultaneously with the submarine attaining the forward velocity appropriate to that nominal point.

In figure 5.2, the submarine is allowed to settle for a short time at the 20 knot nominal conditions before the final step change is applied. In figure 5.3, however, the last step change is applied as soon as the appropriate velocity is reached. Thus the two time histories are identical up to about 35 seconds. A comparison of the two sets of time histories reveals that the cross coupling between yaw rate and pitch angle is not minimized in the second test, although this might be expected since the submarine should be experiencing an attitude very similar to that for which the compensators were designed. Instead, although the curves appear smoother in the second test, a close inspection of the errors and the control surface

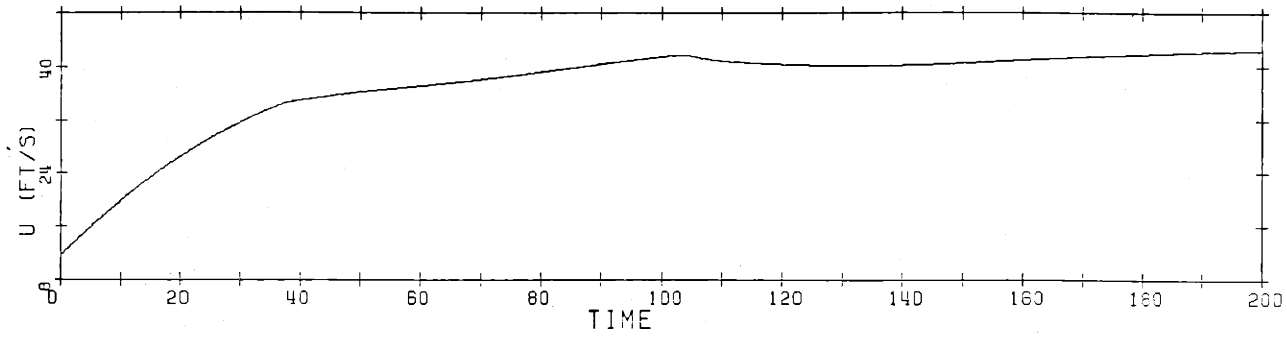

(a) Forward velocity u(t)

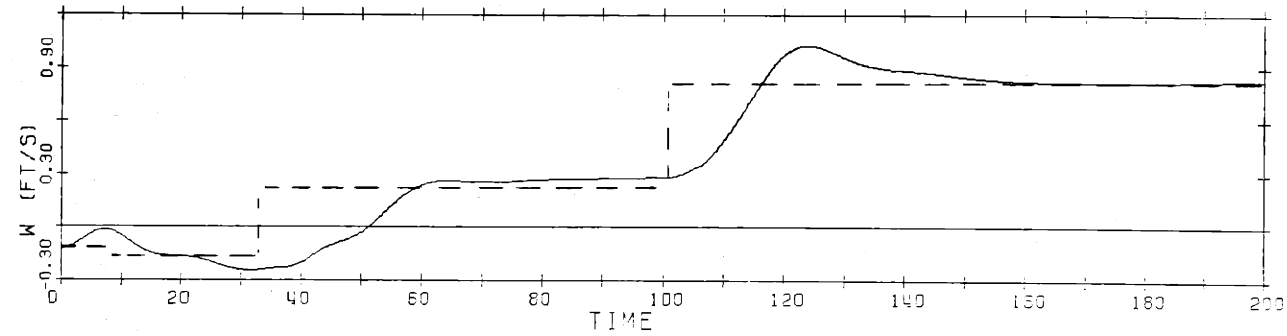

(b) Vertical rate w(t)

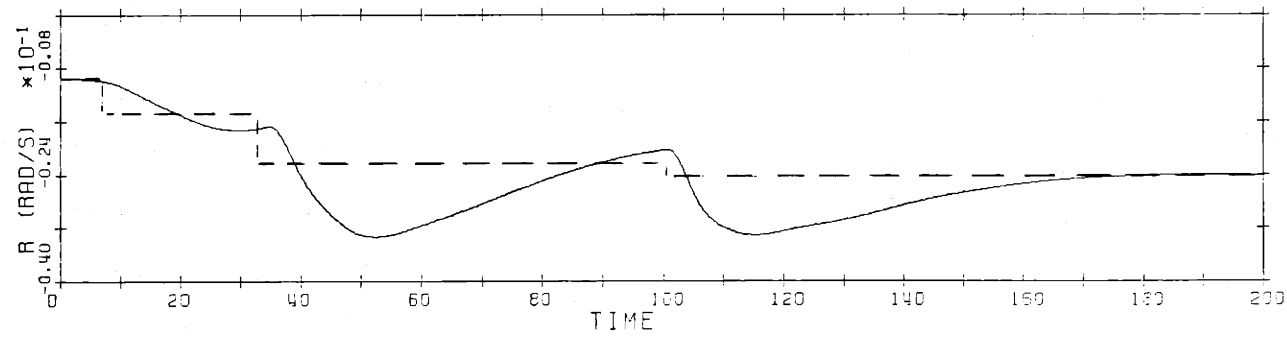

(c) Yaw rate r(t)

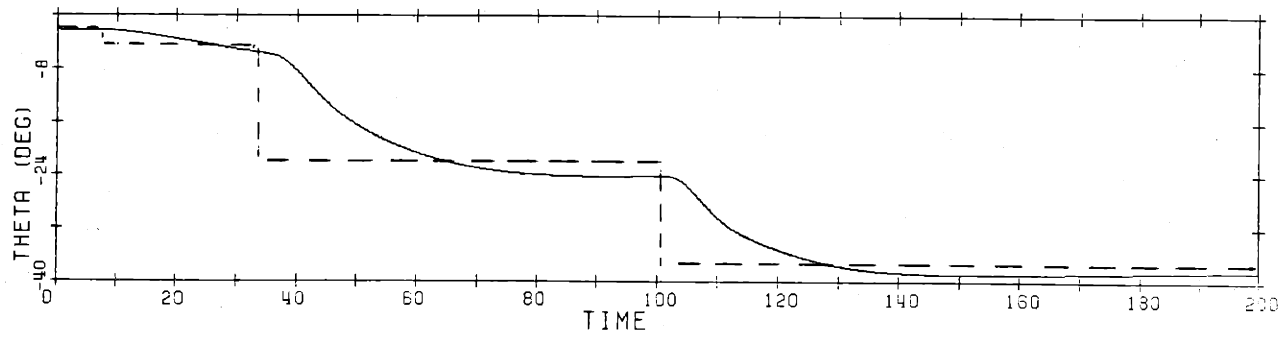

(d) Pitch angle θ(t)

Figure 5.2. Yaw Rate and Pitch Angle Cross Coupling
Test Number 1

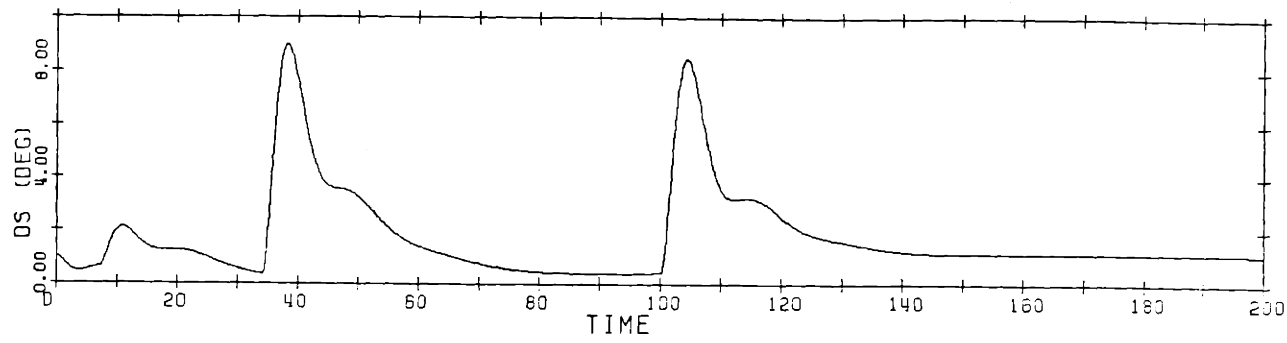

(e) Stern plane deflection

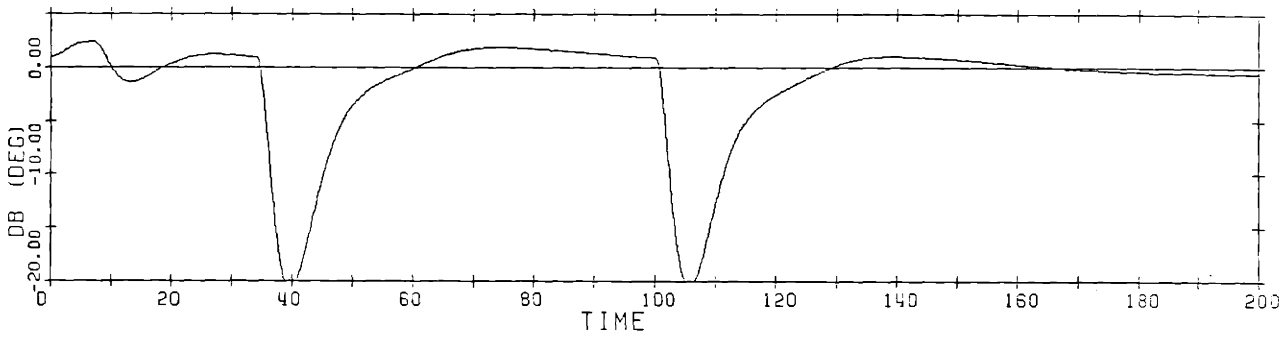

(f) Fairwater plane deflection

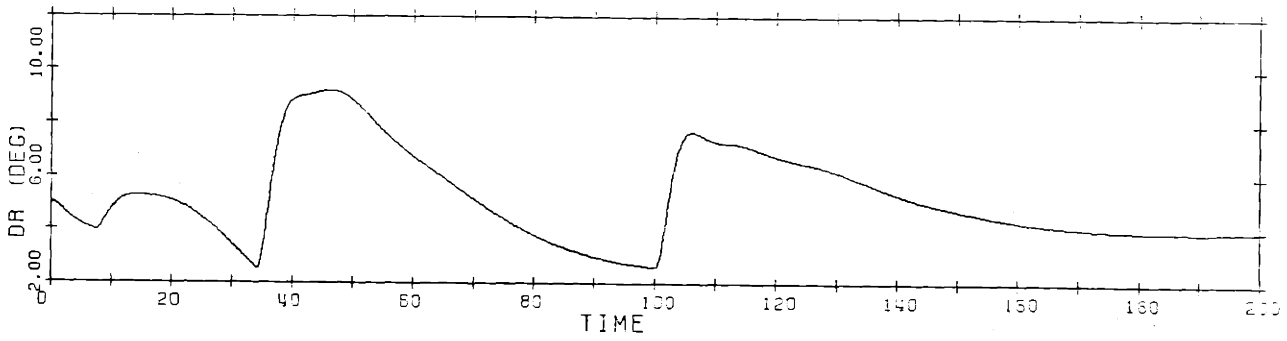

(g) Rudder deflection

Figure 5.2. (Cont'd)

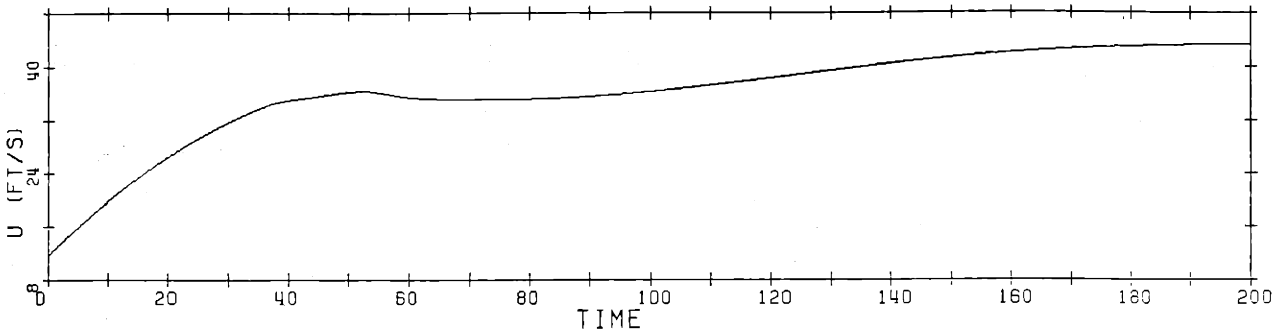

(a) Forward velocity u(t)

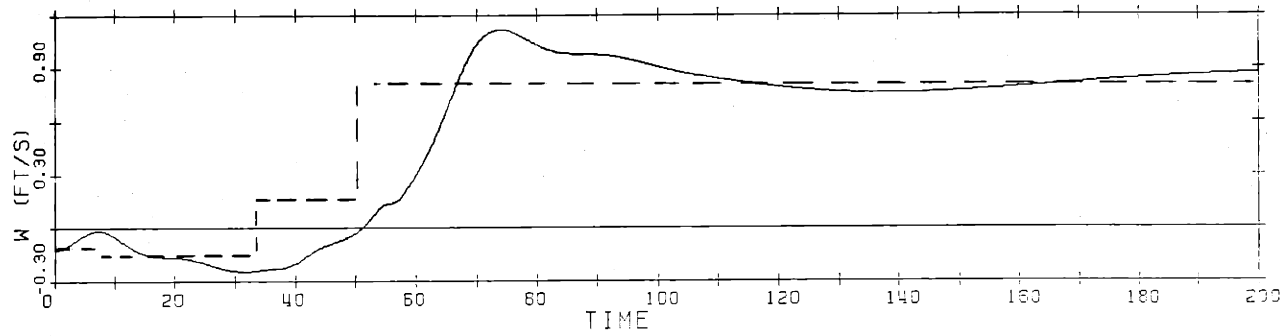

(b) Vertical rate w(t)

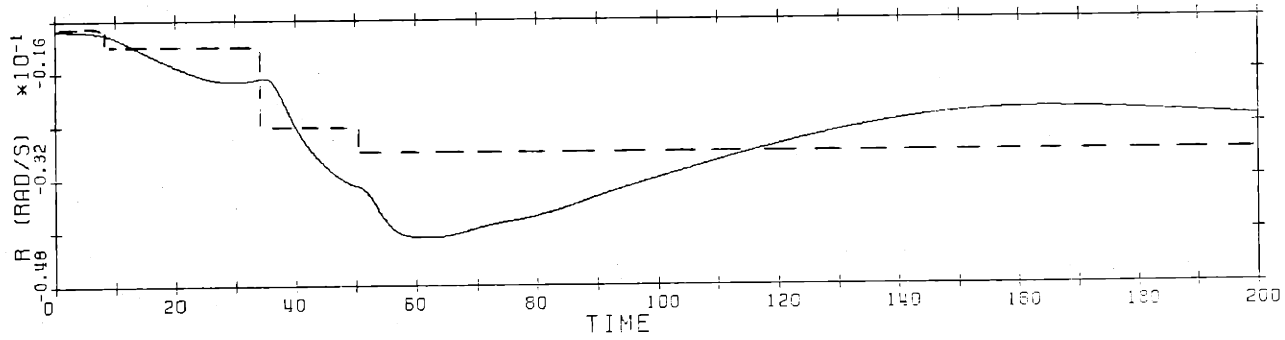

(c) Yaw rate r(t)

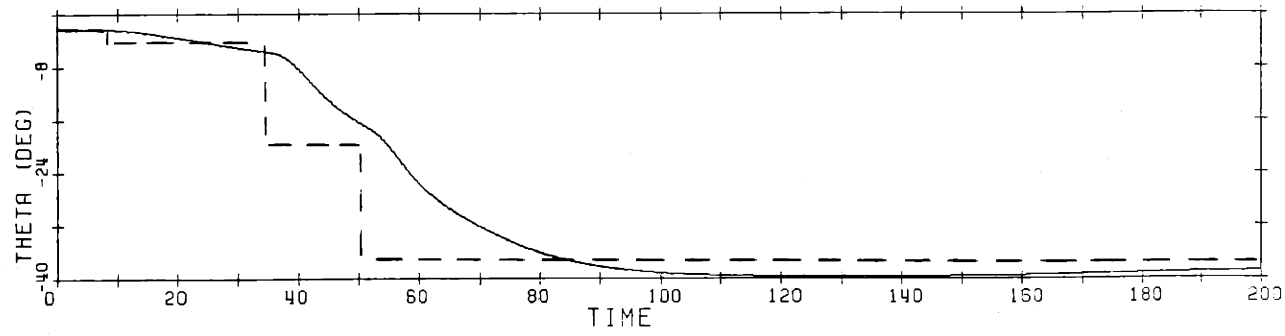

(d) Pitch angle θ(t)

Figure 5.3. Yaw Rate and Pitch Angle Cross Coupling Test Number 2

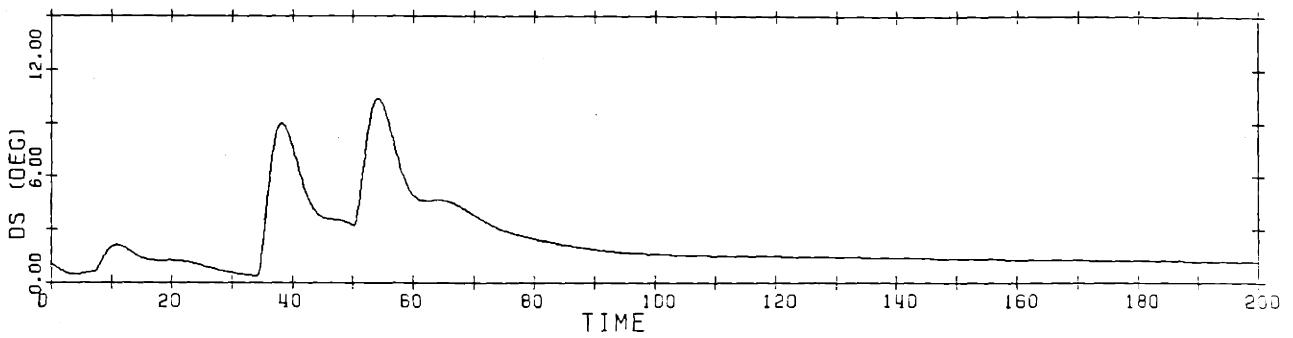

(e) Stern plane deflection

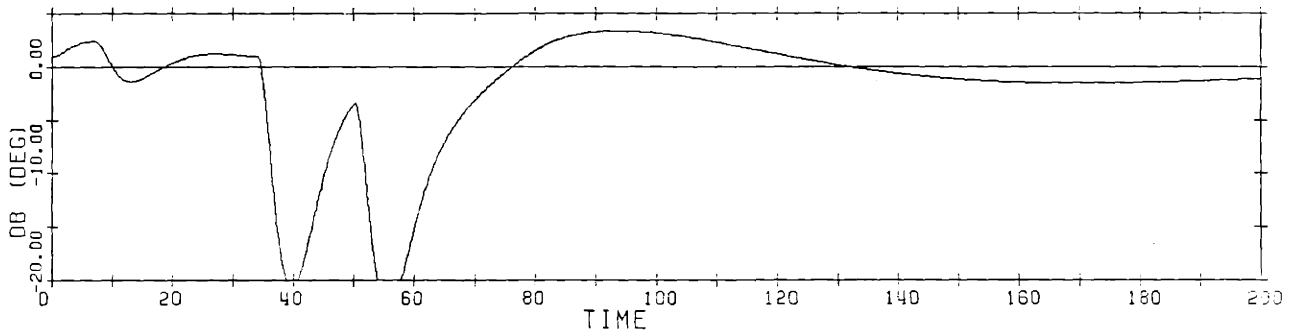

(f) Fairwater plane deflection

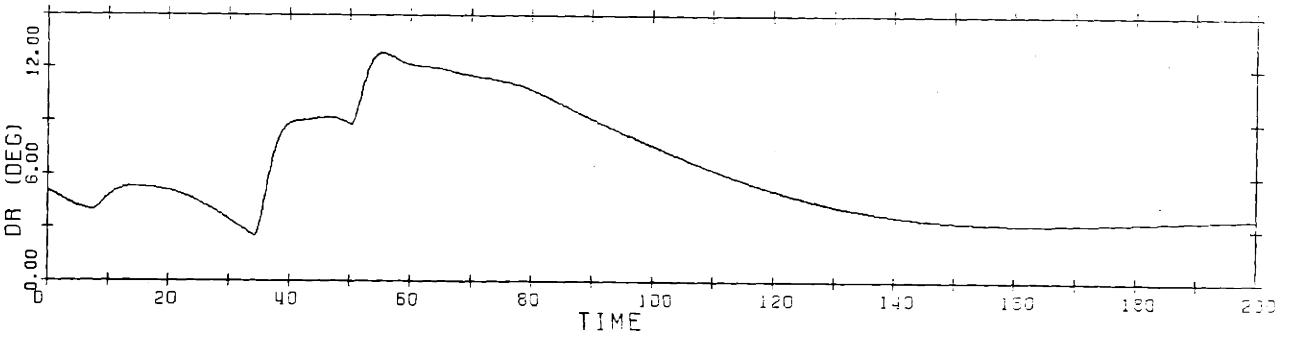

(g) Rudder deflection

Figure 5.3. (Cont'd)

deflections reveal that the degree of cross coupling is a function of the yaw rate error at the time when a step change is applied. In figure 5.2(c), the error in the yaw rate when the third step is applied is approximately 0.003 rad/sec whereas, in figure 5.2(c), it is nearly twice as large. The result is a larger overshoot for all three outputs and an increased rudder deflection. Furthermore, although the third step change was applied 50 seconds earlier in the second test, the errors at 200 seconds are larger than for the first test.

Time did not permit further investigation of the cross coupling present in the submarine model simulations. It should prove informative, however, to compare the simulations of figures 5.1, 5.2, and 5.3 to identical simulations for submarine models linearized about a straight and level trajectory.

The last test, shown in Figure 5.4, illustrates a speed increase from 5 to 25 knots with all commands set to zero. This simulation reveals an oscillatory response not present in any of the simulations presented so far. It occurred consistently for all tests of the nonlinear compensator involving a speed increase to approximately 30 knots and having significant time for settling out to steady state. It should be noted that the oscillations are quite small in

amplitude and are very lightly damped.

Although the cause of the oscillations was not determined, some phase lag appears to be present in the stern plane deflection compared to the error in θ. This indicates the requirement for more data points to accurately predict the model's behavior at higher speeds.

5.4 Summary

This chapter discussed the motivation for including the nonlinear aspects of the submarine model's response into the compensator design. The technique of gain scheduling was introduced as the method by which this could be accomplished, and the specific algorithm used was presented.

The first gain scheduling simulation, figure 5.1, highlights the application of this technique in the time history of the sail planes (figure 5.1(f)). Simulations using the full nonlinear controller were also presented that further demonstrated the cross coupling present in the submarine model.

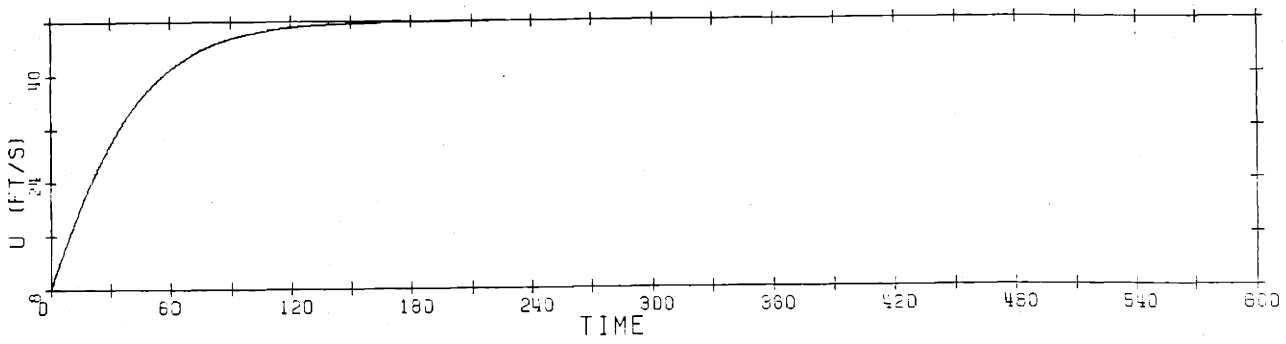

(a) Forward velocity u(t)

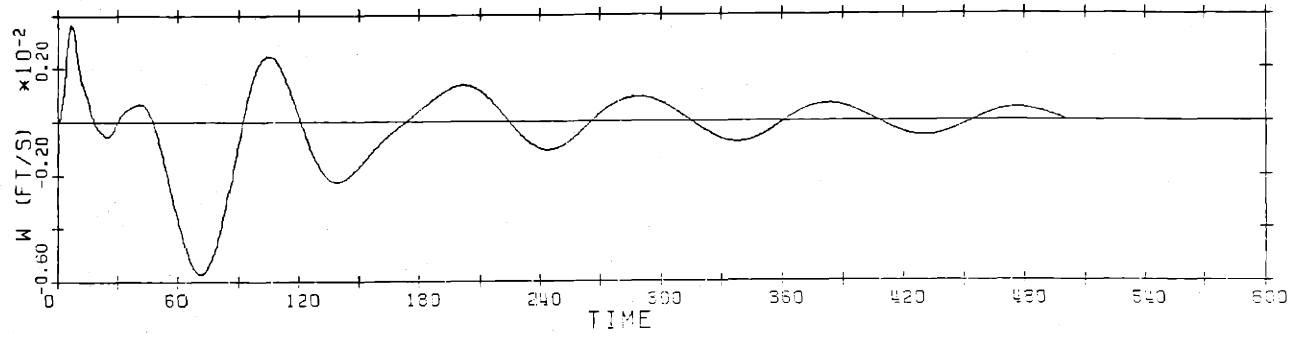

(b) Vertical rate w(t)

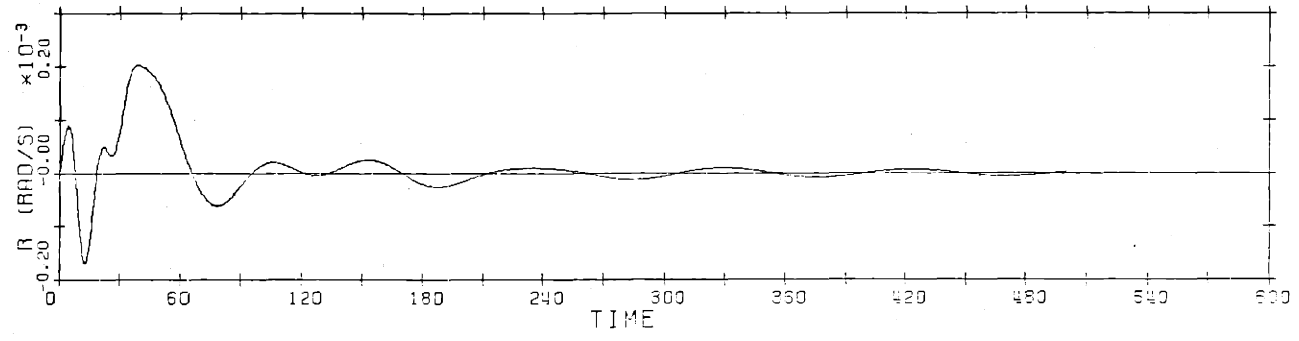

(c) Yaw rate r(t)

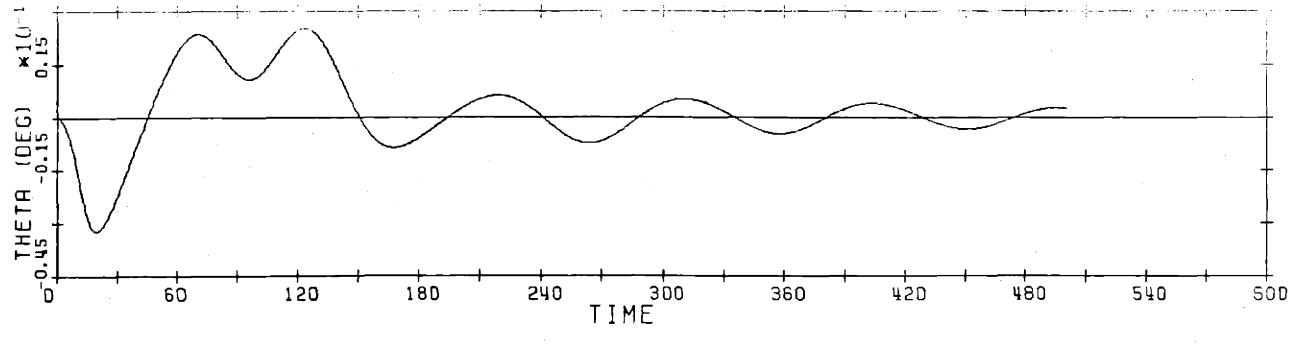

(d) Pitch angle θ(t)

Figure 5.4. High Speed Oscillations Produced by Gain Scheduling

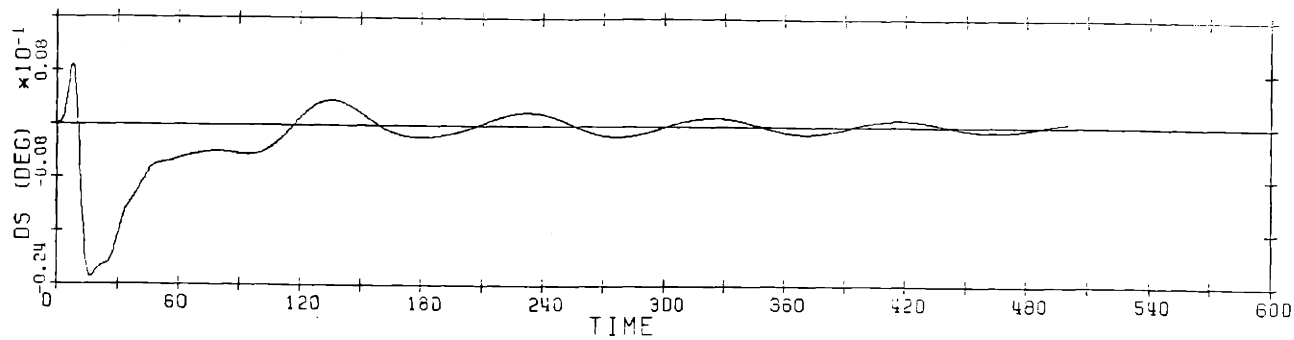

(e) Stern plane deflection

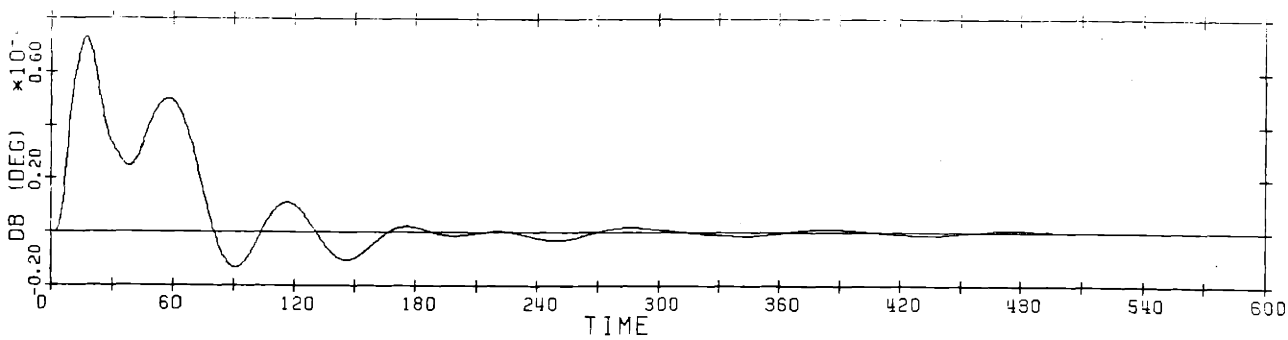

(f) Fairwater plane deflection

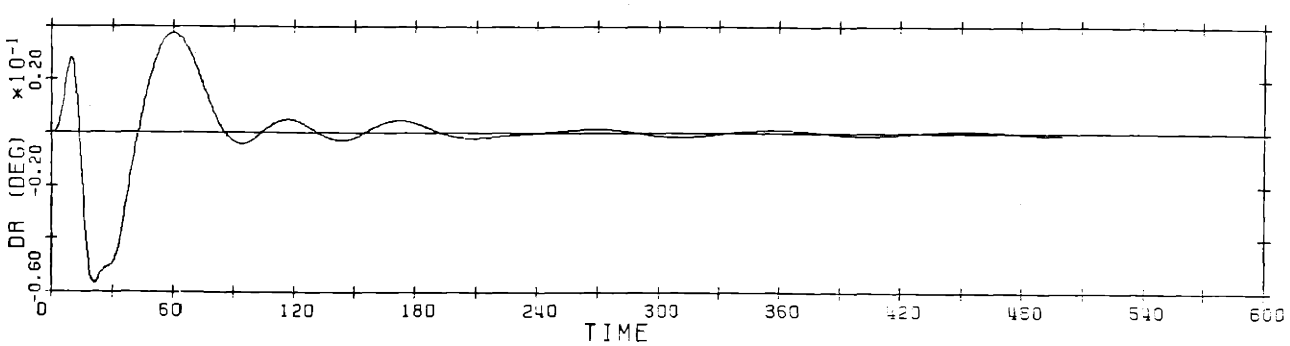

(g) Rudder deflection

Figure 5.4. (Cont'd)

Chapter 6

SUMMARY AND DIRECTIONS FOR FURTHER RESEARCH

6.1 Summary

This thesis has presented a multivariable control design example consisting of the following steps:

1. Four linear models of a full size submarine were developed using a computer implementation of the linear and nonlinear equations of motion.

2. The resulting models were reduced in order by inspection of the $\underline{A}$ and $\underline{B}$ matrices and subjected to modal analysis to determine their suitability for the LQG/LTR design procedure.

3. Response characteristics of the open loop nonlinear model were used to establish guidelines for performance specifications and additional dynamics were included in the models in the form of integrators in each input channel.

4. The controller was designed using the LQG/LTR combined time and frequency domain methodology as formulated by Stein, Doyle, et.al. Loop shaping techniques were independently developed that provided identical behavior of the singular values at both ends of the frequency spectrum for linear models using integral control.

5. A nonlinear capability was added to the controller design using the technique of gain scheduling. A second order polynomial was used to produce coefficients that enabled prediction of the compensator matrices for nominal points not modeled.

6.2 Some Conclusions and Directions for Further Research

Modal analysis should be used as a first step in any multivariable controller design. It not only provides all of the necessary information for proceeding with the design, but also provides invaluable reference material for determining the cause of any anomalies in the behavior of the model.

The techniques used in this thesis to match the singular

values of the Kalman Filter transfer matrix are simple and straight-forward. Unfortunately, they only apply when certain of the matrices used are invertible. An extension of this method to cover the case of noninvertible matrices using a perturbation matrix would provide a useful and general tool to the control system designer.

The extreme usefulness of singular value characterizations for multivariable systems was demonstrated in this thesis. The concept is an easily understood extension of the familiar Bode plots and provides a convenient means of describing and then ensuring the attainment of performance requirements for multivariable systems.

The cross coupling between yaw rate and pitch angle displayed by the submarine models used in this thesis requires further investigation. In particular, performance and transient response for models linearized about a straight and level trajectory should be compared to the simulations presented herein. Such a comparison should allow a determination to be made as to whether or not gain scheduling needs to performed on the basis of roll angle as well as forward velocity.

The gain scheduling algorithm described in the previous chapter is an idealization in that the compensator matrices were updated on each iteration of the integration. An

actual implementation of gain scheduling might require that an overlapping step type of approach be used to decrease both the computational burden and the possibility of introducing instabilities into the controller.

In so far as the purpose of this thesis was to present an LQG/LTR design example and demonstrate the technique of gain scheduling, the reference plane problem was ignored. Unfortunately, controlling a submarine in an inertial reference frame utilizing a body coordinate system somewhat abstracts the state space description of the submarine model. To make the conversion externally, however, presents the control system designer with a time varying C matrix. Replacement of the state variables w and r with the derivatives of z and Ψ would provide a more useful set of state variables for the purposes of controller design.

Although the submarine has six degrees of freedom in its environment, the three control surfaces permit the control of only three output variables. Of course the constant rpm constraint placed on the model in this thesis is artificial, and was intended only to reflect current operating procedures. The addition of propulsion control and differential action for the control surfaces (rudders and stern planes) would provide a total of 6 controls, yielding a much more flexible system.

Appendix A

State Space Matrices for the Linearized Models

The elements of the A and B matrices are presented in the standard row and column format. In the case of the A matrices, the 10 elements of each row are displayed as two rows, containing the first five elements in one row and the second five elements in the next.

Model S5R5

A Matrix

-.8532E-02	-.1166E-01	-.1594E-03	-.1001E-01	.2036E+00
.1590E+01	.0000E+00	.2954E-03	.0000E+00	.0000E+00
.1532E-02	-.4036E-01	.1187E-02	-.3551E+00	.1268E+00
-.2569E+01	.1318E+00	-.2805E-04	.0000E+00	.0000E+00
-.2690E-03	.6475E-03	-.2266E-01	-.8010E+00	.2183E+01
-.1840E-01	.0000E+00	.7616E-02	.0000E+00	.0000E+00
-.3420E-04	-.2184E-02	-.7419E-03	-.8579E-01	-.1323E+00
-.1544E-01	-.1621E+00	.3450E-04	.0000E+00	.0000E+00
-.7759E-05	.6245E-05	.2208E-03	-.6028E-02	-.8562E-01
-.5396E-03	.0000E+00	-.2512E-02	.0000E+00	.0000E+00
-.2941E-04	-.2764E-03	-.7509E-05	-.1346E-02	-.7110E-04
-.8534E-01	.2618E-03	-.5572E-07	.0000E+00	.0000E+00
.0000E+00	.0000E+00	.0000E+00	.1000E+01	.2128E-03
-.2027E-01	.5899E-12	-.6549E-02	.0000E+00	.0000E+00
.0000E+00	.0000E+00	.0000E+00	.0000E+00	.9999E+00
.1050E-01	.6547E-02	.0000E+00	.0000E+00	.0000E+00
.0000E+00	.0000E+00	.0000E+00	.0000E+00	-.1050E-01
.1000E+01	-.2911E-10	.1327E-03	.0000E+00	.0000E+00
.2027E-01	-.1050E-01	.9997E+00	.0000E+00	.0000E+00
.0000E+00	.7882E+00	-.9643E+01	.0000E+00	.0000E+00

B Matrix

-.1122E-02	-.2826E-02	-.1137E-01
.0000E+00	.0000E+00	.8949E-01
-.7633E-01	-.5624E-01	-.2885E-06
.0000E+00	.0000E+00	.1661E-02
-.1845E-02	.5402E-03	.9514E-07
.0000E+00	.0000E+00	-.2266E-02
.0000E+00	.0000E+00	.0000E+00
.0000E+00	.0000E+00	.0000E+00
.0000E+00	.0000E+00	.0000E+00
.0000E+00	.0000E+00	.0000E+00

Model S10R5

A Matrix

-.1491E-01	-.2067E-01	-.7935E-03	-.1777E-01	.2705E+00
.2832E+01	.0000E+00	.2948E-03	.0000E+00	.0000E+00
.2771E-02	-.7168E-01	.1182E-02	-.5860E+00	.2069E+00
-.4562E+01	.1314E+00	-.3061E-03	.0000E+00	.0000E+00
-.4935E-03	.1470E-02	-.4014E-01	-.1427E+01	.3871E+01
-.1274E-01	.0000E+00	.7599E-02	.0000E+00	.0000E+00
-.6136E-04	-.3913E-02	-.1330E-02	-.1522E+00	-.2374E+00
-.2096E-01	-.1616E+00	.3765E-03	.0000E+00	.0000E+00
-.1467E-04	.6635E-05	.3919E-03	-.1069E-01	-.1519E+00
-.1162E-02	.0000E+00	-.2506E-02	.0000E+00	.0000E+00
-.5373E-04	-.4895E-03	-.7697E-05	-.2670E-02	.8318E-03
-.1515E+00	.2611E-03	-.6081E-06	.0000E+00	.0000E+00
.0000E+00	.0000E+00	.0000E+00	.1000E+01	.2328E-02
-.7024E-01	.9818E-10	-.1168E-01	.0000E+00	.0000E+00
.0000E+00	.0000E+00	.0000E+00	.0000E+00	.9995E+00
.3312E-01	.1162E-01	.0000E+00	.0000E+00	.0000E+00
.0000E+00	.0000E+00	.0000E+00	.0000E+00	-.3320E-01
.1002E+01	-.1400E-08	.8189E-03	.0000E+00	.0000E+00
.7011E-01	-.3304E-01	.9970E+00	.0000E+00	.0000E+00
.0000E+00	.1398E+01	-.1709E+02	.0000E+00	.0000E+00

B Matrix

-.3512E-02	-.8903E-02	-.3582E-01
.0000E+00	.0000E+00	.2910E+00
-.2467E+00	-.1772E+00	-.9087E-06
.0000E+00	.0000E+00	.5191E-02
-.5992E-02	.1702E-02	.2997E-06
.0000E+00	.0000E+00	-.7404E-02
.0000E+00	.0000E+00	.0000E+00
.0000E+00	.0000E+00	.0000E+00
.0000E+00	.0000E+00	.0000E+00
.0000E+00	.0000E+00	.0000E+00

Model S20R5

A Matrix

-.2889E-01	-.4046E-01	-.6327E-02	-.3487E-01	-.4169E+00
.5643E+01	.0000E+00	.2754E-03	.0000E+00	.0000E+00
.5539E-02	-.1416E+00	-.8891E-02	-.6934E+00	.1803E+00
-.9060E+01	.1216E+00	-.6676E-02	.0000E+00	.0000E+00
-.1206E-02	.7565E-02	-.8581E-01	-.2851E+01	.7576E+01
.1720E+00	.0000E+00	.7099E-02	.0000E+00	.0000E+00
-.6092E-04	-.8099E-02	-.2414E-02	-.3005E+00	-.4355E+00
.2341E-01	-.1496E+00	.8211E-02	.0000E+00	.0000E+00
-.3405E-04	-.3369E-04	.7281E-03	-.2096E-01	-.2998E+00
-.5757E-02	.0000E+00	-.2342E-02	.0000E+00	.0000E+00
-.1078E-03	-.9620E-03	.4209E-04	-.7928E-02	.1271E-01
-.2994E+00	.2417E-03	-.1326E-04	.0000E+00	.0000E+00
.0000E+00	.0000E+00	.0000E+00	.1000E+01	.5434E-01
-.3853E+00	-.9059E-09	-.2650E-01	.0000E+00	.0000E+00
.0000E+00	.0000E+00	.0000E+00	.0000E+00	.9902E+00
.1397E+00	.2302E-01	.0000E+00	.0000E+00	.0000E+00
.0000E+00	.0000E+00	.0000E+00	.0000E+00	-.1499E+00
.1063E+01	.2498E-08	.9609E-02	.0000E+00	.0000E+00
.3626E+00	-.1302E+00	.9228E+00	.0000E+00	.0000E+00
.0000E+00	.2619E+01	-.3159E+02	.0000E+00	.0000E+00

B Matrix

-.1372E-01	-.3478E-01	-.1399E+00
.0000E+00	.0000E+00	.1137E+01
-.9636E+00	-.6921E+00	-.3550E-05
.0000E+00	.0000E+00	.2028E-01
-.2341E-01	.6648E-02	.1171E-05
.0000E+00	.0000E+00	-.2892E-01
.0000E+00	.0000E+00	.0000E+00
.0000E+00	.0000E+00	.0000E+00
.0000E+00	.0000E+00	.0000E+00
.0000E+00	.0000E+00	.0000E+00

Model S25R5

A Matrix

-.3521E-01	-.4803E-01	-.1255E-01	-.4146E-01	-.1606E+01
.6762E+01	.0000E+00	.2343E-03	.0000E+00	.0000E+00
.6953E-02	-.1718E+00	-.2605E-01	-.3137E+00	-.1038E+00
-.1124E+02	.1017E+00	-.1850E-01	.0000E+00	.0000E+00
-.1901E-02	.1686E-01	-.1060E+00	-.3427E+01	.9191E+01
.4173E+00	.0000E+00	.6039E-02	.0000E+00	.0000E+00
.3581E-04	-.1038E-01	-.2127E-02	-.3679E+00	-.3943E+00
.1083E+00	-.1251E+00	.2275E-01	.0000E+00	.0000E+00
-.4478E-04	-.9358E-04	.8713E-03	-.2491E-01	-.3681E+00
-.1325E-01	.0000E+00	-.1992E-02	.0000E+00	.0000E+00
-.1331E-03	-.1197E-02	.1125E-03	-.1242E-01	.2985E-01
-.3652E+00	.2020E-03	-.3676E-04	.0000E+00	.0000E+00
.0000E+00	.0000E+00	.0000E+00	.1000E+01	.1770E+00
-.7482E+00	-.2864E-08	-.4430E-01	.0000E+00	.0000E+00
.0000E+00	.0000E+00	.0000E+00	.0000E+00	.9731E+00
.2303E+00	.2784E-01	.0000E+00	.0000E+00	.0000E+00
.0000E+00	.0000E+00	.0000E+00	.0000E+00	-.2905E+00
.1227E+01	.4699E-08	.2700E-01	.0000E+00	.0000E+00
.6095E+00	-.1825E+00	.7715E+00	.0000E+00	.0000E+00
.0000E+00	.2750E+01	-.3285E+02	.0000E+00	.0000E+00

B Matrix

-.2061E-01	-.5221E-01	-.2101E+00
.0000E+00	.0000E+00	.1703E+01
-.1444E+01	-.1039E+01	-.5329E-05
.0000E+00	.0000E+00	.3046E-01
-.3508E-01	.9981E-02	.1758E-05
.0000E+00	.0000E+00	-.4333E-01
.0000E+00	.0000E+00	.0000E+00
.0000E+00	.0000E+00	.0000E+00
.0000E+00	.0000E+00	.0000E+00
.0000E+00	.0000E+00	.0000E+00

Appendix B

Modal Analysis Products

All matrices are presented in the standard row and column format. Additionally, the data in appendices B2 through B6 are complex numbers. These numbers are always displayed with the imaginary part directly below the real part. For example, each row of a matrix with complex entries would be displayed as two rows, the real parts in one row and the corresponding imaginary parts in the second row. The eigenvectors are presented as (complex) column vectors.

Appendix B1

Matrices Used to Perform Unit Transformations

1. Matrix used to premultiply both the A and B matrices:

1.0000E+00	0.0000E+00	0.0000E+00	0.0000E+00	0.0000E+00	0.0000E+00	0.0000E+00	0.0000E+00
0.0000E+00	1.0000E+00	0.0000E+00	0.0000E+00	0.0000E+00	0.0000E+00	0.0000E+00	0.0000E+00
0.0000E+00	0.0000E+00	1.0000E+00	0.0000E+00	0.0000E+00	0.0000E+00	0.0000E+00	0.0000E+00
0.0000E+00	0.0000E+00	0.0000E+00	5.7300E+01	0.0000E+00	0.0000E+00	0.0000E+00	0.0000E+00
0.0000E+00	0.0000E+00	0.0000E+00	0.0000E+00	5.7300E+01	0.0000E+00	0.0000E+00	0.0000E+00
0.0000E+00	0.0000E+00	0.0000E+00	0.0000E+00	0.0000E+00	5.7300E+01	0.0000E+00	0.0000E+00
0.0000E+00	0.0000E+00	0.0000E+00	0.0000E+00	0.0000E+00	0.0000E+00	5.7300E+01	0.0000E+00
0.0000E+00	0.0000E+00	0.0000E+00	0.0000E+00	0.0000E+00	0.0000E+00	0.0000E+00	5.7300E+01

2. Matrix used to postmultiply the A matrix only:

1.0000E+00	0.0000E+00	0.0000E+00	0.0000E+00	0.0000E+00	0.0000E+00	0.0000E+00	0.0000E+00
0.0000E+00	1.0000E+00	0.0000E+00	0.0000E+00	0.0000E+00	0.0000E+00	0.0000E+00	0.0000E+00
0.0000E+00	0.0000E+00	1.0000E+00	0.0000E+00	0.0000E+00	0.0000E+00	0.0000E+00	0.0000E+00
0.0000E+00	0.0000E+00	0.0000E+00	1.7452E-02	0.0000E+00	0.0000E+00	0.0000E+00	0.0000E+00
0.0000E+00	0.0000E+00	0.0000E+00	0.0000E+00	1.7452E-02	0.0000E+00	0.0000E+00	0.0000E+00
0.0000E+00	0.0000E+00	0.0000E+00	0.0000E+00	0.0000E+00	1.7452E-02	0.0000E+00	0.0000E+00
0.0000E+00	0.0000E+00	0.0000E+00	0.0000E+00	0.0000E+00	0.0000E+00	1.7452E-02	0.0000E+00
0.0000E+00	0.0000E+00	0.0000E+00	0.0000E+00	0.0000E+00	0.0000E+00	0.0000E+00	1.7452E-02

3. Matrix used to postmultiply the B matrix:

5.7300E+01	0.0000E+00	0.0000E+00
0.0000E+00	5.7300E+01	0.0000E+00
0.0000E+00	0.0000E+00	5.7300E+01

Appendix B2

Modal Decomposition for Model S5R5

Eigenvalues

-1.1277E-02	-2.6709E-02	-2.7689E-02	-2.7689E-02	-4.1686E-02	-4.1686E-02	-5.3308E-02	-9.8265E-02
0.0000E+00	0.0000E+00	1.7643E-02	-1.7643E-02	3.9761E-01	-3.9761E-01	0.0000E+00	0.0000E+00

Eigenvectors

9.9281E-01	7.4178E-01	8.9904E-02	8.9904E-02	-2.9654E-03	-2.9654E-03	-6.5228E-02	2.4125E-01
0.0000E+00	0.0000E+00	3.2552E-02	-3.2552E-02	-3.2693E-03	3.2693E-03	0.0000E+00	0.0000E+00
1.1961E-01	6.6500E-01	2.9770E-02	2.9770E-02	-2.2086E-01	-2.2086E-01	1.6124E-02	-9.7007E-01
0.0000E+00	0.0000E+00	-7.3528E-03	7.3528E-03	-2.7580E-01	2.7580E-01	0.0000E+00	0.0000E+00
-1.8966E-03	8.5962E-02	7.5459E-01	7.5459E-01	-5.5826E-01	-5.5826E-01	-9.6303E-01	-8.9253E-03
0.0000E+00	0.0000E+00	5.9693E-01	-5.9693E-01	-5.4402E-02	5.4402E-02	0.0000E+00	0.0000E+00
-2.9432E-05	2.5411E-04	1.7394E-03	1.7394E-03	-5.1519E-02	-5.1519E-02	-1.3353E-03	-1.8784E-03
0.0000E+00	0.0000E+00	1.3394E-04	-1.3394E-04	2.7309E-01	-2.7309E-01	0.0000E+00	0.0000E+00
7.6272E-05	-2.4696E-04	-6.8074E-03	-6.8074E-03	-4.0647E-03	-4.0647E-03	1.3928E-02	-2.5031E-04
0.0000E+00	0.0000E+00	4.8192E-03	-4.8192E-03	-9.2717E-04	9.2717E-04	0.0000E+00	0.0000E+00
-8.4622E-04	-3.5640E-03	-3.1491E-04	-3.1491E-04	-5.9911E-04	-5.9911E-04	1.1526E-04	-2.0701E-02
0.0000E+00	0.0000E+00	-2.7189E-06	2.7189E-06	-8.6137E-04	8.6137E-04	0.0000E+00	0.0000E+00
-1.7819E-03	-9.0614E-03	1.1554E-03	1.1554E-03	6.9284E-01	6.9284E-01	-6.9590E-03	1.5096E-02
0.0000E+00	0.0000E+00	-6.8116E-03	6.8116E-03	5.6878E-02	-5.6878E-02	0.0000E+00	0.0000E+00
-4.9409E-03	1.2868E-02	2.5288E-01	2.5288E-01	-1.5238E-03	-1.5238E-03	-2.6843E-01	3.7533E-03
0.0000E+00	0.0000E+00	-1.1295E-02	1.1295E-02	-1.0097E-03	1.0097E-03	0.0000E+00	0.0000E+00

Appendix B2 (cont'd)

Model S5R5

Controllability Matrix

3.2358E-03	2.2815E-03	-2.3825E-01
1.8821E-10	-1.2069E-10	1.3580E-11
8.3133E-03	-8.5165E-03	2.8357E-01
4.5045E-11	6.1762E-11	-1.3758E-11
-8.4924E-02	5.7770E-02	-7.9711E-03
8.5281E-02	2.7335E-02	5.7777E-03
-8.4924E-02	5.7770E-02	-7.9711E-03
-8.5281E-02	-2.7335E-02	-5.7777E-03
-1.4243E-03	1.5582E-04	4.9040E-04
7.2981E-05	4.1261E-05	-3.2950E-03
-1.4243E-03	1.5582E-04	4.9040E-04
-7.2982E-05	-4.1261E-05	3.2950E-03
-1.5716E-01	1.1410E-01	4.5351E-03
-7.2641E-10	-6.0431E-10	-1.7913E-10
2.5616E-04	2.5224E-04	7.0342E-02
7.8013E-12	7.6491E-13	3.6112E-13

Observability Matrix

-1.8966E-04	8.5962E-03	7.5459E-02	7.5459E-02	-5.5826E-02	-5.5826E-02	-9.6303E-02	-8.9253E-04
0.0000E+00	0.0000E+00	5.9693E-02	-5.9693E-02	-5.4402E-03	5.4402E-03	0.0000E+00	0.0000E+00
-8.4622E-04	-3.5640E-03	-3.1491E-04	-3.1491E-04	-5.9911E-04	-5.9911E-04	1.1526E-04	-2.0701E-02
0.0000E+00	0.0000E+00	-2.7189E-06	2.7189E-06	-8.6137E-04	8.6137E-04	0.0000E+00	0.0000E+00
-4.9409E-03	1.2868E-02	2.5288E-01	2.5288E-01	-1.5238E-03	-1.5238E-03	-2.6043E-01	3.7533E-03
0.0000E+00	0.0000E+00	-1.1295E-02	1.1295E-02	-1.0097E-03	1.0097E-03	0.0000E+00	0.0000E+00

Appendix B3

Modal Decomposition for Model S10R5

Eigenvalues

-1.9940E-02	-2.2087E-02	-2.2087E-02	-4.7861E-02	-7.2735E-02	-7.2735E-02	-1.4962E-01	-1.7528E-01
0.0000E+00	1.5563E-02	-1.5563E-02	0.0000E+00	3.8643E-01	-3.8643E-01	0.0000E+00	0.0000E+00

Eigenvectors

-9.9044E-01	-5.4762E-03	-5.4762E-03	-7.3665E-01	-9.3156E-03	-9.3156E-03	6.2379E-02	2.3753E-01
0.0000E+00	4.9564E-02	-4.9564E-02	0.0000E+00	4.8473E-03	-4.8473E-03	0.0000E+00	0.0000E+00
-1.2375E-01	2.0387E-03	2.0387E-03	-6.7361E-01	-2.9904E-01	-2.9904E-01	-3.5011E-02	-9.7065E-01
0.0000E+00	4.3490E-02	-4.3490E-02	0.0000E+00	2.2070E-01	-2.2070E-01	0.0000E+00	0.0000E+00
-5.9146E-02	6.5223E-01	6.5223E-01	-5.6862E-02	-2.0650E-01	-2.0650E-01	9.7768E-01	4.7148E-04
0.0000E+00	7.2698E-01	-7.2698E-01	0.0000E+00	7.1837E-01	-7.1837E-01	0.0000E+00	0.0000E+00
1.4378E-04	1.5976E-03	1.5976E-03	-6.4665E-04	1.8240E-01	1.8240E-01	-3.1077E-03	-6.2008E-03
0.0000E+00	-1.8616E-03	1.8616E-03	0.0000E+00	8.5333E-02	-8.5333E-02	0.0000E+00	0.0000E+00
-3.5989E-04	5.0126E-04	5.0126E-04	6.4362E-05	-2.6180E-03	-2.6180E-03	-2.9157E-02	-1.9973E-03
0.0000E+00	5.6592E-03	-5.6592E-03	0.0000E+00	4.7088E-03	-4.7088E-03	0.0000E+00	0.0000E+00
8.7144E-04	-1.0958E-04	-1.0958E-04	3.6271E-03	-1.3168E-03	-1.3168E-03	-2.0260E-04	-2.0382E-02
0.0000E+00	-1.6859E-04	1.6859E-04	0.0000E+00	5.2738E-04	-5.2738E-04	0.0000E+00	0.0000E+00
4.1896E-03	-7.3594E-03	-7.3594E-03	1.6890E-02	1.2725E-01	1.2725E-01	3.6117E-02	2.8127E-02
0.0000E+00	-1.4405E-02	1.4405E-02	0.0000E+00	-4.9625E-01	4.9625E-01	0.0000E+00	0.0000E+00
1.4149E-02	1.0443E-01	1.0443E-01	-7.9559E-03	-2.0542E-03	-2.0542E-03	1.9200E-01	1.3375E-02
0.0000E+00	-1.7467E-01	1.7467E-01	0.0000E+00	3.4431E-03	-3.4431E-03	0.0000E+00	0.0000E+00

Appendix B3 (cont'd)

Model S10R5

Controllability Matrix

2.3370E-02	2.9672E-03	7.7715E-01
-8.5265E-11	1.2147E-10	-1.1231E-10
-2.6650E-01	-1.5615E-02	-2.3874E-02
6.0766E-02	5.3014E-02	-3.6790E-02
-2.6650E-01	-1.5615E-02	-2.3874E-02
-6.0766E-02	-5.3014E-02	3.6790E-02
-1.5316E-02	-5.2494E-03	-9.1870E-01
-1.4236E-10	8.9197E-11	5.8874E-11
-2.1579E-03	-4.6727E-04	1.7865E-02
-1.1457E-02	1.3061E-03	2.6127E-03
-2.1579E-03	-4.6727E-04	1.7865E-02
1.1457E-02	-1.3061E-03	-2.6127E-03
1.7643E-01	-7.9939E-02	-1.8003E-02
-9.0616E-11	3.3785E-10	-1.8464E-10
1.2607E-03	1.0258E-03	2.3037E-01
-9.7488E-12	1.0880E-11	1.6121E-13

Observability Matrix

-5.9146E-03	6.5223E-02	6.5223E-02	-5.6862E-03	-2.0650E-02	-2.0650E-02	9.7768E-02	4.7148E-05
0.0000E+00	7.2698E-02	-7.2698E-02	0.0000E+00	7.1837E-02	-7.1837E-02	0.0000E+00	0.0000E+00
8.7144E-04	-1.0958E-04	-1.0958E-04	3.6271E-03	-1.3168E-03	-1.3168E-03	-2.0280E-04	-2.0382E-02
0.0000E+00	-1.6859E-04	1.6859E-04	0.0000E+00	5.2738E-04	-5.2738E-04	0.0000E+00	0.0000E+00
1.4149E-02	1.0443E-01	1.0443E-01	-7.9559E-03	-2.0542E-03	-2.0542E-03	1.9200E-01	1.3375E-02
0.0000E+00	-1.7467E-01	1.7467E-01	0.0000E+00	3.4431E-03	-3.4431E-03	0.0000E+00	0.0000E+00

Appendix B4

Modal Decomposition for Model S20R5

Eigenvalues

-1.5186E-02	-3.9975E-02	-5.7097E-02	-1.0087E-01	-1.3163E-01	-1.3163E-01	-3.2738E-01	-3.5236E-01
0.0000E+00	0.0000E+00	0.0000E+00	0.0000E+00	3.3086E-01	-3.3086E-01	0.0000E+00	0.0000E+00

Eigenvectors

2.7516E-02	9.6999E-01	-5.5826E-01	-6.9448E-01	2.3784E-02	2.3784E-02	2.2576E-02	-1.8898E-01
0.0000E+00	0.0000E+00	0.0000E+00	0.0000E+00	1.7398E-02	-1.7398E-02	0.0000E+00	0.0000E+00
-8.4185E-02	1.5467E-01	-2.9829E-01	-6.6735E-01	2.3921E-01	2.3921E-01	2.9231E-01	9.6823E-01
0.0000E+00	0.0000E+00	0.0000E+00	0.0000E+00	1.3985E-01	-1.3985E-01	0.0000E+00	0.0000E+00
9.3412E-01	-1.8540E-01	7.7235E-01	-2.6461E-01	8.4294E-01	8.4294E-01	-9.3751E-01	-1.2439E-01
0.0000E+00	0.0000E+00	0.0000E+00	0.0000E+00	-3.4306E-01	3.4306E-01	0.0000E+00	0.0000E+00
-8.6414E-03	4.9216E-04	-5.2264E-04	-3.5415E-03	-1.0906E-02	-1.0906E-02	3.7359E-02	3.5148E-02
0.0000E+00	0.0000E+00	0.0000E+00	0.0000E+00	-1.0192E-01	1.0192E-01	0.0000E+00	0.0000E+00
5.8466E-03	-9.3887E-04	2.9496E-03	-3.2382E-04	5.5002E-03	5.5002E-03	4.3709E-02	1.6220E-02
0.0000E+00	0.0000E+00	0.0000E+00	0.0000E+00	3.7303E-04	-3.7303E-04	0.0000E+00	0.0000E+00
9.0608E-04	-1.0715E-03	1.7350E-03	3.7323E-03	1.5456E-03	1.5456E-03	3.3164E-03	1.9053E-02
0.0000E+00	0.0000E+00	0.0000E+00	0.0000E+00	1.0937E-03	-1.0937E-03	0.0000E+00	0.0000E+00
-2.9824E-02	-2.5064E-03	-6.4512E-03	4.6243E-02	-2.5487E-01	-2.5487E-01	-1.2756E-01	-8.4999E-02
0.0000E+00	0.0000E+00	0.0000E+00	0.0000E+00	1.3604E-01	-1.3604E-01	0.0000E+00	0.0000E+00
-3.4436E-01	2.8443E-02	-5.2797E-02	-1.2540E-02	9.7445E-03	9.7445E-03	-1.2465E-01	-4.7581E-02
0.0000E+00	0.0000E+00	0.0000E+00	0.0000E+00	-3.2606E-03	3.2606E-03	0.0000E+00	0.0000E+00

Appendix B4 (cont'd)

Model S20R5

Controllability Matrix

```
 4.8721E-01 -4.4081E-03 -1.3048E-02
 1.2372E-09 -5.5467E-10 -4.4675E-10

-9.4816E-01 -2.1125E-01 -3.4301E+00
-5.3563E-10  5.5416E-10 -5.0415E-10

-2.7475E+00 -5.9278E-01 -1.1337E+00
-8.4954E-10  1.5149E-09  5.2273E-10

 8.8974E-01  2.5212E-01 -3.4319E+00
-3.4855E-10 -4.6942E-10 -1.0160E-09

 1.3605E-01  1.8850E-03 -2.7789E-01
 1.2245E-01 -2.6434E-02  1.0460E-01

 1.3605E-01  1.8850E-03 -2.7789E-01
-1.2245E-01  2.6434E-02 -1.0460E-01

-4.8970E-01  2.0629E-01  4.0265E-01
-1.1865E-11 -3.3707E-11  1.2161E-10

 7.6635E-02 -4.6328E-02 -9.4790E-01
 7.1173E-10  3.0513E-12 -4.8438E-10
```

Observability Matrix

```
 9.3412E-02 -1.8540E-02  7.7235E-02 -2.6461E-02  8.4294E-02  8.4294E-02 -9.3751E-02 -1.2439E-02
 0.0000E+00  0.0000E+00  0.0000E+00  0.0000E+00 -3.4306E-02  3.4306E-02  0.0000E+00  0.0000E+00

 9.0608E-04 -1.0715E-03  1.7350E-03  3.7323E-03  1.5456E-03  1.5456E-03  3.3164E-03  1.9053E-02
 0.0000E+00  0.0000E+00  0.0000E+00  0.0000E+00  1.0937E-03 -1.0937E-03  0.0000E+00  0.0000E+00

-3.4436E-01  2.8443E-02 -5.2797E-02 -1.2540E-02  9.7445E-03  9.7445E-03 -1.2465E-01 -4.7581E-02
 0.0000E+00  0.0000E+00  0.0000E+00  0.0000E+00 -3.2606E-03  3.2606E-03  0.0000E+00  0.0000E+00
```

Appendix B5

Modal Decomposition for Model S25R5

Eigenvalues

-1.3780E-02	-5.2016E-02	-6.5581E-02	-1.3479E-01	-1.5137E-01	-1.5137E-01	-4.2265E-01	-4.2265E-01
0.0000E+00	0.0000E+00	0.0000E+00	0.0000E+00	2.8421E-01	-2.8421E-01	1.3732E-02	-1.3732E-02

Eigenvectors

2.3608E-01	-9.6049E-01	-8.2586E-01	-6.2030E-01	6.5875E-03	6.5875E-03	-1.1512E-01	-1.1512E-01
0.0000E+00	0.0000E+00	0.0000E+00	0.0000E+00	3.9627E-02	-3.9627E-02	2.6062E-02	-2.6062E-02
-2.2885E-01	-2.1244E-01	-3.7152E-01	-6.0840E-01	3.1678E-02	3.1678E-02	6.5027E-01	6.5027E-01
0.0000E+00	0.0000E+00	0.0000E+00	0.0000E+00	2.4393E-01	-2.4393E-01	5.5980E-01	-5.5980E-01
8.9189E-01	1.7733E-01	4.2192E-01	-4.8881E-01	9.3640E-01	9.3640E-01	6.9853E-02	6.9853E-02
0.0000E+00	0.0000E+00	0.0000E+00	0.0000E+00	-5.0677E-02	5.0677E-02	-4.6114E-01	4.6114E-01
-1.2736E-02	-8.4670E-04	-1.4691E-03	-8.1065E-03	1.9822E-02	1.9822E-02	3.2410E-02	3.2410E-02
0.0000E+00	0.0000E+00	0.0000E+00	0.0000E+00	-7.0970E-02	7.0970E-02	5.3291E-02	-5.3291E-02
4.7857E-03	8.7070E-04	1.7415E-03	-6.5989E-04	4.2094E-03	4.2094E-03	8.5510E-03	8.5510E-03
0.0000E+00	0.0000E+00	0.0000E+00	0.0000E+00	2.2436E-03	-2.2436E-03	3.4444E-02	-3.4444E-02
1.8472E-03	1.4098E-03	2.2594E-03	3.7002E-03	1.3049E-03	1.3049E-03	1.3520E-02	1.3520E-02
0.0000E+00	0.0000E+00	0.0000E+00	0.0000E+00	1.3322E-03	-1.3322E-03	9.9004E-03	-9.9004E-03
-2.9714E-02	9.8925E-03	1.6055E-02	7.5885E-02	-2.2381E-01	-2.2381E-01	-5.4217E-02	-5.4217E-02
0.0000E+00	0.0000E+00	0.0000E+00	0.0000E+00	5.2374E-02	-5.2374E-02	-1.3278E-01	1.3278E-01
-3.0879E-01	-2.7826E-02	-4.0591E-02	-1.7234E-02	1.3502E-02	1.3502E-02	-2.0993E-02	-2.0993E-02
0.0000E+00	0.0000E+00	0.0000E+00	0.0000E+00	-7.3380E-04	7.3380E-04	-7.6633E-02	7.6633E-02

Appendix B5 (cont'd)

Model S25R5

Controllability Matrix

```
 6.2761E-01 -6.4231E-03  4.8521E-02
-4.7501E-09 -3.0469E-10 -8.7641E-09

 4.7783E+00  1.0456E+00  7.0500E+00
-1.8903E-09 -3.9480E-09 -2.8645E-08

-7.1170E+00 -1.5909E+00 -3.8872E+00
 1.5541E-09  5.1546E-09  3.6818E-08

 2.1303E+00  6.7327E-01 -5.0141E+00
-1.8064E-09 -4.6093E-10 -5.5881E-09

 3.2985E-01  7.6203E-03 -8.8275E-01
 2.6104E-01 -5.6660E-02  4.1026E-01

 3.2985E-01  7.6203E-03 -8.8275E-01
-2.6104E-01  5.6660E-02 -4.1026E-01

 3.9653E-01 -1.7981E-01 -1.1051E+00
 5.3461E-01 -2.1880E-01 -3.6675E-01

 3.9653E-01 -1.7981E-01 -1.1051E+00
-5.3461E-01  2.1880E-01  3.6675E-01
```

Observability Matrix

```
 8.9189E-02  1.7733E-02  4.2192E-02 -4.8881E-02  9.3640E-02  9.3640E-02  6.9853E-03  6.9853E-03
 0.0000E+00  0.0000E+00  0.0000E+00  0.0000E+00 -5.0677E-03  5.0677E-03 -4.6114E-02  4.6114E-02

 1.8472E-03  1.4098E-03  2.2594E-03  3.7002E-03  1.3049E-03  1.3049E-03  1.3520E-02  1.3520E-02
 0.0000E+00  0.0000E+00  0.0000E+00  0.0000E+00  1.3322E-03 -1.3322E-03  9.9004E-03 -9.9004E-03

-3.0879E-01 -2.7826E-02 -4.0591E-02 -1.7234E-02  1.3502E-02  1.3502E-02 -2.0993E-02 -2.0993E-02
 0.0000E+00  0.0000E+00  0.0000E+00  0.0000E+00 -7.3380E-04  7.3380E-04 -7.6633E-02  7.6633E-02
```

Appendix B6

Multivariable Zeros for all Models

Model S5R5

1.5030E+07 1.0854E+07 1.5425E+03 -8.4543E-03 -4.2165E-02 -4.2165E-02 -5.3654E-02 -1.5421E+03
0.0000E+00 0.0000E+00 0.0000E+00 0.0000E+00 3.9774E-01 -3.9774E-01 0.0000E+00 0.0000E+00

Model S10R5

9.0004E+10 7.0271E+04 -1.4778E-02 -7.4204E-02 -7.4204E-02 -9.6508E-02 -3.4771E+04 -3.4771E+04
0.0000E+00 0.0000E+00 0.0000E+00 3.8722E-01 -3.8722E-01 0.0000E+00 6.0715E+04 -6.0715E+04

Model S20R5

5.1882E+06 2.5141E+04 -2.8652E-02 -1.4188E-01 -1.4188E-01 -2.0274E-01 -2.5037E+04 -2.0296E+09
0.0000E+00 0.0000E+00 0.0000E+00 3.2942E-01 -3.2942E-01 0.0000E+00 0.0000E+00 0.0000E+00

Model S25R5

4.1257E+02 -3.5002E-02 -1.7204E-01 -1.7204E-01 -2.5599E-01 -1.0904E+03 -1.0904E+03 -1.2896E+04
-1.2806E+03 0.0000E+00 2.6989E-01 -2.6989E-01 0.0000E+00 7.9931E+02 -7.9931E+02 0.0000E+00

Appendix C

Gain Matrices and Properties of the Closed Loop Plant

Appendix C1

Kalman Filter Gain Matrices

Model S5R5

5.0993E-01 1.1576E-02 4.1466E-03 1.9263E-03 -6.8896E-03 -5.6557E-01
5.6308E-01 -4.7120E+01 -2.3271E-01 -7.6189E-01 -7.7504E+00

1.1576E-02 3.2717E-01 -1.5101E-03 -4.5847E-04 -1.0951E-02 -6.9427E-01
5.6803E-01 2.6916E+01 4.2244E-01 -4.4450E-01 5.2359E+00

4.1466E-03 -1.5101E-03 1.5507E-01 1.9535E-03 1.3183E-02 -1.1124E-02
5.3033E-02 -5.8194E-01 -4.7611E+00 -2.9808E-02 -8.5289E-02

Model S10R5

8.1776E-01 8.5743E-02 1.8005E-02 1.7876E-03 -8.3415E-03 -6.2216E-01
1.3793E+00 -3.0833E+01 -5.9833E-01 -7.1770E-01 -7.4749E+00

8.5743E-02 5.3248E-01 -5.2855E-03 -5.8788E-04 -2.1142E-02 -6.5491E-01
1.6640E+00 1.7290E+01 8.3463E-01 -3.7143E-01 6.1774E+00

1.8005E-02 -5.2855E-03 2.8319E-01 2.0265E-03 1.3008E-02 -1.5523E-02
1.3045E-01 -1.0776E+00 -4.8471E+00 -2.8398E-02 -2.5462E-01

Model S20R5

1.4466E+00 3.0242E-01 7.0806E-02 2.0844E-03 -9.0445E-03 -6.6804E-01
1.7005E+00 -1.9263E+01 -1.3559E+00 -6.3832E-01 -6.9217E+00

3.0242E-01 9.2461E-01 -4.6849E-02 -3.7150E-04 -3.2031E-02 -6.0270E-01
2.3851E+00 8.5952E+00 1.6947E+00 1.7106E-01 6.9342E+00

7.0806E-02 -4.6849E-02 5.6766E-01 2.1810E-03 1.4902E-02 -7.3951E-03
5.2001E-02 -2.4884E+00 -5.0834E+00 -6.6319E-02 -1.2386E+00

Model S25R5

1.7170E+00 4.1451E-01 1.0841E-01 2.4834E-03 -1.2226E-02 -6.7828E-01
1.7155E+00 -1.6714E+01 -1.7102E+00 -6.2142E-01 -6.6887E+00

4.1451E-01 1.0844E+00 -9.1668E-02 1.1144E-04 -3.9246E-02 -5.8804E-01
2.3852E+00 6.7242E+00 2.1371E+00 3.6577E-01 7.0179E+00

1.0841E-01 -9.1668E-02 7.0799E-01 2.2573E-03 1.6466E-02 -1.1536E-03
5.4931E-03 -3.3726E+00 -5.3772E+00 -1.3167E-01 -2.0380E+00

Appendix C2

Control Gain Matrices

Model S5R5

-1.0018E-02	-5.9555E-02	-5.0536E-02
-1.4786E-01	-4.9755E-02	4.0136E-02
-1.3888E-01	-9.8459E-01	-2.4462E-01
-2.0376E-02	2.1793E+00	3.7016E-02
-2.5016E-01	-2.2573E+00	-6.4614E-01
3.6744E-01	4.3158E-02	2.3112E-02
2.0608E-04	1.2104E-03	6.4495E-04
1.1480E-04	1.2507E-04	1.2895E-04
4.3158E-03	3.3125E-02	8.1370E-03
-4.6205E-04	1.5528E-02	4.8522E-03
2.3112E-03	8.1370E-03	4.0875E-02

Model S10R5

-6.3100E-03	-2.9297E-02	-2.1827E-02
-1.1706E-01	-1.0929E-01	-2.3457E-03
-1.1104E-01	-6.8330E-01	-1.6012E-01
-4.2047E-02	3.6708E+00	4.1904E-01
-4.0679E-01	-3.2997E+00	-9.9766E-01
4.7272E-01	6.5458E-02	2.1223E-02
9.9092E-04	5.0252E-03	1.8244E-03
3.8495E-05	-9.8181E-04	-1.6970E-04
6.5458E-03	4.2779E-02	1.0618E-02
-3.2026E-04	4.5913E-02	1.5766E-02
2.1223E-03	1.0618E-02	5.1121E-02

Appendix C2 (cont'd)

Control Gain Matrices

Model S20R5

-3.0768E-04	1.8691E-02	-2.6678E-03
-9.9578E-02	-3.1810E-01	-4.3207E-02
-5.2549E-02	-4.0681E-01	-5.9456E-02
-4.0965E-01	6.7546E+00	1.5694E+00
-4.7391E-02	-4.6661E+00	-8.8520E-01
6.1100E-01	5.4639E-02	8.5040E-03
3.8992E-03	2.8093E-02	3.5058E-03
-5.6741E-05	-1.0044E-02	-1.5228E-03
5.4639E-03	5.0574E-02	8.1331E-03
-3.9308E-02	1.6695E-01	3.6961E-02
8.5040E-04	8.1331E-03	5.8230E-02

Model S25R5

2.3797E-03	3.3659E-02	-3.7276E-03
-9.5498E-02	-4.4344E-01	-5.8065E-03
-3.4741E-02	-3.1467E-01	-5.7352E-04
-1.1024E+00	8.0306E+00	1.5822E+00
3.4893E-01	-4.6157E+00	-4.8207E-02
7.7970E-01	3.5628E-02	4.7694E-02
3.2007E-03	4.8469E-02	-4.5751E-03
9.6791E-04	-1.7839E-02	1.5633E-04
3.5628E-03	4.6351E-02	2.2212E-04
-1.1216E-01	2.4663E-01	1.7557E-02
4.7694E-03	2.2212E-04	5.7978E-02

Appendix C3

Poles of the Closed Loop Model

Real Part

-7.6489E-01	-7.6489E-01	-6.2486E-01	-3.1063E-01	-3.1063E-01	-3.9014E-01
-3.9014E-01	-1.3606E-01	-1.3606E-01	-1.5198E-01	-1.5198E-01	-3.2827E-01
-3.5318E-01	-2.0624E-01	-1.2874E-01	-5.7009E-02	-5.7009E-02	-5.7206E-02
	-2.8649E-02	-1.3031E-02	-1.3031E-02	-4.6457E-02	

Imaginary Part

7.7616E-01	-7.7616E-01	0.0000E+00	4.5795E-01	-4.5795E-01	3.4961E-01
-3.4961E-01	3.3397E-01	-3.3397E-01	3.2898E-01	-3.2898E-01	0.0000E+00
0.0000E+00	0.0000E+00	0.0000E+00	5.1976E-02	-5.1976E-02	0.0000E+00
	0.0000E+00	6.1984E-03	-6.1984E-03	0.0000E+00	

Zeros of the Closed Loop Model

Real Part

3.3022E+02	3.3022E+02	1.7580E+02	5.2209E+01	-1.7678E-02	-1.7678E-02
-2.8652E-02	-9.0911E-02	-9.0911E-02	-1.3101E-01	-1.3101E-01-	1.4188E-01
-1.4188E-01	-2.0274E-01	-3.2526E-01	-3.4898E-01	-4.2233E-01	-4.2234E-01
	-5.3055E+01	-8.8860E+01	-8.8860E+01	-8.1268E+02	

Imaginary Part

6.5409E+02	-6.5409E+02	0.0000E+00	0.0000E+00	3.0012E-03	-3.0012E-03
0.0000E+00	2.2508E-02	-2.2508E-02	3.0736E-01	-3.0736E-01	3.2942E-01
-3.2942E-01	0.0000E+00	0.0000E+00	0.0000E+00	5.2639E+01	-5.2639E+01
	0.0000E+00	1.5280E+02	-1.5280E+02	0.0000E+00	

Appendix D

Gain Scheduling Algorithm and Coefficients

The program in appendix D1 is written in Fortran 77 for the Microsoft compiler. It should run on any computer having a Fortran 77 compiler with modifications required only for the input/output statements.

Appendix D1

Fortran Program to Produce the Gain Scheduling Coefficients

```
      program matlsq
c
c     parabolic least squares fit with order of polynomial taken
c     as input from the console (max order = 3)
c     adapted from the Fortran program by Alan R. Miller
c     this version handles matrices up to 11 x 11
c
      integer maxr,maxc,lines,nrow,ncol,matr,matc,maxsiz
      real x(5),ymat(11,11,5),y(5)
      real coef(11,11,5),correl,c(4)
      character*1 answer
      character*15 fname(5), dskfile, prnfile
      character*60 title
      common /sizes/ nrow,ncol,matr,matc
      common /files/ fname
      data maxr,maxc,maxsiz/5, 4, 11/
c
      write(*,'(A)') ' Specify title for this run: (60 chars)'
      read(*,103) title
      call input(x,ymat,maxr,maxc,maxsiz)
c
c   Now do the least squares fit, storing the ncol coeff's for the
c   i,j term in the matrix coeff(i,j,k) for k=1 to ncol.  Store the
c   correlation coefficient in coeff(i,j,ncol+1).
c
      do 20 i=1,matr
         do 20 j=1,matc
            do 10 k=1,nrow
10              y(k) = ymat(i,j,k)
            call linfit(x,y,c,correl,maxr,maxc)
            do 15 k=1,ncol
15              coef(i,j,k) = c(k)
            coef(i,j,ncol+1) = correl
20    continue
```

Appendix D1 (cont'd)

Fortran Program to Produce the Gain Scheduling Coefficients

```
c
c   Determine what type of output is desired
c
        write(*,'(A\)') ' Write coefficients to output device? (Y/N) '
        read(*,100)answer
        if(answer .eq. 'y' .or. answer .eq. 'Y') then
            write(*,'(A\)') ' Disk file for Draper? (Y/N) '
            read(*,100)answer
            if(answer .eq. 'Y' .or. answer .eq. 'y')then
                write(*,'(A)') ' Enter the output filename: '
                write(*,'(A)') ' (example:  ''b:coeff.dat'')'
                read(*,*) dskfile
                write(*,'(A)') ' Writing output file.......'
                open(7, FILE = dskfile, STATUS = 'NEW')
                write(7,104) title
                write(7,'(A)') ' (first coeff is the constant term)'
                do 30 i=1,matr
                    do 30 j=1,matc
30                      write(7,105)i,j,(coef(i,j,k), k=1, ncol)
                write(*,'(A)') ' '
                close(7)
            endif
            write(*,'(A\)') ' Disk file for printing? (Y/N) '
            read(*,100)answer
            if(answer .eq. 'Y' .or. answer .eq. 'y')then
                write(*,'(A)') ' Enter the output filename: '
                write(*,'(A)') ' (example:  ''d:coeff.lst'')'
                read(*,*) prnfile
                write(*,'(A)') ' Writing output file.......'
                open(8, FILE = prnfile, STATUS = 'NEW')
                write(8,104) title
                write(8,101)
                do 35 i=1,matr
                    do 35 j=1,matc
35                      write(8,102) i,j,coef(i,j,ncol+1),
     1                                (coef(i,j,k),k=1,ncol)
                close(8)
            endif
        endif
```

Fortran Program to Produce the Gain Scheduling Coefficients

```
100     format(a1)
101     format(' element',3x,'correlation',3x,
     1             'coefficients(low order to high order)'/)
102     format(' (',i2,',',i2,')',3x,e10.4,3x,5(e10.4,2x))
103     format(a60)
104     format(' ',a60)
105     format(2x,i2,1x,i2,1x,e12.6,2x,e12.6,2x,e12.6,2x,e12.6)
        end
c
        subroutine input(x,ymat,maxr,maxc,maxsiz)
        integer nrow,i,maxr,maxc,ncol,matr,matc,maxsiz
        real x(5),ymat(11,11,5)
        character*15 fname(5)
        common /sizes/ nrow,ncol,matr,matc
        common /files/ fname
c
5       write(*,'(A\)') ' Order of polynomial to use? '
        read(*,*)ncol
        if(ncol .gt. maxc-1)goto 5
        if(ncol .lt. 1) stop
        ncol = ncol+1
10      write(*,'(A\)') ' Number of speeds? '
        read(*,*)nrow
        if(nrow .lt. ncol .or. nrow .gt. maxr)goto 10
        write(*,'(A)') ' Enter the speeds and corresponding filenames: '
        write(*,'(A)') ' (example:  20.0  ''b:abghc.s20'')'
        read(*,*) (x(i),fname(i), i=1,nrow)
15      write(*,'(A\)') ' Specify matrix dimensions: (row,col) '
        read(*,*) matr,matc
        if(matr .gt. maxsiz .or. matc .gt. maxsiz) goto 15
        write(*,'(A)') ' Reading input matrices.....'
        do 20 i=1,nrow
           open(i, FILE = fname(i))
           read(i,100) ((j,k,ymat(j,k,i), m=1,matc), n=1,matr)
           close(i)
20      continue
        write(*,101)
        return
100     format(1x,i2,1x,i2,1x,e16.10,1x,i2,1x,i2,1x,e16.10,
     1         1x,i2,1x,i2,1x,e16.10)
101     format('0')
        end
```

Fortran Program to Produce the Gain Scheduling Coefficients

```
      subroutine linfit(x,y,coef,cor,maxr,maxc)
      logical error
      integer nrow,ncol,i,j,maxr,maxc,matr,matc
      integer index(5,5),nvec
      real x(1),y(1),coef(1)
      real a(5,5),xmatr(5,5)
      real sumy,sumy2,xi,yi,yc,res,cor,srs
      common /sizes/ nrow,ncol,matr,matc
      data nvec/1/
c
      do 10 i=1,nrow
         xi = x(i)
         xmatr(i,1)=1.0
         do 10 j=2,ncol
            xmatr(i,j)= xmatr(i,j-1)*xi
10    continue
      call square(xmatr,y,a,coef,maxr,maxc)
      call gaussj(a,coef,index,nvec,error,maxc)
      sumy = 0.0
      sumy2 = 0.0
      srs = 0.0
      do 20 i=1,nrow
         yi = y(i)
         yc = 0.0
         do 15 j = 1, ncol
15          yc = yc + coef(j) * xmatr(i,j)
         res = yc - yi
         srs = srs + res*res
         sumy = sumy + yi
         sumy2 = sumy2 + yi * yi
20    continue
c   take care of the case where the y(i) are all zero
c   this is guaranteed to produce zero coefficients so cor = 1.0
      if(sumy .eq. 0.0) then
         cor = 1.0
      else
         cor = sqrt(1.0-srs/(sumy2-sumy*sumy/nrow))
      endif
      return
      end
```

Fortran Program to Produce the Gain Scheduling Coefficients

```
      subroutine square(x,y,a,g,maxr,maxc)
      integer nrow,ncol,i,k,l,matr,matc,maxr,maxc
      real x(maxr,maxc),y(maxr),a(maxc,maxc),g(maxc)
      common /sizes/ nrow,ncol,matr,matc
c
      do 40 k=1,ncol
         do 20 l=1,k
            a(k,l)=0.0
            do 10 i=1,nrow
               a(k,l)=a(k,l)+x(i,l)*x(i,k)
               if(k .ne. 1) a(l,k) = a(k,l)
10          continue
20       continue
         g(k) = 0.0
         do 30 i=1,nrow
            g(k)=g(k)+y(i)*x(i,k)
30       continue
40    continue
      return
      end
c
      subroutine gaussj(b,w,index,nvec,error,maxc)
      logical error
      integer nrow,i,j,k,l,nvec,matr,matc,maxsiz,maxc
      integer irow,icol,ll,index(maxc,3)
      real b(maxc,1),w(maxc,1),big,sum,t,pivot,determ
      common /sizes/ nrow,ncol,matr,matc
c
      error = .false.
      n = ncol
      do 10 i=1,n
         index(i,3)=0
10    continue
      determ = 1.0
      do 90 i=1,n
         big = 0.0
         do 20 j=1,n
            if(index(j,3) .eq. 1)goto 20
            do 15 k=1,n
               if(index(k,3) .gt. 1)goto 199
               if(index(k,3) .eq. 1) goto 15
               if(abs(b(j,k)) .le. big)goto 15
               irow = j
               icol = k
               big = abs(b(j,k))
15          continue
20       continue
```

Fortran Program to Produce the Gain Scheduling Coefficients

```
            index(icol,3) = index(icol,3) + 1
            index(i,2) = irow
            index(i,1) = icol
            if(irow .eq. icol)goto 40
            determ = -determ
            do 25 l=1,n
               call swap(b(irow,l),b(icol,l))
25          continue
            if(nvec .eq. 0)goto 40
            do 30 l=1,nvec
               call swap(w(irow,l),w(icol,l))
30          continue
40          pivot = b(icol,icol)
            determ = determ*pivot
            b(icol,icol)= 1.0
            do 45 l=1,n
               b(icol,l)=b(icol,l)/pivot
45          continue
            if(nvec .eq. 0)goto 60
            do 50 l=1,nvec
               w(icol,l) = w(icol,l)/pivot
50          continue
60          do 80 l1=1,n
               if(l1 .eq. icol)goto 80
               t = b(l1,icol)
               b(l1,icol) = 0.0
               do 65 l=1,n
                  b(l1,l) = b(l1,l)-b(icol,l)*t
65             continue
               if(nvec .eq. 0)goto 80
               do 70 l=1,nvec
                  w(l1,l) = w(l1,l)-w(icol,l)*t
70             continue
80          continue
90       continue
         do 120 i=1,n
            l = n - i +1
            if(index(l,1) .eq. index(l,2))goto 120
            irow = index(l,1)
            icol = index(l,2)
            do 110 k = 1,n
               call swap(b(k,irow),b(k,icol))
110         continue
120      continue
```

Fortran Program to Produce the Gain Scheduling Coefficients

```
      do 130 k=1,n
         if(index(k,3) .ne. 1)goto 199
130   continue
      return
199   write(*,999)
      error = .true.
      return
999   format(' ERROR - matrix singular')
      end
c
      subroutine swap(a,b)
      real a,b,hold
      hold = a
      a = b
      b = hold
      return
      end
```

Appendix D2

A-BG-HC matrix coefficients

element	correlation	coefficients (low order to high order)		
(1, 1)	.9999E+00	-.1694E+00	-.6835E-01	.2494E-03
(1, 2)	.9996E+00	.6212E-01	-.1287E-01	-.2528E-03
(1, 3)	.1000E+01	.2333E-02	-.4777E-03	-.1583E-03
(1, 4)	.9998E+00	-.2230E-02	.7932E-04	-.3585E-05
(1, 5)	.9479E+00	.7586E-02	-.1184E-03	.1153E-04
(1, 6)	.9972E+00	.5033E+00	.1461E-01	-.3083E-03
(1, 7)	.9850E+00	.3162E+00	-.2128E+00	.5342E-02
(1, 8)	.9954E+00	.6508E+02	-.4195E+01	.9159E-01
(1, 9)	.9999E+00	-.5577E-01	.6878E-01	.2617E-04
(1,10)	.9987E+00	.8225E+00	-.1267E-01	.1820E-03
(1,11)	.9999E+00	.8144E+01	-.7023E-01	.4817E-03
(2, 1)	.9996E+00	.6212E-01	-.1287E-01	-.2528E-03
(2, 2)	.9999E+00	-.9588E-01	-.4723E-01	.3033E-03
(2, 3)	.9995E+00	.1423E-01	-.3771E-02	.2736E-03
(2, 4)	.9966E+00	.7009E-04	.9534E-04	-.4082E-05
(2, 5)	.9954E+00	.2375E-02	.1945E-02	-.1984E-04
(2, 6)	.9999E+00	.7592E+00	-.1101E-01	.1825E-03
(2, 7)	.9968E+00	.7432E+00	-.3063E+00	.7306E-02
(2, 8)	.9985E+00	-.3801E+02	.2533E+01	-.5170E-01
(2, 9)	.1000E+01	-.1555E-01	-.7298E-01	.2372E-03
(2,10)	.9921E+00	.5869E+00	-.1893E-01	-.8110E-03
(2,11)	.9976E+00	-.4239E+01	-.2394E+00	.5186E-02
(3, 1)	.1000E+01	.2333E-02	-.4777E-03	-.1583E-03
(3, 2)	.9995E+00	.1423E-01	-.3771E-02	.2736E-03
(3, 3)	.9999E+00	-.2462E-01	-.2536E-01	-.8143E-04
(3, 4)	.1000E+01	-.1879E-02	-.1460E-04	-.2144E-07
(3, 5)	.9984E+00	-.1373E-01	.1785E-03	-.1159E-04
(3, 6)	.9912E+00	.2321E-01	.8328E-03	-.6426E-04
(3, 7)	.9227E+00	.2195E-01	-.2131E-01	.8262E-03
(3, 8)	.1000E+01	.2034E+00	.6213E-01	.2590E-02
(3, 9)	.9992E+00	.6111E+01	-.8634E-01	.2780E-02
(3,10)	.9952E+00	.6388E-01	-.8520E-02	.4451E-03
(3,11)	.9999E+00	.4404E+00	-.4512E-01	.4371E-02
(4, 1)	.9998E+00	.1433E-03	-.8452E-04	-.2997E-04
(4, 2)	.9998E+00	.4106E-03	-.2215E-03	-.7572E-04
(4, 3)	.9998E+00	.1652E-02	-.8909E-03	-.3046E-03
(4, 4)	.9998E+00	-.1616E-02	-.1360E-02	.4314E-06
(4, 5)	.9994E+00	-.8778E-03	-.2140E-02	.9642E-05
(4, 6)	.9907E+00	.3420E-01	-.7847E-02	.4101E-03
(4, 7)	.9994E+00	-.7685E-03	-.1833E-02	.7781E-05
(4, 8)	.9958E+00	-.4556E+00	.1650E+00	-.8371E-02
(4, 9)	.9967E+00	-.3616E+00	-.5120E-01	.6185E-03
(4,10)	.1000E+01	.0000E+00	.0000E+00	.0000E+00
(4,11)	.9848E+00	.7706E+00	-.1587E+00	.2462E-02

Appendix D2 (cont'd)

A-BG-HC matrix coefficients

element	correlation	coefficients (low order to high order)		
(5, 1)	.1000E+01	.0000E+00	.0000E+00	.0000E+00
(5, 2)	.1000E+01	.0000E+00	.0000E+00	.0000E+00
(5, 3)	.9998E+00	-.2143E-01	.8462E-02	.2433E-02
(5, 4)	.1000E+01	.3066E-03	.2370E-03	.1173E-05
(5, 5)	.9997E+00	-.5286E-02	-.6884E-02	.7536E-05
(5, 6)	.9998E+00	-.1165E-01	.1008E-01	-.4830E-03
(5, 7)	.9666E+00	.1818E+00	-.1226E+00	.4071E-02
(5, 8)	.9735E+00	-.1456E+00	.6308E-01	-.2428E-02
(5, 9)	.1000E+01	.1911E+00	-.5891E-01	-.8543E-02
(5,10)	.9907E+00	.1214E+00	.2518E-02	-.1306E-03
(5,11)	.9870E+00	-.2566E+00	.2130E+00	-.8000E-02
(6, 1)	.9998E+00	.1688E-01	-.6976E-02	-.2069E-02
(6, 2)	.9998E+00	.8178E-02	-.4408E-02	-.1507E-02
(6, 3)	.9998E+00	.4192E-07	-.2261E-07	-.7728E-08
(6, 4)	.9987E+00	-.2842E-03	.1458E-04	-.3137E-05
(6, 5)	.9952E+00	.4256E-02	-.9237E-03	.5646E-04
(6, 6)	.9998E+00	-.3663E-01	-.4365E-02	-.6024E-04
(6, 7)	.9994E+00	-.6944E-01	-.1435E+00	.3339E-03
(6, 8)	.9997E+00	.3099E+00	.3689E+00	-.4837E-03
(6, 9)	.9990E+00	.6949E-01	-.3453E-01	.1872E-02
(6,10)	.1000E+01	.0000E+00	.0000E+00	.0000E+00
(6,11)	.8381E+00	-.5165E-01	.7623E-02	-.2808E-03
(7, 1)	.1000E+01	.0000E+00	.0000E+00	.0000E+00
(7, 2)	.1000E+01	.0000E+00	.0000E+00	.0000E+00
(7, 3)	.9998E+00	-.2036E-03	.1237E-03	.4434E-04
(7, 4)	.9613E+00	.6191E-04	-.2197E-04	.8259E-06
(7, 5)	.1000E+01	-.5701E-03	-.3009E-03	-.3688E-05
(7, 6)	.9782E+00	.6719E-03	-.2997E-03	.6828E-05
(7, 7)	.9998E+00	-.1383E-01	-.1407E-01	-.5896E-05
(7, 8)	.9847E+00	.7534E-01	-.4371E-01	.9755E-03
(7, 9)	.9872E+00	.3083E-01	-.1128E-01	.4921E-03
(7,10)	.9907E+00	-.1493E+00	-.3097E-02	.1606E-03
(7,11)	.9774E+00	.1430E-01	-.3452E-02	.1564E-03
(8, 1)	.9998E+00	.4363E-03	-.1735E-03	-.5014E-04
(8, 2)	.9998E+00	-.7851E-04	.4234E-04	.1447E-04
(8, 3)	.9998E+00	-.1383E-07	.7456E-08	.2549E-08
(8, 4)	.9998E+00	-.1422E-05	-.1105E-05	-.2545E-07
(8, 5)	.9973E+00	-.2191E-04	.7257E-05	-.4019E-06
(8, 6)	.9964E+00	-.6585E-04	.5711E-04	-.9198E-06
(8, 7)	.9994E+00	-.4591E-03	-.1105E-02	.4811E-05
(8, 8)	.9998E+00	-.1466E-01	-.1386E-01	-.1341E-04
(8, 9)	.9712E+00	-.2680E-02	.3356E-03	-.1202E-05
(8,10)	.1000E+01	.0000E+00	.0000E+00	.0000E+00
(8,11)	.8166E+00	-.4507E-02	.3768E-03	-.1089E-04

Appendix D2 (cont'd)

A-BG-HC matrix coefficients

element	correlation	coefficients (low order to high order)		
(9, 1)	.1000E+01	.0000E+00	.0000E+00	.0000E+00
(9, 2)	.1000E+01	.0000E+00	.0000E+00	.0000E+00
(9, 3)	.9998E+00	.5768E-03	-.2201E-03	-.6176E-04
(9, 4)	.9999E+00	-.3588E-05	-.5043E-05	-.6170E-08
(9, 5)	.9999E+00	-.6080E-04	-.4190E-04	-.1457E-06
(9, 6)	.9919E+00	-.1029E-03	-.8578E-04	.3225E-05
(9, 7)	.9998E+00	-.1297E-02	.8453E-04	-.2108E-04
(9, 8)	.9968E+00	.6898E-02	-.1812E-02	.1082E-03
(9, 9)	.9997E+00	-.3057E-01	-.1769E-01	.9496E-04
(9,10)	.9907E+00	.2412E-03	.5003E-05	-.2594E-06
(9,11)	.9929E+00	-.1026E-02	-.1709E-02	.6912E-04
(10, 1)	.1000E+01	.0000E+00	.0000E+00	.0000E+00
(10, 2)	.1000E+01	.0000E+00	.0000E+00	.0000E+00
(10, 3)	.1000E+01	.0000E+00	.0000E+00	.0000E+00
(10, 4)	.1000E+01	.0000E+00	.0000E+00	.0000E+00
(10, 5)	.1000E+01	.0000E+00	.0000E+00	.0000E+00
(10, 6)	.9931E+00	.3843E-02	-.9352E-03	.4867E-04
(10, 7)	.1$00E+52	.1000E+01	.0000E+00	.0000E+00
(10, 8)	.9871E+00	.6741E-01	-.1600E-01	.8039E-03
(10, 9)	.9994E+00	-.1109E+00	.2537E-01	-.2415E-02
(10,10)	.9935E+00	-.1125E-08	.2765E-09	-.1371E-10
(10,11)	.9883E+00	.1915E-01	-.6268E-02	.1176E-03
(11, 1)	.1000E+01	.0000E+00	.0000E+00	.0000E+00
(11, 2)	.1000E+01	.0000E+00	.0000E+00	.0000E+00
(11, 3)	.1000E+01	.0000E+00	.0000E+00	.0000E+00
(11, 4)	.1000E+01	.0000E+00	.0000E+00	.0000E+00
(11, 5)	.1000E+01	.0000E+00	.0000E+00	.0000E+00
(11, 6)	.8302E+00	-.5870E-03	.7487E-04	-.2739E-05
(11, 7)	.1000E+01	.0000E+00	.0000E+00	.0000E+00
(11, 8)	.9926E+00	.9916E+00	.2057E-02	-.1105E-03
(11, 9)	.9999E+00	.1218E-01	-.4383E-02	.5224E-03
(11,10)	.9996E+00	.7924E-03	.1129E-02	-.1651E-05
(11,11)	.9979E+00	-.2828E-01	-.2926E-02	.6999E-04

Appendix D2 (cont'd)

G matrix coefficients

element	correlation	coefficients (low order to high order)		
(1, 1)	.9999E+00	.1694E+00	.6835E-01	-.2494E-03
(1, 2)	.9996E+00	-.6212E-01	.1287E-01	.2528E-03
(1, 3)	.1000E+01	-.2333E-02	.4777E-03	.1583E-03
(1, 4)	.9998E+00	.2230E-02	-.7932E-04	.3585E-05
(1, 5)	.9479E+00	-.7586E-02	.1184E-03	-.1153E-04
(1, 6)	.9972E+00	-.5019E+00	-.1469E-01	.3090E-03
(1, 7)	.9850E+00	-.3162E+00	.2128E+00	-.5342E-02
(1, 8)	.9954E+00	-.6508E+02	.4195E+01	-.9159E-01
(1, 9)	.9999E+00	.1518E+00	-.7652E-01	.7580E-04
(1,10)	.9987E+00	-.8225E+00	.1267E-01	-.1820E-03
(1,11)	.9999E+00	-.8058E+01	.6203E-01	-.2832E-03
(2, 1)	.9996E+00	-.6212E-01	.1287E-01	.2528E-03
(2, 2)	.9999E+00	.9588E-01	.4723E-01	-.3033E-03
(2, 3)	.9995E+00	-.1423E-01	.3771E-02	-.2736E-03
(2, 4)	.9966E+00	-.7009E-04	-.9534E-04	.4082E-05
(2, 5)	.9954E+00	-.2375E-02	-.1945E-02	.1984E-04
(2, 6)	.1000E+01	-.7411E+00	.1023E-01	-.1646E-03
(2, 7)	.9968E+00	-.7432E+00	.3063E+00	-.7306E-02
(2, 8)	.9985E+00	.3801E+02	-.2533E+01	.5170E-01
(2, 9)	.1000E+01	.1813E-01	.7974E-01	.2015E-03
(2,10)	.9921E+00	-.5869E+00	.1893E-01	.8110E-03
(2,11)	.9982E+00	.4116E+01	.2580E+00	-.5719E-02
(3, 1)	.1000E+01	-.2333E-02	.4777E-03	.1583E-03
(3, 2)	.9995E+00	-.1423E-01	.3771E-02	-.2736E-03
(3, 3)	.9999E+00	.2462E-01	.2536E-01	.8143E-04
(3, 4)	.1000E+01	.1879E-02	.1460E-04	.2144E-07
(3, 5)	.9984E+00	.1373E-01	-.1785E-03	.1159E-04
(3, 6)	.9820E+00	-.5691E-02	-.1567E-02	.7094E-04
(3, 7)	.9227E+00	-.2195E-01	.2131E-01	-.8262E-03
(3, 8)	.1000E+01	-.2034E+00	-.6213E-01	-.2590E-02
(3, 9)	.9955E+00	-.4802E+01	.1219E-01	-.1385E-02
(3,10)	.9952E+00	-.6388E-01	.8520E-02	-.4451E-03
(3,11)	.1000E+01	-.1199E+00	.2822E-01	-.4200E-02

Appendix D2 (cont'd)

H matrix coefficients

element	correlation	coefficients (low order to high order)		
(1, 1)	.9999E+00	-.1391E-01	.8202E-03	-.6807E-05
(1, 2)	.9999E+00	-.9601E-01	.7746E-02	-.1019E-03
(1, 3)	.9976E+00	-.8577E-01	.8209E-02	-.1985E-03
(2, 1)	.9911E+00	-.1806E+00	.7790E-02	-.1782E-03
(2, 2)	.9997E+00	-.2579E-02	-.6763E-02	-.4387E-03
(2, 3)	.9815E+00	.1236E+00	-.1863E-01	.5326E-03
(3, 1)	.9988E+00	-.1752E+00	.7341E-02	-.6687E-04
(3, 2)	.9975E+00	-.1309E+01	.7416E-01	-.1394E-02
(3, 3)	.9974E+00	-.3206E+00	.1690E-01	-.1708E-03
(4, 1)	.9921E+00	-.3611E+00	.8359E-01	-.4474E-02
(4, 2)	.9998E+00	.4895E+00	.3388E+00	-.1437E-02
(4, 3)	.9848E+00	-.7704E+00	.1587E+00	-.2462E-02
(5, 1)	.9978E+00	.4290E-01	-.7944E-01	.3686E-02
(5, 2)	.9983E+00	-.7009E+00	-.3402E+00	.7286E-02
(5, 3)	.9870E+00	.2508E+00	-.2115E+00	.7923E-02
(6, 1)	.9903E+00	.3376E+00	.6572E-02	.4228E-03
(6, 2)	.9804E+00	.1273E-01	.7745E-02	-.2754E-03
(6, 3)	.8302E+00	.5870E-01	-.7487E-02	.2739E-03
(7, 1)	.9561E+00	-.2202E-02	.4746E-03	-.9889E-05
(7, 2)	.1000E+01	.3365E-02	-.9604E-03	.1104E-03
(7, 3)	.8933E+00	-.7054E-02	.1677E-02	-.6174E-04
(8, 1)	.9153E+00	.9755E-03	-.1880E-03	.7340E-05
(8, 2)	.1000E+01	-.9334E-03	.4378E-03	-.4459E-04
(8, 3)	.7781E+00	.2180E-02	-.4215E-03	.1319E-04
(9, 1)	.9804E+00	.1273E-02	.7745E-03	-.2754E-04
(9, 2)	.9983E+00	.1790E-01	.3460E-02	-.9251E-04
(9, 3)	.9929E+00	.1014E-02	.1712E-02	-.6928E-04
(10, 1)	.9931E+00	-.3843E-01	.9352E-02	-.4867E-03
(10, 2)	.9998E+00	-.2817E-02	.1807E-02	.3286E-03
(10, 3)	.9140E+00	-.2804E-01	.6996E-02	-.2021E-03
(11, 1)	.8302E+00	.5870E-02	-.7487E-03	.2739E-04
(11, 2)	.9929E+00	.1014E-02	.1712E-02	-.6928E-04
(11, 3)	.9979E+00	.2828E-01	.2926E-02	-.6999E-04

---

1. M.S. Idelchik, An Application of Modern Control Theory to a High-bypass Variable Compressor Geometry Jet Engine, S.M. Thesis, MIT, 1981.

2. Efthimios Kappos, Robust Multivariable Control for the F100 Engine, E.E., S.M. Thesis, MIT, 1980.

3. G. Stein, J. Doyle, Multivariable Feedback Design: Concepts for a Classical Modern Synthesis, IEEE Transactions on Automatic Control, AC-26, Feb. 1981.

4. G. Stein, LQG-Based Multivariable Design: Frequency Domain Interpretation, AGARD-LS-117.

5. G. Stein, N. Sandell, Classical and Modern Methods for Control System Design, Notes, MIT, 1979.

6. M. Inoue, Control System Synthesis of a Computer Piloted Submarine, S.M. Thesis, MIT, 1979

7. M. Saylor, Electronics Systems Design and Control Algorithm for a Robot Submarine, S.M. Thesis, MIT, 1979

8. M. Athans, Multivariable Control System Design Using the LQG/LTR Methodology, 6.232 class notes, MIT, 1983.

9. B. Bonnice, L. Valavani, Submarine Configuration and Control, CSDL memo SUB 1-1083, 1983.

10. B. Bonnice, CONSTRPS Fortran and Executive Command Computer Programs, CSDL, May, 1984.

11. Gertle, Hagan, Standard Equations of Motion for Submarine Simulation, NSRDC Report 2510, June 1967.

12. S. Crandall, et al., Dynamics of Mechanical and Electromechanical Systems, McGraw-Hill, 1968.

13. Takahashi, Rabins, and Auslander: Control, Addison-Wesley, 1970, pp 65-86.

14. Kevin Boettcher, Analysis of Multivariable Control Systems with Structured Uncertainty, Area Examination Paper, MIT, May 13,1983.

15. Lawrence Dreher, Robust Rate Control System Designs for a Submersible, O.E., S.M. Thesis, MIT, May 11,1984.

16. J.N. Newman, Marine Hydrodynamics, MIT Press, 1977

17. Alan Miller, Fortran Programs for Scientists and Engineers, Sybex, 1982.